JUSTUS-LIEBIG-
UNIVERSITÄT
GIESSEN

# The SMARCAD1-orthologue Fft2 is a novel RNA binder and linked to the nuclear RNA exosome

Inaugural-Dissertation
to obtain the academic degree
Doctor rerum naturalium (Dr. rer. nat)

submitted to the Department of Biochemistry
of Justus Liebig Universität, Gießen

by

Philip Fleischhauer

February, 2023

1st reviewer: Dr. Cornelia Kilchert

2nd reviewer: Prof. Dr. Sigurd Braun

# Danksagung,

Ich möchte mich zu Beginn dieser Danksagung von ganzem Herzen bei all jenen bedanken, die mich während meiner Doktorarbeit unterstützt haben.

Zunächst möchte ich meiner Doktormutter Dr. Cornelia Kilchert danken, die mich mit Ihrem Fachwissen, Ihrer Geduld und Ihrem Engagement inspiriert hat. Ohne sie hätte ich diese Arbeit nicht erfolgreich abschließen können. Des Weiteren danke ich Dr. Katja Sträßer für die zur Verfügungstellung von Labor Ressourcen sowie Ihrem stets konstruktiven Feedback innerhalb der Doktorandenseminare.

Bedanken möchte ich mich außerdem bei Dr. Birte Keil für die experimentelle Durchführung der ChIPseq, sowie der experimentellen Evaluierung des Heterochromatinstatus von *S. pombe* innerhalb meiner Doktorarbeit. Auch möchte ich mich bei Dr. Nadine-Bianca Wäber für die Bereitstellung Ihrer Daten der RNase behandelten Dichtegradientenzentrifugationen wie auch einer ausführlichen Einarbeitung in den „Äkta Purifier" bedanken.
Ebenfalls bedanke ich mich bei Dr. Stefan Günther vom MPI Bad Nauheim für die Sequenzierung und Bearbeitung der RNAseq wie auch der ChIPseq. Bei Dr. Oliver Rossbach und Sophie Stebel (Doktorandin) möchte ich mich ebenfalls für die Einführung in der Arbeit im Radionukleotid Labor bedanken.
Ein großer Dank geht ebenfalls an Jan Weber (B. Sc.), welcher mir experimentell bei der Durchführung diverser ChIP-Experimente assistierte. Auch möchte ich mich bei Melanie Bingel (ehem. tech. Assistentin) für Ihre Hilfe bedanken, welche einen wichtigen Beitrag für die Generierung verschiedener Stämme leistete. Ebenfalls bedank
ich mich bei Jacqueline Böhme (Doktorandin) und Ebru Aydin (Doktorandin) für ihre Hilfe im Labor, die kreativen Denkanstöße bei experimentellen Sackgassen sowie die aufbauenden Gespräche.
Ich danke auch allen anderen Kollegen an der AG Sträßer, die mir wertvolle Hilfe und Anregungen gegeben haben.
Insbesondere bedanke ich mich bei Dr. Matthias Miosga, für die großartigen wissenschaftlichen Diskurse aber nicht zuletzt für die großartige Zeit innerhalb und außerhalb des Labors.

Zuletzt bedanke ich mich bei meiner Freundin Sandra Stullgys. Ihr ständiger Beistand hat mich durch die anspruchsvolle Zeit getragen und zu diesem erfolgreichen Abschluss verholfen. Ich bin unendlich dankbar für alles, was sie für mich getan hat.

# eidesstattliche Erklärung

Ich erkläre:
Ich habe die vorgelegte Dissertation selbstständig und ohne unerlaubte fremde Hilfe und nur mit den Hilfen angefertigt, die ich in der Dissertation angegeben habe. Alle Textstellen, die wörtlich oder sinngemäß aus veröffentlichten Schriften entnommen sind, und alle Angaben, die auf mündlichen Auskünften beruhen, sind als solche kenntlich gemacht. Ich stimme einer evtl. Überprüfung meiner Dissertation durch eine Antiplagiat-Software zu. Bei den von mir durchgeführten und in der Dissertation erwähnten Untersuchungen habe ich die Grundsätze guter wissenschaftlicher Praxis, wie sie in der „Satzung der Justus-Liebig-Universität Gießen zur Sicherung guter wissenschaftlicher Praxis" niedergelegt sind, eingehalten.

_____ _____

Datum Unterschrift

# Table of contents

# List of Figures

# List of abbreviation

| | |
|---|---|
| cDNA | complementary DNA |
| ChIP | Chromatin immunoprecipitation |
| CLIP | Crosslink immunoprecipitation |
| Comp. RIC | comparative oligo d(T) RNA interactome capture |
| CUT | Cryptic unstable transcripts |
| DEG | Differently expressed gene |
| DNA | Deoxyribonucleotide acid |
| DUT | Dicer unstable transcripts |
| EAC | Exosome adaptor complex |
| EDM | Exosome deficiency mutants |
| ESF | Exosome specificity factor |
| FC | Fold change |
| Fft | Fissionyeast fun thirty |
| gDNA | genomic DNA |
| HTP | His-TEV-proteinA |
| LD | Loading dye |
| LF | Left flanking |
| LTR | Long terminal repeat |
| MTREC | Mtl1-Red1-core |
| o.n. | overnight |
| PAR-CLIP | Photoactivatable-Ribonucleoside-Enhanced Crosslinking and Immunoprecipitation |
| PCR | Polymerase chain reaction |
| qPCR | Quantitative PCR |
| RF | Right flanking |
| RNA | Ribonucleotide acid |
| RT-PCR | Reverse transcription PCR |
| *S.pombe* | *Schizosaccharomyces pombe* |
| SDS-PAGE | Sodium Dodecyl Sulfate – Polyacrylamide Gel Electrophoresis |
| seq | sequencing |

| | |
|---|---|
| TSS | Transcription start site |
| TES | Transcription end site |
| XUT | Xrn1 unstable transcripts |
| YPCK | Yeast Pombe Cornelia Kilchert |
| YPLV | Yeast Pombe Lidia Vasiljeva |

# Abstract

In this study, the role of Fft2, a member of the SMARCAD1 family, is investigated for the ability of posttranscriptional regulation an nuclear RNA exosome interaction in the model organism *S. pombe*. Using a combination of functional and biochemical approaches, a novel RNA-binding activity mediated by the N-terminal extension was demonstrated for Fft2. It was also shown that Fft2 is recruited to specific chromatin regions in an exosome-dependent manner and that this recruitment is negatively affected by mutations of the exosome components Rrp6 and Mtl1. The author also demonstrated that Fft2 is recruited in an Rrp6-dependent manner to long terminal repeats (LTRs). He also shows that deletion of Fft2 accelerates spore formation but does not lead to impaired chromosome segregation. However, the members of the Fft family show a diverse response to environmental factors, suggesting a functional division of tasks. Overall, this work provides new insights into the role of Fft2, its connection to exosome-dependent regulation of gene expression in *S. pombe* and a potential crosstalk between the SMARCAD1 family and RNA metabolism.

# Zusammenfassung

In dieser Studie wird die Rolle von Fft2, einem Mitglied der SMARCAD1-Familie, im Hinblick auf die Fähigkeit zur posttranskriptionellen Regulierung sowie der Interaktion mit dem nukleären RNA Exosome im Modellorganismus *S. pombe* untersucht. Mit einer Kombination aus funktionellen und biochemischen Ansätzen konnte eine neue RNA-Bindungsaktivität für Fft2 gezeigt werden, welche durch den N-terminalen Bereich des Proteins vermittelt wird. Ebenfalls konnte gezeigt werden, dass Fft2 Exosom- abhängig an spezifische Chromatinregionen rekrutiert wird und dass diese Rekrutierung durch Mutationen der Exosom-Komponenten Rrp6 und Mtl1 negativ beeinflusst wird. Der Autor konnte ebenso zeigen, dass Fft2 Rrp6-abhängig an Chromatinregionen rekrutiert wird, die long terminal repeats (LTRs) enthalten. Er zeigt auch, dass die Deletion von Fft2 die Sporulierung beschleunigt, ohne dabei zu einer gestörten Chromosom Segregation zu führen. Die Mitglieder der Fft-Familie zeigen indes eine diverse Reaktion auf Umweltfaktoren wodurch eine funktionelle Aufgabenteilung nahe liegt. Insgesamt bietet diese Arbeit neue Einblicke in die Rolle von Fft2, seine Verbindung zur Exosom-abhängigen Regulierung der Genexpression von *S. pombe* und dem Zusammenhang zwischen der SMARCAD1-Familie und dem RNA-Metabolismus.

# 1 Introduction

## 1.1 *Schizosaccharomyces pombe* as a model organism

The fission yeast, *Schizosaccharomyces pombe* (*S. pombe*) belongs to the division of *Ascomycota* and the family of *Schizosaccharomycetaceae* [Sipiczki 2000] and is the best-studied member in the *Schizosaccharomyces* genus [Hoffman et al. 2015]. The first description and isolation of *S. pombe* were performed by Paul Lindner from east African millet beer, dated back to the year 1893 [Lindner 1893]. The name "pombe" originates in the language Swahili, can be translated to beer and is the name of the local brew in this region [Burton 1859].

As an eukaryotic model system, *S. pombe* shows typical characteristics including splicing of transcripts, intracellular compartmentalization like a nucleus and organelles and the processes of transcription, translation and cytoskeletal organisation is comparable to metazoan [Hoffman et al. 2015]. On the other hand, *S. pombe* is a unicellular organism that can be easily grown in large amounts using simple and robust conditions as ambient temperature. This opportunity drastically increases the number of organisms managed in the experimental procedure, and the simple and robust conditions for *S .pombe* growth enable plain changes in environmental growth conditions [Hoffman et al. 2015]. These characteristics make *S. pombe* an popular eukaryotic model organism.

In direct comparison to the model organism like the budding yeast *Saccharomyces cerevisiae* (*S. cerevisiae*), *S. pombe* contains more intronic regions [Wood et al. 2002]. The *S. pombe* binary fission is more closely related to asexual cell division of metazoan cells [Balasubramanian et al. 2004] and the overall protein conservation between *Homo sapiens (H. sapiens)* and *S. pombe* is much higher than overall protein conservation between *S. cerevisiae* and *S. pombe* [Vo et al. 2016].

These cellular and molecular distinctions are due to the genetic divergence *between S. cerevisiae* and *S. pombe* that developed after the evolutionary split of these two organisms, which took place 420 to 330 million years ago, with 300 deleted and 300 altered genes in *S. cerevisiae,* representing around 10% of its translatome [Sipiczki 2000].

The cells of the fission yeast are rod-shaped and typically measure 3 to 4 µm in diameter and 7 to 14 µm in length. *S. pombe* is relatively well described and has become an relevant model organism in cell biology, cell cycle studies and genetics over time [Fantes and Hoffman 2016]. While investigations of meiosis in homothallic and heterothallic *S.pombe* strains date back to the year 1949 [Leupold 1949; Fantes and Hoffman 2016], the finding of the sexual

reproduction cycle research, studies on the control of cell growth and asexual binary fission control advanced in the 1950s [Mitchison 1990]. Adding to these early cytological investigations, interest in *S. pombe* strongly increased in the early 1990s (Figure 1), which opened the door for sequencing of the full genome in 2002 [Wood et al. 2002].

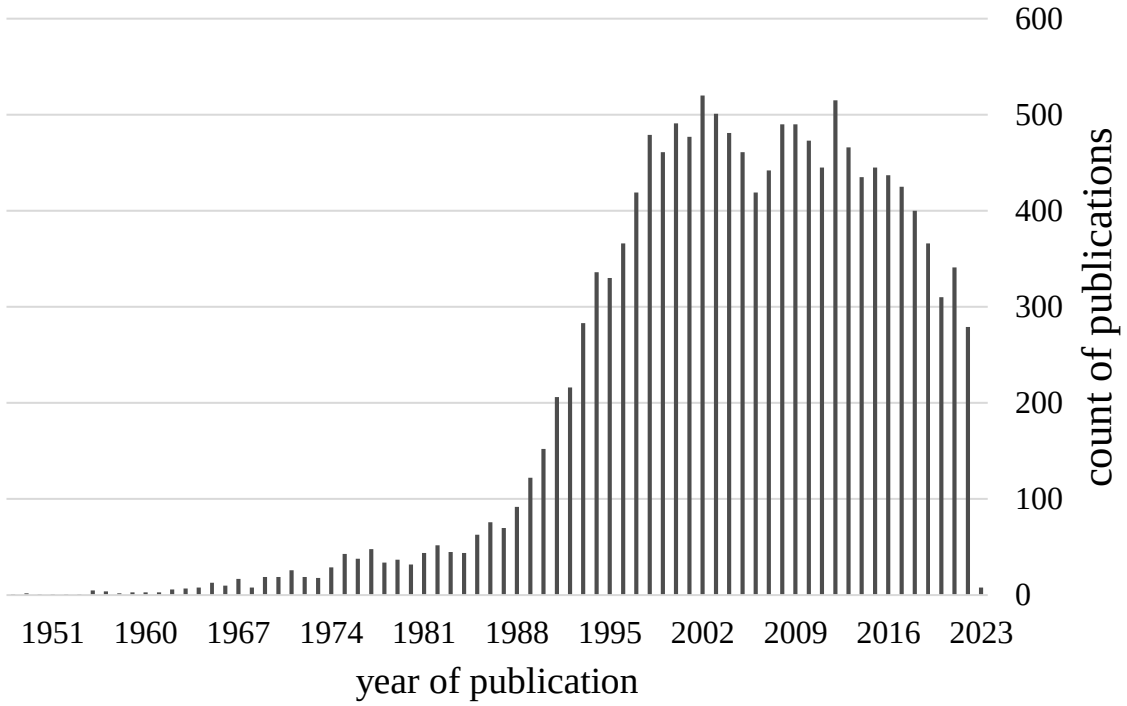


*Figure 1 publication history of scientific researches on S.pombe*

Representation of published papers in NCBI containing the term "*S. pombe*" between the years 1949 and 2023 as a bar chart. In the 1990s, the number of publications rose sharply, reaching a maximum of 520 publications in 2002, when the genomic sequence was published [Wood et al. 2002]

The genome of *S. pombe* has a size of 13.8 Mb and is distributed between three chromosomes named I, II and III [Smith et al. 1987] with a respective size of 5.7 Mb, 4.6 Mb and 3.5 Mb [Wood et al. 2002]. The genome itself contains a total amount of 4,940 genes with 50 potential genes, whose have *H.sapiens* orthologues, where then known as diseases associated [Wood et al. 2002]. Current researches associate 1,299 *S. pombe* genes in a disease context by their human orthologue [Harris et al. 2022]. The overall amount of genes is substantially lower than many other known eukaryotes, including *S.cerevisiae* and *H. sapiens* [Wood et al. 2002] which simplifies the translatome and makes deletion viability investigation of protein-coding genes much easier, as demonstrated in genome-wide research from 2010 [Kim et al. 2010].

### 1.1.1 Sporulation as strategy for sexual differentiation

While the mitotic reproduction cycle leads to a genetically identical offspring of the origin cell, sexual differentiation (meiosis and sporulation) is necessary to genetically recombine genomes from two individual *S.pombe* cells and generate durable stages in the form of ascospores [Tanaka and Hirata 1982].

Meiosis in *S. pombe* is induced by metabolic stress due to nitrogen starvation[Egel 1971] in a homothallic strain (h90) or two heterothallic strains with the opposite sex (h+/h-)[Egel 1971]. The initiation of meiosis is controlled by mating of two cells in a homothallic strain, heterothallic strains instead need a partner cell with expressed opposite mating type, to initiate the mating process. Nitrogen starvation in *S.pombe* reduces intracellular cAMP [Mochizuki and Yamamoto 1992], which directly controls expression of the central meiotic gene *mei2* [Watanabe et al. 1988].

The sexual differentiation of *S. pombe* ends with meiotic recombination [Yamashita et al. 2017] and the formation of four haploid ascospores [Ohtsuka et al. 2022]. The azygotic meiosis describes the process of meiosis in diploid cells, while the sexual reproduction in haploid cells is called zygotic meiosis (Figure 2). The zygotic meiosis is coordinated by specific pheromones[Nielsen and Davey 1995], namely P-Factor (h+ factor, *map2* [Imai and Yamamoto 1994]) and M-Factor (h- factor: *mfm1, mfm2* and *mfm3* [Kjaerulff et al. 1994]) [Nielsen and Davey 1995; Seike and Niki 2022]. These factors are separately expressed by h+ and h- genotypes and afterwards exported into the extracellular media[Nielsen and Davey 1995]. h- cells expressing the M-factor and detect the respective P-factor via the receptor *mam2* [Kitamura and Shimoda 1991] while the M-factors itself is bound by *map3* in h+ cells [Tanaka et al. 1993].

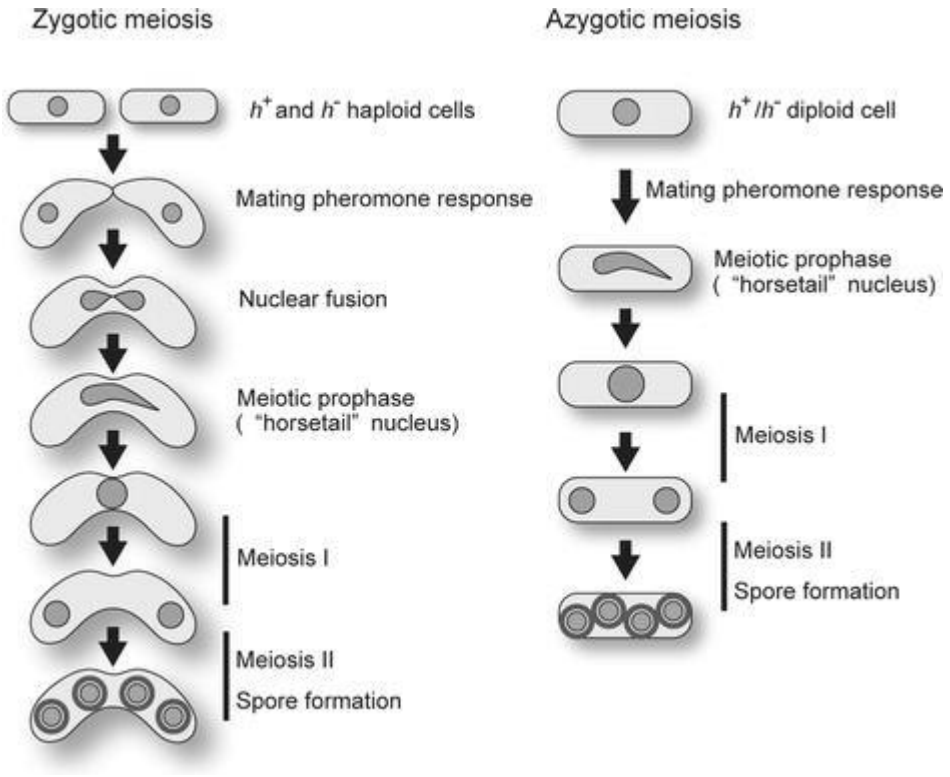


*Figure 2 schematic representation of zygotic and azygotic meiosis*

The figure shows a schematic overview of zygotic and azygotic meiosis in *S. pombe* published in [Asakawa and Hiraoka 2009]. While zygotic meiosis is initiated after mating und nuclear fusion of haploid cell with different mating type, the azygotic meiosis starts from a diploid cell. The processes of meiotic prophase, Meiosis I and Meiosis II is similar, but ascospores differentiating in their shape, caused by the lack of cellmating.

Azygotic and zygotic meiosis both activate the protein Spk1, which activates the initial transcription factor Ste11 through phosphorylation [Kjaerulff et al. 2005]. Ste11 initiates the transcription of Mei2, which binds the *sme2* transcript (meiRNA)[Watanabe et al. 1997; Yamashita et al. 2017] and therefore blocks degradation of *mei4* RNA by the nuclear RNA exosome (chapter 1.3).

While the nuclear fusion takes place, the haploid genomes merge into a single diploid genome and the genetic composition is rearranged by meiotic recombination. The oscillatory motion of the fused nucleus, which is important for this purpose, is controlled by tubulin and uses the spindle pole body as anchor point [Ding et al. 1997]. Additional investigations demonstrated the involvement of dynein heavy chain (Dhc1) not just in the movement of the nucleus, but also in the meiotic recombination [Yamamoto et al. 1999]. After that, meiosis I and meiosis II takes place, which results in the formation of four ascospore [Tanaka and Hirata 1982; Bennett and Turgeon 2016; Ohtsuka et al. 2022]. The survival period of the spores is significantly longer than that of cells from the stationary phase[Ohtsuka et al. 2022]. To

achieve this resistance to environmental factors [Egel 1977], the spore wall contains a composition of chitosan, mannan, and glucan while the surface is covered with a proteinaceous fibrillar structure consisting mainly Isp3 [Tahara et al. 2020; Ohtsuka et al. 2022].

## 1.2 Posttranscriptional gene regulation

The switch of gene activity is essential for unicellular organisms, like *S.pombe*, for precise control of metabolism, the cell cycle and the switch between meiosis and mitosis as well as cellular responses to environmental stress factors or cellular damage [Ghedira 2018].
It is necessary to distinguish between processes which affect the direct transcriptional gene regulation and posttranscriptional gene regulation [Ghedira 2018]. The regulation of polymerase-mediated transcription is mostly based on the accessibility of the respective chromatin region.
Processes that affect the transcriptional regulation are therefore nucleosome rearrangement, histone variant exchanges, histone modifications, heterochromatin maintenance, transcription factors and enhancer/repressor elements. Instead, molecular functions that alter the expression post-transcriptionally are RNA degradation, RNA modification, alternative splicing, export stalling and many more. Because the Fft2 orthologue in *S. cerevisiae* (FUN30) [Neves-Costa et al. 2009; Strålfors et al. 2011] and of its paralogue Fft3 [Strålfors et al. 2011; Steglich et al. 2015; Taneja et al. 2017] involved in heterochromatin maintenance, as well as RNA degradation pathway [Birot et al. 2022]. These two functional pathways are described in more detail.

### 1.2.1 Heterochromatin formation

Heterochromatin is highly packed chromatin with strictly reduced transcriptional activity, when compared to euchromatin which shows high transcriptional activity [Allis et al. 2007]. Beside of transcription regulation, the function of heterochromatin in *S. pombe* ranges from prevention of chromatin missegregation [Bernard et al. 2001], mating type switch [Grewal and Moazed 2003] and telomere packaging [Nimmo et al. 1994]. A hallmark of heterochromatin is the epigenetic modification of histone 3 by methylation of the lysine at position nine (H3K9) as di- and trimethylation [Padeken et al. 2022]. In addition, DNA methylation, ncRNA transcription and recruitment of the "RNA-induced initiation of transcriptional gene silencing complex" RITS complex [Verdel et al. 2004] are characteristic in these regions. While lysine trimethylation is characteristic for constitutive, constantly non-transcribed, heterochromatin (H3K9me3) [Trojer and Reinberg 2007], lysine dimethylation is

present in facultative formed heterochromatin at transcription sites [Trojer and Reinberg 2007]. This process is known for lineage-specific gene repression [Allshire and Madhani 2018] . Critical for this process are histone methyltransferases (HMT). While six different H3K9-HMTs are known in Mammalia [Padeken et al. 2022], *S.pombe* contains only one H3K9-HMT (namely Clr4) which is known and in charge for all histone methylations in heterochromatin regions [Harris et al. 2022]. The Clr4 HMT is therefore the essential pivot point for heterochromatin maintenance [Nakayama et al. 2001]. Also, a Clr4-dependent methylation of Mlo3 has been reported [Reyes-Turcu et al. 2011] and links the Clr4 activity to posttranscriptional gene regulation as well.

The complete loss of the K9 methylation, by HMT depletion, leads to a complete abolishment of heterochromatin organization in mouse model organism[Gao et al. 2008], which indicates the importance of H3K9 methylation in heterochromatin maintenance [Montavon et al. 2021]. Proteins which are capable to recognize methylated histones often contain one or more chromodomains. Chromodomain are protein domains that specifically bind to methylated histones. They are also found in other proteins that are involved in various cellular processes such as DNA repair, chromatin remodeling and cell cycle regulation [Eissenberg 2012] The binding of chromodomains to methylated histones is an important mechanism for the regulation of gene expression [Yap and Zhou 2011]. Chromodomain proteins are also involved in the regulation of other epigenetic processes such as DNA methylation [Du et al. 2015].

While the function of Clr4 is evaluated in multiple studies [Ivanova et al. 1998; Rea et al. 2000] the recruitment to chromatin is still under investigation. Additionally, Clr4 is not able to function as a solitary protein, but fulfils its function as the main component of the Clr4 methyltransferase complex (CLRC) [Horn et al. 2005; Jia et al. 2005; Kuscu et al. 2014]. CLRC consists of six proteins and has a ubiquitin ligase- in addition to its methyltransferase activity, which helps to sequester Clr4 to the heterochromatin regions [Oya et al. 2019; Shan et al. 2021].

In *S. pombe*, studies suggest an additional "RNA-induced transcriptional silencing" complex (RITS) which is essential in initiation of transcriptional silencing by the formation of heterochromatin [Verdel et al. 2004; Zhang et al. 2008]. As part of the complex RNAi machinery, RITS consist of Ago1 (which is also found in the RISC complex of *D.melanogaster* [Murchison and Hannon 2004]), Tas3 and Chp1. Chp1 contains a chromodomain and is therefore able to recognize H3K9 methylation [Verdel et al. 2004]. The RITS complex is guided by siRNA to complementary nascent transcripts and which leads to the recruitment the CLRC complex over a direct interaction between Stc1 and Ago1 [Bayne et al. 2010] which links the RNA interference to the formation of heterochromatin in a given region like the

heterochromatin formation in mating type locus [Martienssen and Moazed 2015].
In contrast to the RITS-complex, the silencing of chromatin in higher eukaryotes involves also an additional Agonaut protein containing RNA interference (RNAi) machinery, namely the "RNA-induced silencing complex" (RISC) [Sigova et al. 2004; Reyes-Turcu et al. 2011]. RNAi is a mandatory process for posttranscriptional silencing of centromeric regions [Volpe et al. 2002], as well as for silencing of the mating type locus [Sigova et al. 2004]. This posttranscriptional processs of gene regulation involves agonaut driven mRNA cleavage, guided by siRNA nucleotide sequence and/or binding on mRNA by its complementary miRNA nucleotide sequence. Also miRNA/mRNA hybridisation results in stalling of ribosomes on mRNA and the stop of translation [Pratt and MacRae 2009]. In summary, while both RITS and RISC complexes involve Argonaute proteins and small RNAs, they operate in different cellular compartments and have distinct functions. RITS is involved in transcriptional gene silencing at nucleus, guided by siRNAs [Verdel et al. 2004], whereas RISC operates in the cytoplasm and is involved in post-transcriptional gene silencing [Pratt and MacRae 2009]

### 1.2.2 RNA degradation

A major control factor in gene expression is the specific RNA turnover rate [Bevilacqua et al. 2003] and the overall stability of a specific RNA which results in a respective half-life time. This turnover rate is tightly regulated by selected RNA degradation-specific cis-acting sequences and trans-acting factors [Bevilacqua et al. 2003]. In mammalian cells, AU-rich elements are the most abundant sequence identified in unstable mRNA at the respective 3'-untranslated regions (UTR) [Caput et al. 1986; Wilson et al. 2001; Mignone et al. 2002]. In contrast, secondary structures, like hairpins and stem loops present in the UTR have been described to positively affect RNA stability. While many structural elements are known to inflict RNA stability, the majority of RNA is not degraded by chance, but proteins control the degradation process.
Enzymes that are able to degrade RNA can be separated into three major classes: endonucleases, 5' exonucleases and 3' exonucleases [ Houseley and Tollervey 2009]. Because of overlapping functions, the knockdown of a single RNase does not critically inhibit RNA degradation in most cases. This characteristic decrease the vulnerability of RNA degradation pathways in general [Houseley and Tollervey 2009]. The observed flexibility is represented in yeast and bacteria by the involvement of nucleases in degradation and RNA processing [Allmang et al. 1999; Diederichs and Haber 2007; Delan-Forino et al. 2017]. To prevent uncontrolled RNA degradation by exo- and endonucleases, cofactors are often assembled into complexes that target the respective RNA to the catalytic centre. An important RNA-degrading

complex in eukaryotes is the nuclear RNA exosome complex, which holds also endo- and 3'-exonuclease activity (chapter 1.3). Important cofactors for the RNA exosome are ATP-dependent helicases, in *S. cerevisiae* Mtr4 and Ski2. *S. pombe,* in contrast, has an additional "Mtr4-like helicase" (Mtl1), which is involved in RNA substrate selection via the MTREC complex (chapter 1.4). In bacteria, a complex with similar functions, namely the degradasome [Górna et al. 2012], with the corresponding RNA helicase RhlB [Tejada-Arranz et al. 2020].
Because extensive RNA secondary structure can inhibit degradation [Deutscher 2006], poly(A) polymerases are used to generate substrates for 3' exonucleases. Studies suggest that the vast majority of RNA is polyadenylated and that non polyadenylated RNA are more robustly expressed [Marguerat et al. 2012]. In *S. cerevisiae* [LaCava et al. 2005], and in *S. pombe* [Bühler et al. 2007], the TRAMP complex is essential for RNA degradation and processing of certain exosome substrates. The TRAMP complex contains a poly(A) polymerase (*S. cerevisiae:* Trf4/5, *S. pombe*: Cid14), which tags the bound RNA with short poly(A) tails. This polyadenylation was identified as a necessary step in the process of RNA depletion [LaCava et al. 2005; Tudek et al. 2018]. This is reminiscent of bacteria, where polyadenylation of RNA is exclusively connected to the degradation process [Deutscher 2006], suggesting that polyadenylation in eukaryotes has stabilizing function in the cytoplasm, and destabilizing function in the nucleus, depending on the polyadenylating polymerase [Stevenson and Norbury 2006; Houseley and Tollervey 2009]. In addition to poly(A) polymerases, poly(U) polymerases are also involved in destabilizing RNA by tagging them for degradation [Lehrbach et al. 2009].

## 1.3 The nuclear RNA exosome

The nuclear exosome complex is one of the most important RNA processing units in the cell nucleus [Ambro and Parker 1999; Bernstein and Toth 2012; Kilchert et al. 2016] and was described for the first time in 1997 [Mitchell et al. 1997]. Especially, the structural composition of the RNA exosome is a very essential characteristic in a broad range of species [Mitchell et al. 1997; Kim et al. 2010; Wan et al. 2012] and it was shown, that the RNA exosome has important functions in RNA surveillance and RNA processing in the nucleus and cytoplasm [Doma and Parker 2007; Kilchert and Vasiljeva 2013]. In addition, it was found that mutated exosome components can cause neuronal diseases in humans [Wan et al. 2012], which underlines the importance of the RNA exosome in the steady-state system of the cell.

### 1.3.1 EXO9

The exosome has 9 subunits that constitute the exosome core, namely EXO9, which is found in all archaea and eukaryota [Liu et al. 2006]. All components of EXO9 are essential [Mitchell et al. 1997]. Six of the exosome core subunits form a hexameric ring with a centric pore [Lorentzen et al. 2005] and show homology with bacterial PNPase and RNase PH [Lorentzen and Conti 2005]. The archaeal exosome contains triplicates of Rrp41 and Rrp42 in an alternating pattern, with only Rrp41 possessing catalytical activity [Lorentzen et al. 2005]. Although catalytic activity is observed in PH domains in the archaea EXO9, there is no RNase PH-like subunit activity *in vitro* or *in vivo* in either *S. cerevisiae* [Liu et al. 2006; Dziembowski et al. 2007] or in *H. sapiens* [Liu et al. 2006]. The hexameric ring in higher eukaryotes contain Rrp41 and Rrp42, but in contrast to archaea Rrp43, Rrp45, Rrp46 and Mtr3 in a very similar arrangement [Liu et al. 2006; Januszyk and Lima 2010; Kilchert et al. 2016].

The other 3 subunits Cls4, Mtr3 and Rrp43 contain S1 and KH domains which are capable to bind RNA in Prokaryota [Zhonghao Shi et al. 2008]. These 3 EXO9 components form a 'cap' structure on top of the hexameric ring [Liu et al. 2006]. Due to a lack of EXO9 RNase activity in Eukaryota, EXO9 cannot be found isolated in eukaryotes. Other proteins are necessary to maintain the functions of RNA quality control and RNA processing supported by the RNA exosome.

### 1.3.2 $EXO10^{Dis3/Rrp44}$ and $EXO10^{Rrp6}$

The smallest functional exosomal subunit in *S. cerevisiae* is the Exosome core with an additional processive 3′ to 5′ exo- and endoribonuclease. In *S. cerevisiae* this ribonuclease is named Rrp44, in *H. sapiens* and *S. pombe* it is annotated as Dis3. Dis3 shows similarities with RNase II in *E.coli* [Mitchell et al. 1997] and its exo- and endonuclease activity is functionally independent of the exosome core complex [Mitchell et al. 1997; Liu et al. 2006]. This functional complex is named $EXO10^{Dis3/Rrp44}$ because it's containing 10 subunits in total [Dziembowski et al. 2007]. $EXO10^{Dis3/Rrp44}$ is localized in the nucleus of *S. cerevisiae* and *H. sapiens* and also at minor levels in the cytoplasm of *H. sapiens* [Kilchert et al. 2016]. It should be noted that in *H. sapiens* a Dis3 orthologue (Dis3L) exists [Staals et al. 2010; Tomecki et al. 2010]. In contrast to Dis3, Dis3L is located exclusively in the cytoplasmatic $EXO10^{Dis3/Rrp44}$ complex and is not found in the nucleus [Tomecki et al. 2010]. Besides this compartmenting, Dis3L has no endonuclease activity based on aspartic amino acid exchanges in the PIN domain [Tomecki et al. 2010]. In *S. cerevisiae* *H. sapiens* and *S. pombe* the additional orthologue Dis3L2 [Chang et al. 2013; Malecki et al. 2013] is also described as a cytoplasmatic variant, but Dis3L2 is not interacting with exosome components [Malecki et al. 2013]. These findings

support the functional independence of Dis3 from the EXO9 core.
Dis3 is positioned at the bottom of the EXO9 barrel [Liu et al. 2016; Vo et al. 2016] and is bound to Rrp41 and Rrp45 [Bonneau et al. 2009], which makes it necessary for RNA to be funneled through the pore of the core complex to reach the catalytic exonuclease region of Dis3 [Wang et al. 2007; Bonneau et al. 2009]. Besides the canonical route, an alternative route is described which recruits RNA directly to the Dis3 exonuclease subunit. For this process, a nicking of the Dis3 domain is necessary to enable free access to the exonuclease domain. This nicking has already been described as a critical step in processing tRNA and 5s rRNA [Han and Ambro 2016; Delan-Forino et al. 2017].
In addition to the EXO10$^{Dis3/Rrp44}$ complex, a diverse functional EXO10 complex could be identified in *H. sapiens* nucleolus, EXO10$^{Rrp6}$ [Tomecki et al. 2010; Januszyk and Lima 2014]. Rrp6 is, like Dis3, an exoribonuclease but lacks an endonuclease activity. The Rrp6 protein is positioned at the top of the EXO9 barrel and is anchored over the-terminal α-helix to Cls4 and Mtr3 and with an unstructured, but conserved, region to the surface of Rrp43. An additional contact to EXO9, between the HRDC (helicase and RNase D C-terminal) domain of Rrp6 and a conserved loop (149-151) in Rrp4 is published [Wasmuth et al. 2014], which is important for exosome function *in vivo* [Malet et al. 2010].
Rrp6 and Dis3 also have in common that nucleolytic activity is observed for EXO9-independent Rrp6, which could be demonstrated *in vivo* [Callahan and Butler 2008]. In contrast to Dis3, Rrp6 is not essential, but a lack of the protein is resulting in temperature-sensitive growth in *S. cerevisiae* [Briggs et al. 1998] and leads to the accumulation of pre-rRNA, snRNA and inhibition of the trimming process of pre-snoRNA [Allmang et al. 1999]. Also, polyA-RNA is accumulating within the nucleolus in *S. cerevisiae* when Rrp6 is depleted [Carneiro et al. 2007].

Another crucial difference between Dis3 and Rrp6 is, that the exonucleolytic domain is exposed and is therefore accessible for RNA without contacting different subunits. Cryo-EM structures show an alternative way to access the Rrp6 exonuclease domain, which shows RNA within the hexameric ring and the S1-KH cap structure to the exonucleolytic domain of Rrp6 [Wasmuth et al. 2014]. A conclusion for the RNA accessibility pathway for Rrp6 needs further investigations.

### 1.3.3 EXO11$^{Dis3/Rrp6}$ Cofactors

While EXO10$^{Dis3/Rrp44}$ can be found as a functional complex in the cytoplasm of *H. sapiens, S. cerevisiae* and *S. pombe*, EXO10$^{Rrp6}$ is present in the nucleolus of *H. sapiens* solely. The majority of exosome complexes in the cell nucleus are composed of an EXO9 core with both

nuclease proteins Rrp6 and Dis3. This complex is referred to as EXO11$^{Dis3/Rrp6}$ or as nuclear RNA exosome [Kilchert et al. 2016]. Nevertheless, small quantities of Rrp6 were found in cytoplasm *H. sapiens* which suggests the occurrence of EXO11$^{Dis3/Rrp6}$ outside of the nucleus [Lejeune et al. 2003].

## 1.4 Exosome specificity factors and exosome adaptor complexes

While the structure of the exosome complex and its subcomponents was characterized in the past, it remains largely unclear how substrate targeting is performed in detail. Former studies found four different proteins (Mmi1 [Harigaya et al. 2006; Kilchert et al. 2015], Nop53p [Thoms et al. 2015], Utp18p [Thoms et al. 2015] and Nrd1p [Porrua and Libri 2015]) which are critical for RNA targeting to the exosome. These four so-called exosome-specific factors (ESF) make up only for a subset of exosome substrates, and therefore enable the possibility that other ways of exosome targeting take place and allow cells to adapt in response to environmental factors.

Later investigation assumed that the well-described ESF are components of larger functional complexes which guide the exosome to the target RNA, namely the exosome adaptor complexes (EAC) (Figure 3 [Ogami 2018]).

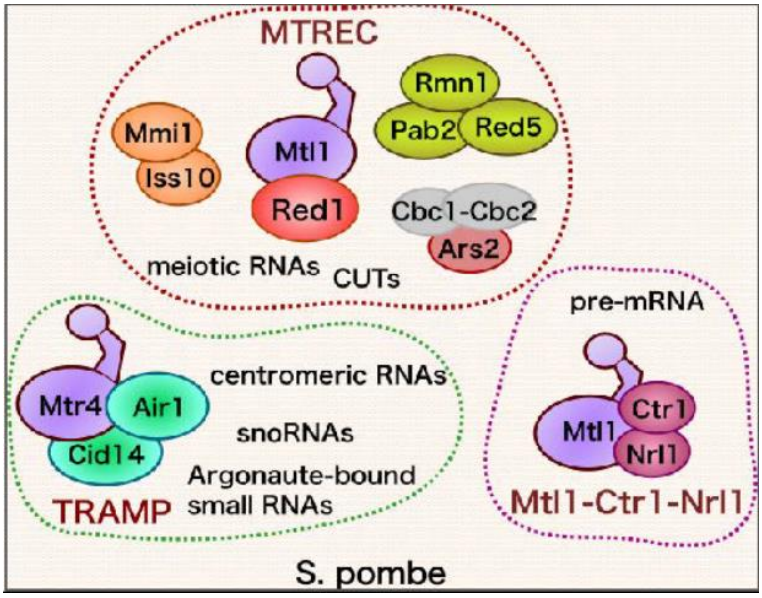


*Figure 3 variation of exosome adaptor complexes in S.pombe*

Schematic overview, adapted from [Ogami 2018], illustrate main exosome adaptor complex described in *S. pombe*. The central molecule is a Mtr4-like helicase 1 (Mtl1), or Mtr4 which interconnects all three complexes into the family of EAC. While MTREC is the largest complex which is responsible for CUT and meiotic RNA regulation, splicing events are mediated by Mtl1-Ctr1-Nrl1 and

TRAMP is involved in the regulation of centromeric transcripts. All of these complexes are found separate from each other which lead to the hypothesis of independent subunits including Mtl1.

Three major nuclear EACs have been described in *S. pombe* and are known to be involved in various exosome-driven processes [Bühler et al. 2007; Lee et al. 2013; Yang Zhou et al. 2015; Ogami 2018]. The three described complexes are Mtl1-Red1-core (MTREC) [Yang Zhou et al. 2015], TRAMP [Bühler et al. 2007] and the Mtl1–Ctr1–Nrl1 complex, which is also involved in the splicing of pre-mRNA [Yang Zhou et al. 2015; Ogami 2018]. Importantly, all of these complexes contain a Ski2-like RNA helicase as a central protein. The MTREC complex and the Mtl1–Ctr1–Nrl1 complex contain the core helicase Mtl1 [Yang Zhou et al. 2015; Mikolaskova et al. 2021], TRAMP, in contrast, contains Mtr4 [Bühler et al. 2007]. The Mtl1 protein has been proposed to funnel the bound RNA into the exosome channel [Weick et al. 2018], which leads to its decay [Kilchert et al. 2016].

Newer structural studies suggest that Nrl1 forms a link between Mtl1 and Ctr1 [Mikolaskova et al. 2021], suggesting that Mtl1 is not the central connector of this complex and could be assembled directly on target pre-mRNA. TRAMP is involved in the processes of the RNA interference (RNAi) machinery via Cid14 and is therefore associated with the regulation of centromeric transcripts and heterochromatin maintenance [Bühler et al. 2007; Reyes-Turcu et al. 2011].

In human, PAXT and NEXT are known adaptor complexes of the exosome. These two main exosome adaptors exist in the nucleoplasm of *H. sapiens*: The core of the PAXT consist of the proteins Mtr4-ZFC3H1 (orthologue of *S. pombe*: Mtl1-Red1) [Wu et. Al., 2020] while the NEXT complex contains the Zn knuckle protein ZCCHC8 and the RNA-binding protein RBM7 [Wu et. Al., 2020; Lubas et. Al. 2011]. The PAXT complex is primarily associated with long polyadenylated transcripts, the NEXT complex instead recruits on PROMPTs, replication-dependent histone mRNAs, snRNAs and snoRNAs [Wu et. Al., 2020]. The PAXT and NEXT complexes share a set of RNA substrates, but they differ significantly in their ability of binding to polyadenylated RNA [Wu et. Al., 2020].

Another exosome adaptor complex, present in the cytoplasm, is the superkiller complex (SKI complex). This complex is found in the cytoplasm of *S. cerevisiae* [Araki et. al., 2001; Brown et.al. 2000] and *H. sapiens* [Kögel et.al. 2022]. Orthologues of the central SKI-complex proteins (SKI2, SKI3 and SKI8) have also been described for *S. pombe* [Rhind et. al. 2011]. The SKI protein complex regulates RNA degradation by recruiting the exosome complex in the cytoplasm and is responsible for mRNA quality control in the cell [Brown et.al. 2000]. In humans, it has been shown that the SKI complex is essential for regulating the turnover of

RNA molecules and that the complex is closely associated with ribosomes and post-translational mRNA degradation [Kögel et.al. 2022].

The MTREC complex (alt. NURS) in *S. pombe* is therefore the orthologous complex to the PAXT complex in *H.sapiens* with the central helicase Mtr4 [Meola et al. 2016] instead of the MTREC helicase Mtl1 [Yang Zhou et al. 2015]. The MTREC is, in contrast to Mtl1-Ctr1-Nrl1, known for its involvement in the exosome-mediated decay of cryptic unstable transcripts (CUT) and meiotic transcripts [Andersen et al. 2013; Egan et al. 2014; Yang Zhou et al. 2015; Yuichi Shichino et al. 2020]. Also, MTREC is involved in the maintenance of facultative heterochromatin (Figure 4). In addition to the Mtl1-Red1 core, the complex can assemble up to three additional submodules to a full 11-subunit complex [Yang Zhou et al. 2015], which may be able to assemble independently to a variety of individual subcomplexes[Ogami 2018]. Which proteins are assigned to the "core", and which proteins are considered as transient interactors are evaluated differently by various studies [Lee et al. 2013; Egan et al. 2014; Yang Zhou et al. 2015].

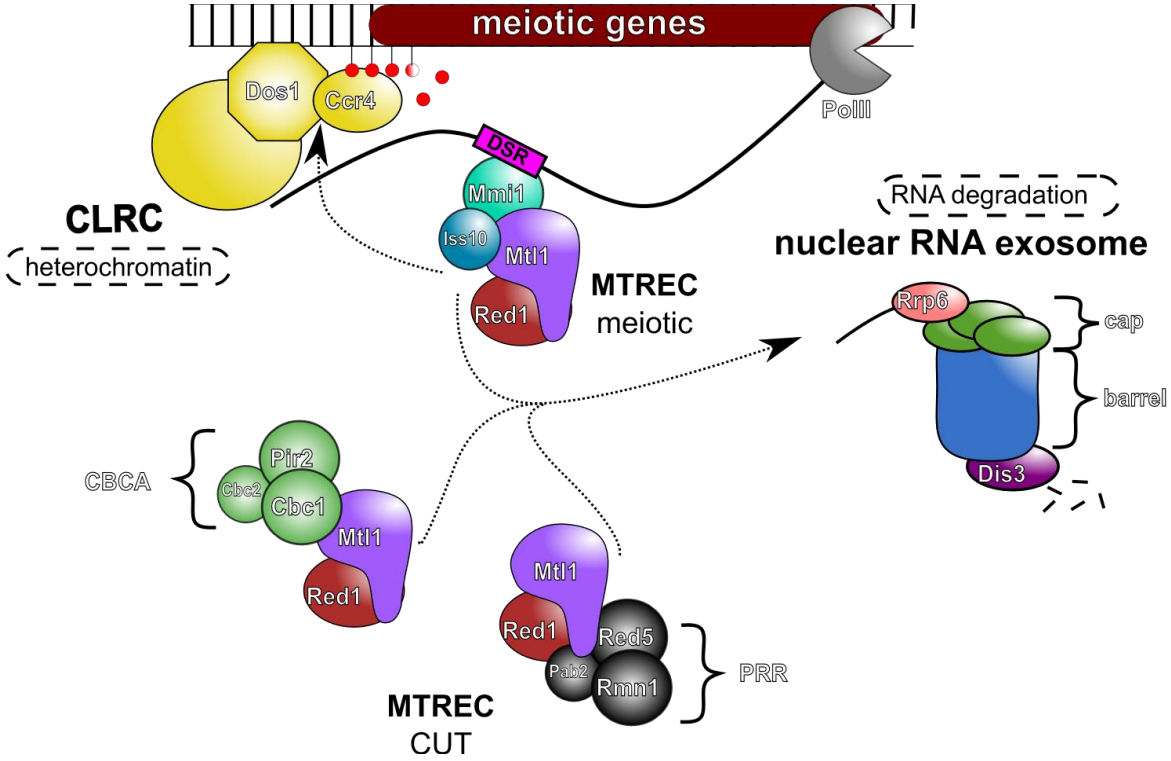


*Figure 4 schematic model of posttranscriptional regulation of meiotic genes mediated by MTREC*

Models illustrate the regulation of genes and transcripts by the exosome target complex MTREC. The Mtl1-Red1 core assembles in three separate subcomplexes: 1. meiotic subcomplex which bind to meiotic RNA by DSR, 2. CBCA subcomplex and 3. PRR subcomplex which targets cryptic unstable transcripts (CUT). All subcomplexes recruits RNA to the nuclear RNA exosome via Rrp6 where the RNA is threaded into the exosome core and therefore degraded. When the nuclear RNA exome is connected at meiotic gene sites by MTREC, the CLRC is recruited, which is responsible for facultative heterochromatin establishment.

The first group of MTREC target genes is classified by the direct binding of the exosome specificity factor Mmi1, a negative regulator of meiosis [Harigaya et al. 2006; Kilchert et al. 2015]. The RNA-binding protein Mmi1 [Shichino et al. 2018; Yuichi Shichino et al. 2020] interacts directly with RNA and recognizes determinants of selective removal (DSR) consisting of multiple repetitions of the base sequence U(U/C)AAAC [Yamashita et al. 2012; Yuichi Shichino et al. 2020] . Efficient degradation requires interaction with Erh1, which promotes dimerization. The binding of Mmi1 leads to the recruitment of Iss10, which is necessary to assemble MTREC on Mmi1-bound RNA [Yamashita et al. 2013; Yuichi Shichino et al. 2020]. The MTREC component Red1 links the MTREC to Rrp6 [Yang Zhou et al. 2015], a component of the nuclear RNA exosome with distributive 3'→5' exoribonuclease activity [Januszyk et al. 2011; Januszyk and Lima 2014; Yang Zhou et al. 2015]. This recruitment cascade results in the degradation of meiotic transcripts by the nuclear exosome [Yuichi Shichino et al. 2020]. Mmi1 is also an essential protein and its absence leads to untimely induction of meiosis [Harigaya et al. 2006]. In contrast, most other proteins involved in the pathway are not necessary for cell survival. In later studies, weak physical interactions of Mmi1/Rrp6 was verified in *Δred1* background [Yuichi Shichino et al. 2020], which could explain the general viability for Red1 and Rrp6 deletion strains, even in double deletion backgrounds [Sugiyama and Sugioka-Sugiyama 2011].
Interestingly, impairment of MTREC function additionally leads to a loss of facultative heterochromatin islands at meiotic genes like *mei4* or *ssm4* [Zofall et al. 2012; Tashiro et al. 2013]. The lack of heterochromatin in a *Δred1* background correlate with the loss of Clr4 at *mei4* and *ssm4* sites, while a deletion of *clr4* results in loss of RITS subunit Chp1 on *mei4* and *ssm4* loci [Zofall et al. 2012]. These findings implicate an independent pathway for heterochromatin formation without RITS which is part of the RNAi machinery.

Cryptic unstable transcripts (CUTs) were first characterized as transcripts that accumulate in a *Δrrp6* background in *S. cerevisiae* [Davis and Ares 2006]. CUTs can be separated into the major classes of PROMPTs (antisense promotor transcripts), AS (antisense gene) transcripts and 3'IGTs (intergenic transcripts) [Yang Zhou et al. 2015]. The targeting of CUTs is mediated in *S. pombe* by an assembly of the MTREC core with two individual submodules: the CBCA (Cbc1, Cbc2, Pir2/Ars2), which has also been described in mammals [Lubas et al. 2011; Andersen et al. 2013] and the PRR (Pab2, Red5, Rmn1)[Yang Zhou et al. 2015]. Both submodules are involved in targeting PROMPTs to the nuclear exosome [Andersen et al. 2013; Yang Zhou et al. 2015], which leads to their degradation, but are not required for turnover of AS transcripts and 3' IGT [Yang Zhou et al. 2015].

In addition to the important role of the various protein complexes, recent studies suggest that the nuclear scaffold is also essential for exosome regulation. Mmi1-dependent posttranscriptional RNA degradation takes place in nuclear foci where most of the exosome factors assemble [Harigaya et al. 2006; Shichino et al. 2014]. Additionally, the nuclear membrane-associated protein Lem2 is necessary to repress meiotic and ncRNA expression in a foci-independent pathway [Martín Caballero et al. 2022], which indicates a wider area of potential EAC components than already known.

## 1.5 ATP-dependent chromatin remodelling complexes

A mechanistical process that regulate the accessibility of chromatin are for example histone sliding, as well as ejection and incorporation of histone variants which modify the chromatin scaffold. ATP-dependent chromatin remodelers that fulfill this function can be subdivided into the ISWI subfamily, CHD subfamily, SWI/SNF subfamily and the INO80 subfamily [Clapier et al. 2017]. ISWI complexes are mostly involved in nucleosome spacing and the formation of repressive chromatin structures [Kagalwala et al. 2004]. The CHD subfamily in *S. cerevisiae* functions as a monomer [Tran et al. 2000], whereas the metazoan CHD remodeler complex (NuRD) has a wider variety of functions [Allen et al. 2013] and is also involved in nucleosome sliding and spacing [Clapier et al. 2017]. The subfamilies INO80 and SWI/SNF are both associated with active and inactive chromatin modifications. While INO80 is known to exchange histone variants like H2A.X [van Attikum et al. 2007] and H2A.Z [Papamichos-Chronakis et al. 2011], SWI/SNF is the most versatile complex, which can assemble with a broader variety of proteins depending on the tissue and developmental stage in metazoan[Ho and Crabtree 2010]. SWI/SNF subfamily remodellers typically facilitate chromatin access as they slide and eject nucleosomes, and promote either gene activation or gene repression [Clapier et al. 2017].

The NuRD complex, as well as the SWI/SNF complex, are involved in cancer biology [Lai and Wade 2011; Wilson and Roberts 2011] which implies the importance of correct regulation for the cell fate. The Fft-family and the human orthologue SMARCAD1, are members of the SWI/SNF family and are reviewed in greater detail.

### 1.5.1 The human SMARCAD1 protein and the Fft-family

The SMARCAD1 protein is classified as SNF-ATPase [Stelzer et al. 2016] and is known for its involvement in maintaining genome integrity [Lo et al. 2021], nucleosome exchange activity [Markert et al. 2021] and DNA double-strand break repair [Chakraborty et al. 2018].

A specific heterozygous mutation in the SMARCAD1 gene connected with exon skipping results in Basan syndrome [Xiong et al. 2022]. Basan syndrome is a rare autosomal-dominant disease and up to the year 2021, just 14 cases have been described in the literature [Xiong et al. 2022]. The symptoms are ectodermal dysplasia and adermatoglyphia (loss of fingerprints) [Valentin et al. 2018], without an link to skin malignancy [Xiong et al. 2022]. In all tested individuals with Basan syndrome, results implicated the specific pointmutation of SMARCAD1 gene cause splicing variations by exon skipping and therefore a loss of function [Valentin et al. 2018].

The Fft proteins are classified as members of the SMARCAD1 family of ATPases in *S. pombe* and *S. japonicus* [Harris et al. 2022]. The Fft-family in the *Schizosaccharomyces* genus consists of the three members Fft1, Fft2, and Fft3, which are considered as paralogues [Harris et al. 2022] which stands in contrast to other species, which express just a single protein variant (*S. cerevisiae*: FUN30, *H. sapiens*: SMARCAD1, *D. melanogaster*: Etl1) (Figure 5). Fft-family proteins contain a DNA-binding DEXDc domain and a HELICc domain, which are conserved in all orthologues.
Fft3 is the best-investigated family member in *S. pombe* and is known to be involved in meiotic recombination [Storey et al. 2018], heterochromatin maintenance [Strålfors et al. 2011; Steglich et al. 2015], and regulation of retrotransposons in centromeric regions and telomeric regions in combination with Fft2 [Persson et al. 2016]. Retrotransposons are important repetitive sequences of the genome regulation [Mita and Boeke 2016] and need a high level of regulation to control their mutational activity which drives genomic evolution [Göke and Ng 2016] and cancer growth. A subclass of retrotransposons are long terminal repeats (LTR), which are recognizably regulated by Fft3 and Fft2 in pombe [Persson et al. 2016] and drives evolution and gene expression in mammalian [Franke et al. 2017]. Also, specific activation of retrotransposons in *S. cerevisiae* meiosis progression is described, but its function is not finally uncovered [Laureau et al. 2021]. Other studies instead, associate specific retrotransposons with tumour suppressor activity [Wu et al. 2021] , giving the SMARCAD1 family studies significance in terms of a potential medical implication.

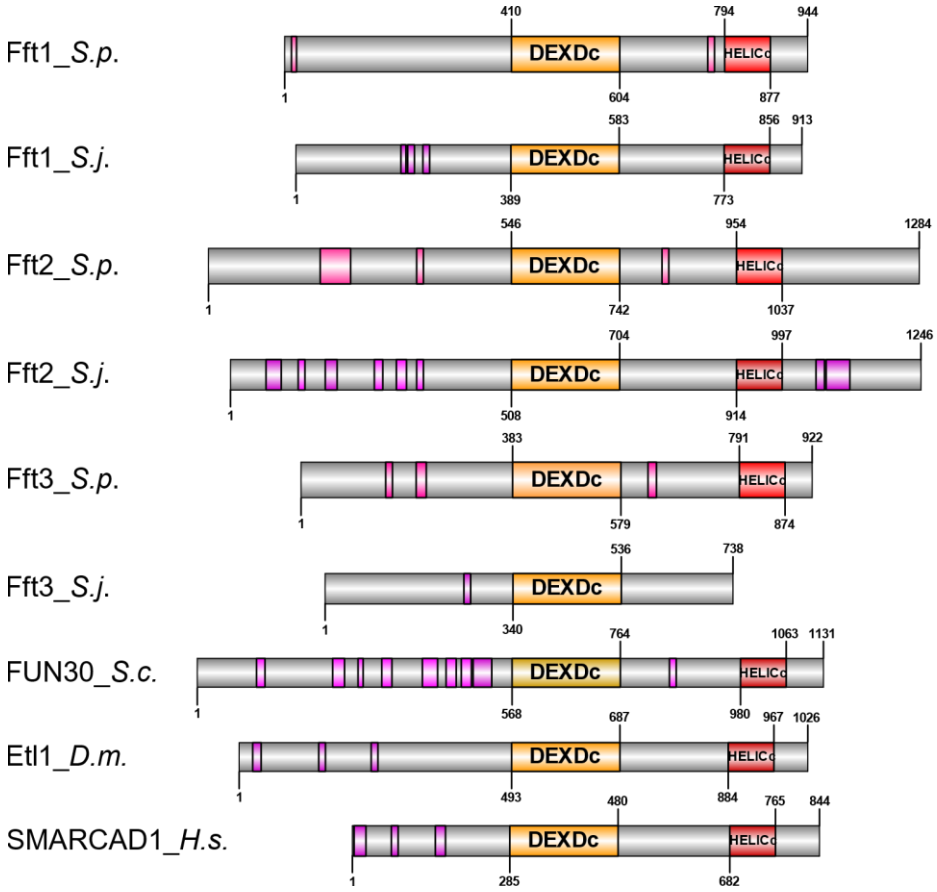


*Figure 5 SMARCAD1-family and their orthologues in different species*

Schematically illustrated are various variants of proteins which belong to the SNF/ATPase SMARCAD1- family. Characteristic domains are a DEXDc (yellow) and a HELICc (red) domain which is annotated by SMART sequence annotation tool (Letunic 2021) and present in a highly structured domain (for details see chapter 4.2). Beside of these regions, the N-terminal and C-terminal extensions are very unstructured, whith islands of conserved intrinsical disordered domains (IDD, pink). In *S. pombe* and *S. japonicus* three paralogues are known, which is a unique characteristic of this genus. While Fft2 is the longest variant, Fft3 is the shortest, which is due to the shortened N-terminal extension and a near loss of C-terminal extension.

## 1.6 Objective of this work

The primary objective of this PhD thesis is to comprehensively investigate and elucidate the role of Fft2, a member of the SMARCAD1 family, within the model organism *S. pombe*. Employing a combination of functional and biochemical methodologies, the study aims to specifically unravel the details of RNA-binding activity of Fft2. Furthermore, this work should reveal insights into the mechanisms underlying the recruitment and interconnection of Fft2 to distinct chromatin regions, with a particular emphasis on the relation to the nuclear RNA exosome and its adaptor complexes. Finally, an effect of Fft2 deletion on cell survival and sexual differentiation is tested to evaluate the importance of Fft2 in cellular processes.

# 2 Material

## 2.1 Fission yeast strains

In this work, fission yeast *Schizosaccharomyces pombe* strains with different genotypes were used for all carried experiments. If sexus is not determined by mating test, a "?" is noted. The strains used in this thesis are listed below:

| **clone number** | **genotype** | **characteristics** | **sexus** | **reference** |
|---|---|---|---|---|
| YF336 | met15Δ0 | *S. c.* BY4741 | / | *S.c.* genome deletion project - Fred Winston |
| YPCK217 | leu1-32 ura4D18 ade6-M216 mtl1-his6-TEV-Prot A::kanMX; *Δfft2*::NATMX4 | Mtl1-HTP; *Δfft2*::NATMX4 | h+ | this study |
| YPCK306 | leu1-32 ura4D18 ade6-M216; *Δfft2*::NATMX4 | *Δfft2*::NATMX4 | h+ | this study |
| YPCK328 | ade6-M216 leu1-32 lys1-131? ura4-D18 his7+::LacI-GFP A30:lacOP-ura4+-kanr | FY38780 - A30 | h90 | [Ding et al. 2019] |
| YPCK349 | leu1-32 ura4D18 ade6-M216; *Δfft1*::NATMX4 | *Δfft1*::NATMX4 | h + | this study |
| YPCK416 | leu1-32 ura4D18 ade6-M216 Fft3-6His-TEV-ProteinA::kanMX | Fft3-HTP | h + | this study |
| YPCK426 | leu1-32; ura4D18; ade6-M216 | wild type, h+, high sporulation | h+ | this study |
| YPCK427 | leu1-32; ura4D18; ade6-M216 | wild type, h-, high sporulation | h- | this study |
| YPCK434 | leu1-32 ura4D18 ade6-M216, his3D::1?? , imr1R(NcoI)::ura4+??? *Δrrp6*::NATMX4 Fft2-6xHIS-TEV-ProtA::KanMX | Fft2-HTP *Δrrp6*::NATMX4 | h- | this study |

| | | | | |
|---|---|---|---|---|
| YPCK489 | leu1-32 ura4D18 ade6-M216 his2?? otr1T(SphI)::ura4+?? his3?::1?? mtl1-1-FLAG::natMX; Fft2-6xHIS-TEV-ProtA::KanMX6 | Fft2-HTP Mtl1-1-FLAG | ? | this study |
| YPCK490 | leu1-32 ura4D18 ade6-M216 his3?::1 mei4D(828-1554nt)::GFP-hph *Δmmi1*::NATMX4 ; Fft2-6xHIS-TEV-ProtA::KanMX6 | Fft2-HTP *Δmmi1*::NATMX4 | ? | this study |
| YPCK491 | leu1-32, ura4D18, ade6-M216, his3?::1; Mmi1-his6-TEV-ProtA::KAN MX ; *Δfft2*::NatMx4 | Mmi1-HTP; *Δfft2*::NATMX4 | ? | this study |
| YPCK520 | ura4D18 leu1-32 ade6-M210 otr1R(Sph1)::ura4+ *Δclr4*::NatMx4, Fft2-6xHIS-TEV-ProtA::KanMX | Fft2-HTP *Δclr4*::NATMX4 | ? | this study |
| YPCK541 | ade6-M216 leu1-32 lys1-131? ura4-D18 his7+::lacI-GFP A30:lacOP-ura4+-kanr , *Δfft2*::NatMx4 | FY38780 - A30 *Δfft2*::NAT h90 | h90 | this study |
| YPCK543 | leu1-32 ura4D18 ade6-M216 *Δfft2*::NatMX4 , Pht1-HTP-kanMX dFft2::NAT | *Δfft2*::NAT, Pht1-HTP | h+ | this study |
| YPCK551 | leu1-32; ura4D18; ade6-M216?; his3?::1?; imr1R(NcoI)::ura4+?? *Δpht1*::HygMX, Fft2-6xHIS-TEV-ProtA::KanMX | *Δpht1*::Hyg, Fft2-HTP | ? | this study |
| YPCK552 | leu1-32 ura4D18 ade6-M216 *Δfft2*::NatMX4, Pht1-6xHis-TEV-ProteinA::kanMx | Pht1-HTP | ? | this study |

| | | | | |
|---|---|---|---|---|
| YPCK560 | leu1-32 ura4-D18 ade6-M216 Fft2_truncated_AA1-392-6xHis-TEV-ProtA-kanMX | Fft2-T1-HTP (M-->AA392) | h+ | this study |
| YPCK561 | leu1-32 ura4-D18 ade6-M216 Fft2_truncated_AA1-751-6xHis-TEV-ProtA-kanMX | Fft2-T2-HTP (M-->AA751) | h- | this study |
| YPCK562 | leu1-32 ura4-D18 ade6-M216 Fft2_truncated_AA1-1073-6xHis-TEV-ProtA-kanMX | Fft2-T3-HTP (M-->AA1073) | h+ | this study |
| YPCK57 | leu1-32 ura4D18 ade6-M216 mtl1-his6-TEV-Prot A::kanMX | Mtl1-HTP | h+ | this study |
| YPCK620 | leu1-32 ade6-216 ura4-D18 ; *Δfft3*::NATMX4 | *Δfft3*::KANMX | h+ | Supplied by Sigurd Braun |
| YPCK9 | leu1-32; ura4D18; ade6-M216; Fft2-6xHIS-TEV-ProtA::KanMX | Fft2-HTP | h+ | Cornelia Kilchert |
| YPLV144 | leu1-32; ura4D18; ade6-M216 | WT | h+ | [Lemieux et al. 2011] |
| YPLV353 | leu1-32, ura4D18, ade6-M216, his3?::1; mmi1-his6-TEV-ProtA::KAN MX | Mmi1-HTP | h+ | [Kilchert et al. 2015] |
| YPLV411 | leu1-32 ura4D18 ade6-M216? his3?::1? imr1R(NcoI)::ura4 *Δrrp6*::NATMX4 | ΔRrp6::NATMX4 | h+ | [Kilchert et al. 2015] |
| YPLV729 | leu1-32, ura4D18 ,ade6-M216, his2?? otr1T(SphI)::ura4+?? his3?::1??; mtl1-1-FLAG::kanMX | Mtl1-1-FLAG | h+ | Cornelia Kilchert, original strain by [Lee et al. 2013] |
| YPLV742 | leu1-32 ura4D18 ade6-M216 spac3c7.04-his6-TEV-ProtA::KAN MX | SPAC3c7.04-HTP | h+ | Cornelia Kilchert |

## 2.2 Laboratory equipment

| **Name** | **Company** | **notes** |
|---|---|---|
| Mini agarose gel chamber | | |
| UV detection table | | |
| cooling centrifuge 5425 R | Eppendorf | |
| centrifuge 5425 | Eppendorf | |
| NanoDrop ND-1000 | | |
| arrested pipette Eppendorf Reference® 2-20µl | Eppendorf | EP4924000037 |
| QuantStudio 3 | Thermofisher | |
| ThermoMixerC | Eppendorf | 5382000015 |
| Trans-Blot Turbo | Biorad | |
| Semidry Blotter | | |
| Biowave CO8000 Cell Density Meter | Biochrom | OD600 cell density measurement |
| FastPrep-24 5G | MP Biomedicals | |
| autoclave DX-150 | Systec | |
| ice machine | Manitowoc | |
| Autoclave VX-150 | Systec | |
| HERAfreeze HFU T Series | ThermoScientific | -80°C freezer |
| Bio-Link 365 | Vilber | 365nm UV crosslinker |
| 6870D Freezer/Mill | SPEX SamplePrep | |
| Avanti JXN-26 | Beckman Coulter | harvest centrifuge |
| Multitron Pro | Infors HT | |
| Innova 44 | New Brunswick | |
| DeltaVision Ultra High Resolution Microscope | Cytiva Life Sciences | 29206348 / 29254706 |
| Äkta system Purifier 100 | Amersham Biosciences | HPLC |
| Superose 6 Increase 10/300 GL | GE healthcare | Gel filtration column |
| Unichromat 1500 | UniEquip | Climate chamber for "äkta purifier" |
| Äkta start | cytvia | |

| | | |
|---|---|---|
| Optima XPN-80 Ultracentrifuge | Beckman Coulter | |
| Roller mixer SRT6 | stuart | |
| T advance | Biometra | 2-Block PCR cycler |
| XCell SureLock | Invitrogen | |
| HEP-1 Semi-Dry Blotter | Peqlab | 20cm x 20cm |
| Gel IX imager | Intas | geldocumentation chamber |
| Perfection 3200 Photo | Epson | scanner for agarplates |
| Typhoon FLA 9500 | GE healthcare | |
| Phosphor stage | GE healthcare | |
| UV transilluminator | | |
| Rotator 10UpM fix | NeoLab | 2-1175 |
| Electrophoresis system B1A | Easy-Cast | |
| Advantage A10 | Milli-Q | |
| Megafuge 40R | Heraeus | Centrifuge tube and plate centrifuge |
| ECL chemocam imager | intas | scanner for western blot |
| PM 2000 | Mettler | analyzer scale |
| AM 1000 | Mettler | precision scale |
| Rainin-classic starter KitPR-START | Mettler-Toledo | 17008708 |
| Rainin-classic 0.1µl - 2.0µl | Mettler-Toledo | 17008648 |
| PSU-20i | Grant-bio | multi-functional orbital shaker |
| KS 4000 ic control | IKA | heat able incubation shaker |
| EPS 600 | pharmacia biotech | electrophoresis Power Supply |
| PROTEAN II XL cell | Biorad | / |
| Bioanalyzer 2100 | Agilent Biotechnologie | |
| RNA 6000 Pico | Agilent Biotechnologie | chip for Bioanalyzer |
| XCell SureLock™ Mini-Zelle | Invitrogen | EI0001 |

## 2.3 Chemicals and ingredients

All used chemicals are listed in alphabetical order.

| Name | Company | Purity | catalogue number |
|---|---|---|---|
| dNTP | | | |
| HDGreen® Safe DNA Dye | Intas | / | ISII-HDGreen |
| Agarose | | | |
| 4-Thiouracile | Sigma | 97% | 440736-1G |
| Acidic Phenol/Chloroform 5:1 | Ambion | MB grade, purity >99% | AM9720 |
| RNasin RNase Inhibitor, 10,000u | Promega | | N2515 |
| Clarity™ Western ECL Substrate | Bio-Rad | | 1705060 |
| TEMED | VWR | | A1148.0025 |
| Phenylmethylsulfonylfluorid (PMSF) | | | |
| ROTI®Phenol/Chloroform/Isoamylalkohol | Roth | | A156.2 |
| glycogen blue | Boehringer | | |
| PowerUp SYBR Green Mastermix | ThermoFisher Scientific | | A25742 |
| Acrylamid 4K - solution (30 %) - Mix 37,5 : 1 | AppliChem | | A1672 |

## 2.4 Material and consumeables

All used materials and tools are listed in alphabetical order.

| Name | Company | notes |
|---|---|---|
| MN NucleoSpin Gel and PCR Clean-up Kit | Macherey-Nagel | 740609.250 |
| 15ml TPX tubes | diagenode | C30010009 |
| Micro tube 2ml with screwcap | Sarstedt | 72.693.005 |
| Multiply®-µStrip 0,2ml 8 well stripe + lids | Sarstedt | 65.989.002, 72.985.092 |
| Whatman® Gel-Blotting-Papiere, 20 cm x 20 cm | Merck | WHA10426981 |
| Rabbit IgG-Agarose | Sigma | A2909-5ML |
| Nitrocellulose Membrane, Roll, 0.45 µm | Bio-Rad | 1620115 |

| | | |
|---|---|---|
| Cover glasses No. 1.5H | Marienfeld | 0107032 |
| NuPAGE™, 4 to 12 %, Bis-Tris, 1.0–1.5 mm | invitrogen | NP0321BOX |

## 2.5 Enzymes

| Name | Company | Catalogue no. |
|---|---|---|
| Phire Hot Start II DNA-Polymerase | ThermoFisher Scientific | F122L |
| Q5 polymerase | NEB | M0491LVIAL |
| Protease inhibitor cockatil (PIC) | Sigma | P8215 |
| Pronase | Merck | 53702 |

## 2.6 Software/web resources

If not stated otherwise, all software in this project was used with commercial/academic licences or in a time-limited trial phase.

| name | version | creator |
|---|---|---|
| APE – a plasmid editor | 3.1.3 | M. Wayne Davis[Davis and Jorgensen 2022] |
| Primer3 | 4.1.0 | Whitehead Institute for Biomedical Research[Koressaar and Remm 2007] |
| OriginLab Pro 2023 | 10.0.0.154 (Academic) | OriginLab Corporation[OriginLab Corporation 2022] |
| Gimp2 | 2.10.32 | Spencer Kimball, Peter Mattis[Spencer Kimball 2022] |
| Inkscape | 1.2.1 | Inkscape-development team[Inkscape-development team 2022] |

| | | |
|---|---|---|
| FIJI | 1.53t | Johannes Schindelin et.al.[Schindelin et al. 2012] |
| integrated genome browser | 9.1.10 | Nowlan H. Freese, David C. Norris, Ann E. Loraine[Freese et al. 2016] |
| Pombase.org | Last updated: 2022-11-27 | Val Wood, Kim Rutherford[Harris et al. 2022] |
| IBS | 1.0.3 | Wenzhong Liu[Liu et al. 2015] |
| Jalview | 2.11.2.0 | Andrew Waterhouse, David Martin[Waterhouse et al. 2009] |
| CLUSTAL omega | 2.1 | |
| usegalaxy.org | | The galaxy community |

## 2.7 Custom DNA oligos

All DNA oligos were designed with the assistance of primer3 webpage and PCR product size was verified by APE.

| # | name | sequence |
|---|---|---|
| 586 | clr4-L3 | CTGCTGGCACGTTTATCACT |
| 587 | clr4-L4-pFA | ttaattaacccggggatccgACCGAAAAGCCAGCCACGACAATT |
| 588 | clr4-L5-pFA | cgagctcgaattcatcgatGGTCATTCATTTTCTAAGCAACGA |
| 589 | clr4-L6 | GCTCTCAGGTTTGGTGCAAA |
| 624 | fft1-L1 | ACGAAGAGGATTGGAAGGCT |
| 625 | fft1-L2 | gtcgacctgcagcgtacgACCCTCTCTTTTCTATAATCTATTTCACT |
| 627 | fft1-L4-pFA | ttaattaacccggggatccAACAACGGACCCATCCATAGTATCCACCCG |
| 628 | fft1-L5-pFA | cgagctcgaattcatcgatTCACACAAAGCAATAGAAACACTT |
| 629 | fft1-L6 | AACCCAACACAAGTGCATGT |
| 4 | fft2-L1 | TGCGGTGAGTTTTCCTTGTG |
| 5 | fft2-L2 | gtcgacctgcagcgtacgCGGTAATTATCGCAATGCCG |
| 9 | fft2-L3 | AGATTTAGACACCGAGGCGT |
| 10 | fft2-L4-HTP | aatcatggtgatggtgatggtgGTCTTTAGCAGCATTATTGTCAACCTCC |
| 36 | fft2-L4-pFA | ttaattaacccggggatccgGTCTTTAGCAGCATTATTGTCAACCTCC |

| | | |
|---|---|---|
| 11 | fft2-L5-HTP | gacgaggcaagctaaacaggACTTTCGATATCCTAGAATATTGTTGGT |
| 6 | fft2-L5-pFA | cgagctcgaattcatcgatACTTTCGATATCCTAGAATATTGTTGGT |
| 37 | fft2-L5-pFA | cgagctcgaattcatcgatACTTTCGATATCCTAGAATATTGTTGGT |
| 7 | fft2-L6 | CCCAGAATTGCTAACTCGATGA |
| 875 | Fft2-T1_fw | CAGCGATCTCGTTCCTCCTC |
| 845 | Fft2-T1_reverse_HTP | aatcatggtgatggtgatggtgGTGAACTATGGCTTCAGGCT |
| 876 | Fft2-T2_fw | GGACACCACGGACCTCATTT |
| 846 | Fft2-T2_reverse_HTP | aatcatggtgatggtgatggtgCGCATCTGCGGTTGGTTTAG |
| 877 | Fft2-T3_fw | ATAATGCAAGAGGAACAATA |
| 847 | Fft2-T3_reverse_HTP | aatcatggtgatggtgatggtgAGAGCTTAAGCTCATGTCAA |
| 202 | Fft3-L3 | GATGAACCTTGGATGGACGC |
| 679 | Fft3-L4-HTP | aatcatggtgatggtgatggtgATCATCGTCATCTTCAGCCTCCACAGTTTCG |
| 680 | Fft3-L5-HTP | gacgaggcaagctaaacaggATTGATTAGGTTTCTACTTTATTCGAGT |
| 205 | Fft3-L6 | GGGCCATGCAAAACTAGACC |
| 19 | HTPA-L5-rc | cctgtttagcttgcctcgtc |
| 18 | HTP-L4-rc | caccatcaccatcaccatgatt |
| 20 | KanMX-C2-rc | CGGATCCCCGGGTTAATTAA |
| 21 | KanMX-L2-rc | CGTACGCTGCAGGTCGAC |
| 22 | KanMX-L5-rc | ATCGATGAATTCGAGCTCG |
| 172 | mtl1-L3 | ACAAAGGGTTTTACGGCGAC |
| 176 | mtl1-L4-HTP | aatcatggtgatggtgatggtgGAGGTATAGAGAGGCCGAAAAT |
| 177 | mtl1-L5-HTP | gacgaggcaagctaaacaggGACAATGATCGTTTGGCCTATC |
| 175 | mtl1-L6 | CTCCACCTTTCCAAACCAGC |
| 983 | NCRNA.5066-f | TTGAAGGGACGGTGAATTGC |
| 984 | NCRNA.5066-r | CCACTTAACTCAACGGGGAC |
| 867 | Pht1-L1-f | ACGCTTAACTGCAGTGATCG |
| 868 | Pht1-L2pFA-rc | gtcgacctgcagcgtacgTTTGACCAGCCAACTTGTCG |
| 869 | Pht1-L3-f | GTCTGGAGGCGGTAAAGGTA |
| 871 | Pht1-L4HTP-rc | aatcatggtgatggtgatggtgAATAATTTCTTCCTCCTCGG |
| 870 | Pht1-L4pFA-rc | ttaattaacccggggatccgAATAATTTCTTCCTCCTCGG |
| 873 | Pht1-L5HTP-f | gacgaggcaagctaaacaggTGGAAAGTAAAATGTGCATGCG |

| | | |
|---|---|---|
| 872 | Pht1-L5pFA-f | cgagctcgaattcatcgatTGGAAAGTAAAATGTGCATGCG |
| 874 | Pht1-L6-rc | TCACACTATATTGAACGCTAAGC |
| 967 | SPBC32H8.15-f | CCCGCCCAGCATTTCAATTA |
| 968 | SPBC32H8.15-r | TCCACTTCTTTGCATTGCGG |
| 977 | SPLTRB.35-f | GAGCTGCGGTAAGTTTTCCT |
| 978 | SPLTRB.35-R | ACTGAACTGAGGAACGAGGT |
| 979 | SPLTRC.50-f | ACCTCGTTCCTCAGTTCAGTTAT |
| 980 | SPLTRC.50-r | TGCGGTGAGTTTTCCTTGTG |
| 987 | Ssa2-f | TCCATGGGTATCGAGACTGC |
| 988 | Ssa2-r | CACGCTCACCTTCAAACACT |

## 2.8 Antibodies

| Name | Company | notes |
|---|---|---|
| Anti-Histone H3 | Abcam | ab1791 |
| Anti-Histone H3 (di methyl K9) | Abcam | ab1220 |
| Anti-flag M2 monoclonal antibody | Sigma | F3165-1MG |
| Peroxidase-Anti-Peroxidase (PAP) | Jackson ImmunoResearch | 323-005-024 |
| peroxidase conjugate-goat anti-rabbit | Sigma | A2304-1ML<br>secondary antibody, |

## 2.9 Buffer and media

| YES media | EMM-G media | EMM-N media | 10000 x mineral stock |
|---|---|---|---|
| Glucose 30 g | l-Glutamic acid, monosodium salt 3.38 g | Potassium hydrogen phthalate 3 g | Boric acid 5g |
| Yeast extract 5 g | Potassium hydrogen phthalate 3 g | $Na_2HPO_4$ 2.2 g | $MnSO_4$ 4 g |
| Adenine 225 mg | $Na_2HPO_4$ 2.2 g | | $ZnSO_4 \cdot 7\ H_2O$ 4 g |

| | | | |
|---|---|---|---|
| Uracil 225 mg | Ad 750ml and autoclave | Ad 750ml and autoclave | $FeCl2 \cdot 6H2O$ 2 g |
| Histidine 225 mg | 50 x salt stock 20ml | 50 x salt stock 20ml | Molybdic acid 0.4 g |
| Leucine 225 mg | 1000 x vitamin stock 1ml | 1000 x vitamin stock 1ml | Kalium Iodid 1 g |
| Lysine 225 mg | 10000 x mineral stock 0.1ml | 10000 x mineral stock 0.1ml | $CuSO4 \cdot 5H_2O$ 0.4g |
| Agar (for solid medium only) 20 g | 10x aminoacid stock 100ml | 10x aminoacid stock 100ml | Citric acid 10 g |
| ad 1L with $H_2O$ and autoclave | 20% Glucose stock 150ml | 20% Glucose stock 150ml | ad 1L and sterile filter and store at 4°C |

| 50x salt stock | 1000x vitamine stock | 10x (low uracile) aminoacid stock | 20% glucose stock |
|---|---|---|---|
| $MgCl_2 \cdot 6\ H_2O$ 52.5 g | Pantothenic acid 1 g | 2.25 g adenine | 200g glucose |
| $CaCl2 \cdot 2H2O$ 0.735 g | nicotinic acid 10 g | 0,1 g (low uracile)/ 2.25 g uracile | |
| KCl 50 g | inositol 10 g | 2.25 g histidine | |
| $Na_2SO_4$ 2 g | biotin 10 mg | 2.25 g leucine | |
| | | 2.25 g lysine | |
| Ad 1L, autoclave and store at RT | Ad 1L and sterile filter and store at 4°C | Ad 1L, autoclave and store at RT | Ad 1L, autoclave and store at RT |

| TBS | TBS-T | TE | AE-buffer |
|---|---|---|---|
| 20 mM Tris-HCl pH 7.5 | 20 mM Tris-HCl pH 7.5 | 10mM Tris-Cl (pH 8.0) | 10 mM Tris-HCl |
| 150 mM NaCl | 150 mM NaCl 0,5ml tween20 | 1mM EDTA (pH 8.0) | 0.5 mM EDTA |

| Buffer I | Buffer II | Buffer III | Buffer IV |
|---|---|---|---|
| 50 ml 2x FA lysis buffer<br>1 ml 10% SDS<br>2.5 ml 5M NaCl | 50 ml 2x FA lysis buffer<br>1 ml 10% SDS<br>7 ml 5M NaCl | 10 ml 1M Tris-HCl, pH 8.0<br>6.25 ml 4M LiCl<br>0.2 ml 0.5M EDTA<br>5 ml 10% NP-40<br>5 ml 10% Na-Deoxycholate | 10ml 1M Tris-HCl, pH 8.0<br>2ml 0.5M EDTA |
| ad 100ml | ad 100ml | ad 100ml | ad 100ml |

| ChIP elution buffer | 6x laemmli buffer | Buffer A | 1M LiAc |
|---|---|---|---|
| 2,5ml 1M Tris-HCl pH7,5<br>1ml 0,5M EDTA,<br>5ml 10% SDS<br>ad 100ml | 630 µl 1 M Tris-HCl pH 6.5<br>2 ml 100% glycerol<br>2 ml 10% SDS<br>500 µl ß-mercapthoethanol<br>+ bromphenol blue | 2% Triton X-100<br>1% SDS<br>100 mM NaCl<br>10 mM Tris-HCl pH 8.0<br>1 mM EDTA pH 8.0 | 102.02g lithium acetate |
| | Ad 10 ml with $H_2O$ | | ad 1L with H2O and adjust pH to 7.5 |

| PLATE | LiTE | RIPA | E-TCA |
|---|---|---|---|
| 80 ml 50% PEG (3000-5000)<br>10 ml 1M LiAc<br>10 ml 10x TE pH 7.5 | 10ml 1 M LiAc<br>10 ml 10x TE pH 7.5 | 500µl Tris-HCl pH 7.4<br>300µl 5M NaCl<br>100µl 0.5M EDTA<br>100µl NP-40<br>100µl 10% SDS | 10 ml 100% TCA<br>10 ml 0.15% deoxycholate<br>80 ml aceton 100% |
| Ad 100ml | Ad 100ml | Ad 10 ml | |

| RNase mix | ChIP diluent | glycine buffer | 2 x FA buffer |
|---|---|---|---|
| 100 µl RNase A (10 mg/ml) | 14.3 ml 5M NaCl | 225 g glycine | 4.77 g HEPES-KOH |

| | | | |
|---|---|---|---|
| 100 µl RNase T1 (1000 u/µl)<br>2 µl RNase III (250 u/ml)<br>1 µl RNase H (5000 u/ml)<br>50 µl RNase I (100 u/ml)<br>247 µl dd$H_2O$ | 1.43 ml 0.5M EDTA<br>8.51 g HEPES | 2.4 g Tris | 12 ml 5M NaCl<br>0.8 ml 0.5 M EDTA<br>4 ml 100% Triton-X<br>4 ml 10% sodium deoxycholate |
| | ad 500ml | ad 1 L | ad 200ml |

| 4 M LiCl | DNA loading dye | 0.5 M EDTA | Semidry blotting buffer |
|---|---|---|---|
| 16.985 g LiCl | 3 ml Glycerol<br>+ bromphenole blue<br>+ xylencyanol | 96.02 g EDTA | 11.7 g tris<br>5.84g glycine<br>0.74 g SDS<br>200 ml methanol |
| | Ad 10 ml | ad 500 ml and adjust pH to 8.0 | Ad 2 L |

| ME agar plate | 5 x SDS-PAGE running buffer |
|---|---|
| 30 g malt extract<br>20 g agar<br>225 mg Uracil<br>225 mg Histidine<br>225 mg Leucine<br>225 mg Lysine | 60.4 g tris<br>288 g glycine<br>14.88 g EDTA<br>20 g SDS |
| Ad to 1L and adjust pH to 5.5 | Ad to 4L |

# 3 Methods

Water, which is used in this study, is autoclaved milli-Q water when not stated otherwise. Also, incubation of agar plates is performed standardized at 30°C, top-down with parafilm closed lids.

The used methods are split into "basic methods", where a shorter summary of published standard methods is presented and "methods of the study", where more details of the methodical procedure are provided.

## Basic methods

## 3.1 Polymerase chain reaction (PCR)

### 3.1.1 Quantitative PCR

Quantitative PCR (qPCR) is performed with PowerUP master mix in 96well plates. The working mix is prepared in a 1.5ml reaction tube with PowerUp master mix, autoclaved Milli-Q water and respective forward/reverse primer pair in the following ratios:

| | **for each reaction** |
|---|---|
| PowerUp SYBR green master mix | 7.5 µl |
| Oligo forward | 0.1875 µl |
| Oligo reverse | 0.1875 µl |
| $H_2O$ | 2.125 µl |
| **Total** | **10µl** |

The working mix is then submitted into a 96-well plate with arresting pipette and 5µl of DNA template is added to a final volume of 15µl. The plate is then sealed with foil and centrifuged for 1min at 500rpm. The program of the qPCR cycler (QuantStudio3) is prepared in the corresponding software with the following conditions:

| **volume:** | **15µl** | **cover:** | **105°C** | |
|---|---|---|---|---|
| | | temperature | time | ramping speed |
| hold stage | step 1 | 50 °C | 2 min. | 1.6 °C/sec. |
| | step 2 | 95 °C | 10 min. | 1.6 °C/sec. |
| PCR stage | step 1 | 95 °C | 5 sec. | 1.6 °C/sec. |
| | step 2 | 60 °C | 30 sec. | 1.6 °C/sec. |

40x

| | | | | |
|---|---|---|---|---|
| melt curve stage | step 1 | 95 °C | 15 sec. | 1.6 °C/sec. |
| | step 2 | 60 °C | 1 min. | 1.6 °C/sec. |
| | step 3 | 95 °C | 15 sec. | 0.1 °C/sec. |

Software-determined Ct value is interpreted with ddCt methode as published [Livak and Schmittgen 2001] in excel.

## 3.2 Fluorescence and DIC microscopy

All microscopy images are recorded with DeltaVision Ultra™ with 60x objective, cover slipe (high quality) and immersion oil RE 1.6.

### 3.2.1 Live cell imaging

For live cell imaging, cells are inoculated in liquid YES and incubated at 30°C, 160rpm o.n. to an OD of 0.5OD/ml. 1 ml of the cell suspension is centrifuged in a 1.5 ml reaction tube at 3000rpm for 2 minutes and washed once with 1 ml H2O. The cells are resuspended in an adjusted volume on EMM-N and 10 µl of the cell suspension is applied to a slide. The slide is positioned over the mounted sample without air bubbles, the corners are covered with nail varnish and dried for 10 minutes at RT. The slide must be microscoped immediately.

## 3.3 SDS-PAGE

### 3.3.1 Discontinuous gel casting

Mini gels are prepared with a Mini-PROTEAN® set and casting stand, large gels are prepared with the PROTEAN® II xi set and casting stand according to the instruction supplied by Bio-Rad. For standard resolution, 10% resolving gel and 4% stacking gel mixture are prepared as followed:

| | Resolving gel (10%) | | Stacking gel (4%) | |
|---|---|---|---|---|
| | mini gel (~ 10ml) | large gel | mini gel (~ 5ml) | large gel |
| $H_2O$ | 4.1 ml | 11.85 ml | 3.05 ml | 6.615 ml |
| 1.5 M Tris-HCl pH 8.8 | 2.5 ml | 7.5 ml | - | |
| 0.5 M Tris-HCl pH 6.5 | - | | 1.25 ml | 3.125 ml |

| | | | | |
|---|---|---|---|---|
| 30% Acrylamide / Bis-Acrylamide | 3.3 ml | 10 ml | 0.65 ml | 2.5 ml |
| 10% SDS (w/v) | 0.1 ml | 0.33 ml | 0.05 ml | 0.125 ml |
| TEMED | 10 µl | 45 µl | 5 µl | 17.5 µl |
| 10% APS | 50 µl | 150 µl | 25 µl | 62.5 µl |

Gel cassettes with 1mm spacer are prepared in the respective stand as described in the instruction manual and filled with water to test for their seal. Water is poured out and the inner area is dried with whatman paper. APS is added to the resolution gel mixture and blended properly by swirling. The mixture is poured into the cavity between glass plates, covered with distilled water and the gel is left for polymerizates for 10 min. at ambient temperature.

When the resolution gel is cured, the supernatant water is poured off and the cavity is dried with whatman paper. APS is added to the stacking gel mixture and blends properly by swirling. The mixture is poured on top of the resolution gel, comb with the required number of wells inserted into the glass chamber and polymerizates for 10 min. at RT. The gel can be stored with a comb at 4 °C, wrapped in wet tissue or the comb is removed, and the gel is used immediately.

### 3.3.2 Gel electrophoresis

Gel cassettes are installed into the electrode assembly as described in the manual. The gasket and tank are filled with 1x SDS running buffer, till the gel is fully covered. Raw cell lysates are diluted in a 1.5ml reaction tube to a concentration of 40 ng/µl and mixed 1:1 with 6x laemmli buffer to a final concentration of 20 ng/µl. The laemmli-lysate mix is heated at 85 °C for 10min in thermos block. 5µl of protein ladder and 10-15µl of samples are loaded with a 20µl pipette or syringe into wells of polyacrylamide gel. The tank is then closed and connected to the power supply. Mini gels are treated with 200V const. for around 50min, and large gels are treated with 200V for around 2.5h at 4 °C. The gel is then released from the glass cassette by spatula and used gel in staining or western blot procedure.

## 3.4 Semi dry western blot

original western blot protocol is described in a paper from 1981 [Burnette 1981] and is modified in different points.

Nitrocellulose membrane and thick whatman filter are cut into 6.5cm x 8cm pieces for mini gels and 8.5cm x 17cm for large gels. The membrane and the filter are soaked in a gasket filled with cold semi-dry running buffer. The Polyacrylamide gel after successful SDS-PAGE is released from the glass cassette and also equilibrated in semi-dry running buffer for 5min. The blot "sandwich" is built in the semi-dry blotter (mini gel = Trans-Blot Turbo, large gel = semidry blotter) from bottom to top: one thick whatman filter, nitrocellulose membrane, polyacrylamide gel and one thick whatman filter. Possible air bubbles are rolled out by WB roller, the lid is closed and a total current amount of 0,5 A is applied (Trans-Blot Turbo: 30min, 1000 mA const., Semidry blot: 1h15min, 400mA const.). After the transfer is completed, the membrane is removed, and the quality of the transfer is probed with a ponceau stain.

## 3.5 Extraction of nucleic acids

### 3.5.1 Extraction of genomic DNA

The protocol is adapted from the method of Hoffman and Winston from 1987. Grow 5 ml yeast cultures to saturation and collect cells by centrifugation and transferred to a 1.5 ml reaction tube. Wash cells in 1ml $H_2O$ pour off supernatant and briefly vortex to resuspend cells in residual liquid. Add 0.2 ml of Buffer A, 0.2 ml glass beads, and 0.2 ml phenol:chloroform:isoamyl alcohol (25:24:1; ~ pH7). The mixture is vortexed for 3 minutes and quick spinned. 0.2ml $H_2O$ is added and the tube vortexed briefly to mix. The tube is centrifuged for 5 minutes at 10,000 g. The aqueous phase is transferred to a new tube and 1 ml of 100% EtOH at RT. The tube must be inverted to mix and afterwards centrifuged for 2 minutes at full speed. The white pellet is washed once with 70% EtOH and resuspended in 0.4ml $H_2O$. For PCR, 1µl of a 1:10 dilution is used.

### 3.5.2 Extraction of total RNA

all water used in RNA extraction procedure is DMPC water.

5ml of cells were grown to an OD of 0.5 in YES at 30 °C. Cells are pelleted in a 1.5ml safelock reaction tube at 5000rpm. Pellet is washed once in 1ml AE-buffer and vortexed in 500µl of acidic phenol/chloroform with additional 25µl 10% SDS. The reaction tube is placed in ThermoMixer and shaked for 5min. at 65°C and placed on ice afterwards. The reaction tube is shortly centrifuged and 500µl AE buffer is additionally added and the tube is vortexed at max speed for 30". The tube is then centrifuged for 5min in a cooling centrifuged at maximum speed. After centrifugation is over the upper phase, which contains the extracted RNA, is

transferred to a new reaction tube. 500µl of acidic phenol/chloroform is added and the process is repeated as second phenol chloroform cleanup. The upper phase of the second extraction is mixed with 500µl of chloroform, vortexed at max speed for 30" and centrifuged for 5min in a cooling centrifuged at maximum speed. The final 500µl top phase is transferred into a fresh 1.5ml reaction tube and mixed with 1ml of ice cold 100% ethanol and 1µl glycogen blue. The tube is inverted for 20 times and stored for 30min at -20°C for precipitation of RNA. The RNA is pelleted in cooling centrifuge at maximum speed for 20min at 4°C. The pellet is then washed once with 70% ethanol and centrifuged for 5min. The ethanol is decanted, and the pellet is dried till the ethanol is completely evaporated. The RNA is resuspended in a respective amount of $H_2O$ and the RNA concentration is determined by nanodrop.

# Methods of the study

## 3.6 Strain creation

### 3.6.1 Creation of transformation products

Insertion of DNA into the genome (stable transformation) of *S. pombe* is achieved by creating DNA constructs which include a fitting region at the genomic region of interest and the cassette with artificial DNA to be inserted, as first demonstrated in 1981 by D. Beach [Beach and Nurse 1981]. To achieve this goal, a so-called, two-step PCR is performed for the 3 main goals: gene deletion, c-terminal protein tagging and c-terminal gene truncations. While in 1$^{st}$ step flanking regions with complementary parts to the genomic region and the corresponding cassette are produced, in the 2$^{nd}$ step PCR creates DNA fragments which contain a flanking part for the genomic region and the desired cassette. It can be used directly for the transformation of *S.pombe* cells. All primers can be found under "2.6 Custom DNA oligos"

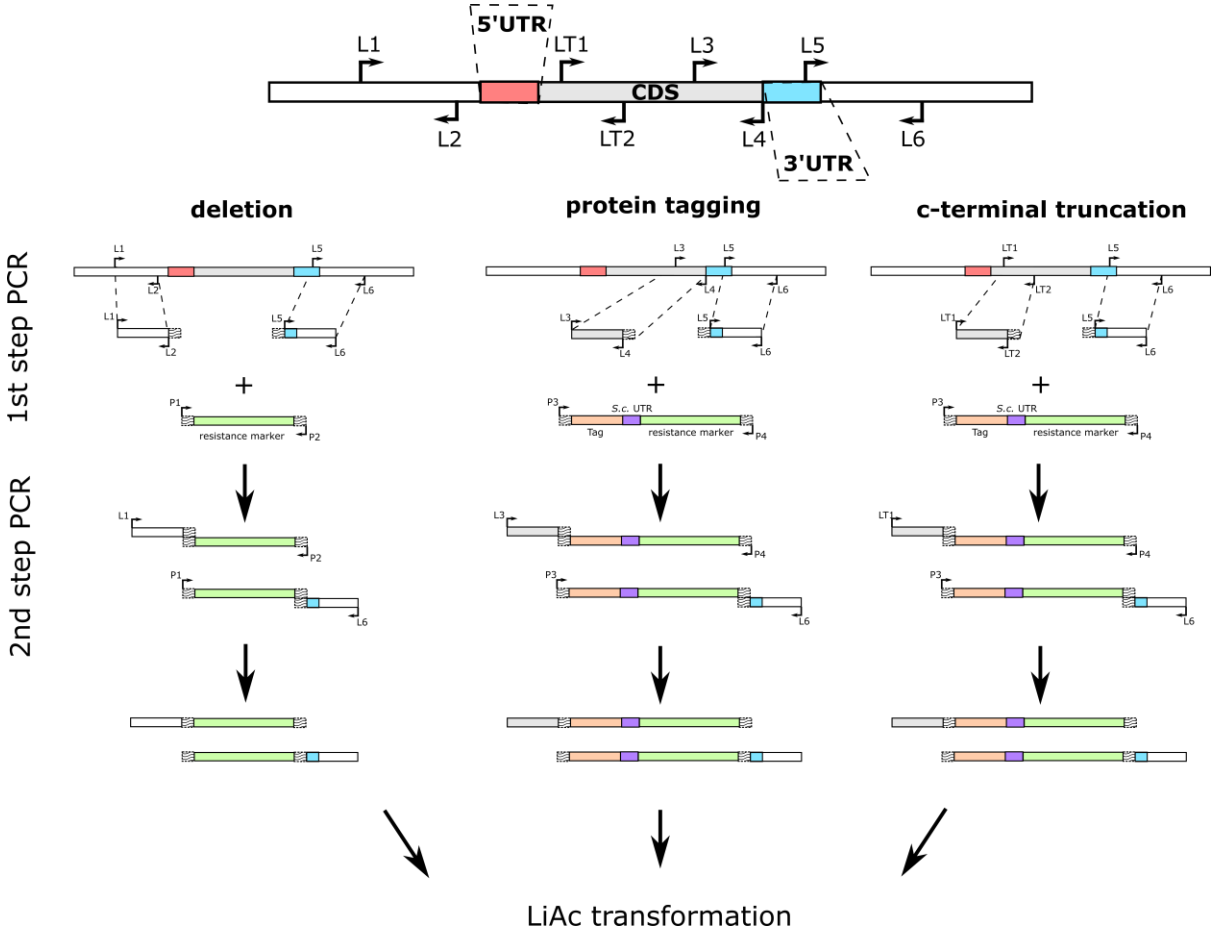


*Figure 6 schematic procedure of "two-step" PCR to create transformation products*

### 3.6.1.1 Transformation products for deletions

PCR reaction for the left flanking (LF) region of GOI with respective L1 and L2 primer, the right flanking (RF) region with respective L5 and L6 and the deletion cassette with P1 and P2 were set up as follows:

| | **LF** | | **RF** | | **DC** |
|---|---|---|---|---|---|
| $H_2O$ | 13,5 µl | $H_2O$ | 13,5 µl | $H_2O$ | 13,5 µl |
| 5x Q5 reaction buffer | 5 µl | 5x Q5 reaction buffer | 5 µl | 5x Q5 reaction buffer | 5 µl |
| dNTP (2mM) | 2,5 µl | dNTP (2mM) | 2,5 µl | dNTP (2mM) | 2,5 µl |
| L1 (10nmol) | 1,25 µl | L5 (10nmol) | 1,25 µl | P1 (10nmol) | 1,25 µl |

| | | | | | |
|---|---|---|---|---|---|
| L2 (10nmol) | 1,25 µl | L6 (10nmol) | 1,25 µl | P2 (10nmol) | 1,25 µl |
| Template (gDNA) | 1 µl | Template (gDNA) | 1 µl | Template (Plasmid) | 1 µl |
| Q5 Polymerase | 0,5 µl | Q5 Polymerase | 0,5 µl | Q5 Polymerase | 0,5 µl |
| | 25 µl | | 25 µl | | 25 µl |

The template for this 1st-step PCR is YPLV144(WT) gDNA and plasmid DNA with respective AB resistance cassette which is used for deletion. The PCR was performed in a thermocycler with the following conditions:

| | temperature | time | |
|---|---|---|---|
| pre denaturation | 95 °C | 120 sec. | |
| denaturation | 95 °C | 10 sec. | 36x |
| annealing | 60 °C | 10 sec. | |
| elongation | 72 °C | 30 sec./kb | |
| final elongation | 72 °C | 300 sec. | |
| hold | 10 °C | ∞ | |

Afterwards, PCR products are loaded on 1% mini agarose gel with 0.004% HDgreen besides 1kB DNA ladder and 100V is applied for 30min. Hereafter, PCR products are checked for correct size by comparing with DNA ladder height, gel is cut on the UV table and cleaned up with "MN PCR and agarose cleanup kit". DNA concentration is measured by nanodrop and is diluted to 25ng/µl with water.

For 2nd step PCR, the following reaction mix is used:

| | **2nd step A** | | **2nd step B** |
|---|---|---|---|
| $H_2O$ | 12,5 µl | $H_2O$ | 12,5 µl |
| 5x Q5 reaction buffer | 5 µl | 5x Q5 reaction buffer | 5 µl |
| dNTP (2mM) | 2,5 µl | dNTP (2mM) | 2,5 µl |
| L1 (10nmol) | 1,25 µl | P1 (10nmol) | 1,25 µl |
| P2 (10nmol) | 1,25 µl | L6 (10nmol) | 1,25 µl |
| LF PCR product (25ng/µl) | 1 µl | RF PCR product (25ng/µl) | 1 µl |
| DC PCR product (25ng/µl) | 1 µl | DC PCR product (25ng/µl) | 1 µl |
| Q5 Polymerase | 0,5 µl | Q5 Polymerase | 0,5 µl |
| | 25 µl | | 25 µl |

The conditions for the thermocycler are similar to the conditions of the 1st step PCR. After finishing off 2nd step of PCR, 4µl are mixed with 6x agarose LD load on 1% mini agarose gel with 0.004% HD green besides 1kB DNA ladder and 100V is applied for 30min. Hereafter, 2nd step PCR product A/B are checked for the correct size and the product leftover is used in the transformation process.

### 3.6.1.2 Transformation products for protein tagging

PCR reaction for the left flanking (LF) region of GOI with respective L3 and L4 primer, the right flanking (RF) region with respective L5 and L6 primer and the tagging cassette (TC) with P3 and P4 were set up as follows:

| **LF** | | **RF** | | **TC** | |
|---|---|---|---|---|---|
| $H_2O$ | 13,5 µl | $H_2O$ | 13,5 µl | $H_2O$ | 13,5 µl |
| 5x Q5 reaction buffer | 5 µl | 5x Q5 reaction buffer | 5 µl | 5x Q5 reaction buffer | 5 µl |
| dNTP (2mM) | 2,5 µl | dNTP (2mM) | 2,5 µl | dNTP (2mM) | 2,5 µl |
| L1 (10nmol) | 1,25 µl | L5 (10nmol) | 1,25 µl | P1 (10nmol) | 1,25 µl |
| L2 (10nmol) | 1,25 µl | L6 (10nmol) | 1,25 µl | P2 (10nmol) | 1,25 µl |
| Template (gDNA) | 1 µl | Template (gDNA) | 1 µl | Template (Plasmid) | 1 µl |
| Q5 Polymerase | 0,5 µl | Q5 Polymerase | 0,5 µl | Q5 Polymerase | 0,5 µl |
| | 25 µl | | 25 µl | | 25 µl |

The template for this 1st-step PCR is YPLV144(WT) gDNA and plasmid DNA with a respective cassette which is used for tagging. The PCR was performed in a thermocycler with the following conditions:

| | temperature | time | |
|---|---|---|---|
| predenaturation | 95 °C | 120 sec. | |
| denaturation | 95 °C | 10 sec. | 36x |
| annealing | 60 °C | 10 sec. | |
| elongation | 72 °C | 30 sec./kb | |
| final elongation | 72 °C | 300 sec. | |

| | | |
|---|---|---|
| hold | 10 °C | ∞ |

Afterwards, PCR products are loaded on 1% mini agarose gel with 0.004% HDgreen besides 1kB DNA ladder and 100V is applied for 30min. Hereafter, PCR products are checked for correct size by comparing them with DNA ladder height. The gel parts are cut on the UV table and cleaned up with an "MN PCR and agarose cleanup kit". DNA concentration is measured by nanodrop and is diluted to 25ng/µl with water.

For 2nd step PCR, the following reaction mix is used:

| | **2nd step A** | | **2nd step B** |
|---|---|---|---|
| $H_2O$ | 12,5 µl | $H_2O$ | 12,5 µl |
| 5x Q5 reaction buffer | 5 µl | 5x Q5 reaction buffer | 5 µl |
| dNTP (2mM) | 2,5 µl | dNTP (2mM) | 2,5 µl |
| L3 (10nmol) | 1,25 µl | P3 (10nmol) | 1,25 µl |
| P4 (10nmol) | 1,25 µl | L6 (10nmol) | 1,25 µl |
| LF PCR product (25ng/µl) | 1 µl | RF PCR product (25ng/µl) | 1 µl |
| TC PCR product (25ng/µl) | 1 µl | TC PCR product (25ng/µl) | 1 µl |
| Q5 Polymerase | 0,5 µl | Q5 Polymerase | 0,5 µl |
| | 25 µl | | 25 µl |

The conditions for the thermocycler are similar to the conditions of the 1st step PCR. After finishing off the 2nd step PCR, 4µl are mixed with 6x agarose LD load on 1% mini agarose gel with 0.004% HDgreen besides 1kB DNA ladder and 100V is applied for 30min. Hereafter, 2nd step PCR product A/B are checked for the correct size and the product leftover is used in the transformation process.

### 3.6.1.3 Transformation products for c-terminal truncations

PCR reaction for the left flanking region of GOI with respective LT1 and LT2 primer, the right flanking region with respective L5 and L6 primer and the tagging cassette with P3 and P4 were set up as follows:

| | **LF** | | **RF** | | **TC** |
|---|---|---|---|---|---|
| $H_2O$ | 13,5 µl | $H_2O$ | 13,5 µl | $H_2O$ | 13,5 µl |

| | | | | | |
|---|---|---|---|---|---|
| 5x Q5 reaction buffer | 5 µl | 5x Q5 reaction buffer | 5 µl | 5x Q5 reaction buffer | 5 µl |
| dNTP (2mM) | 2,5 µl | dNTP (2mM) | 2,5 µl | dNTP (2mM) | 2,5 µl |
| L1 (10nmol) | 1,25 µl | L5 (10nmol) | 1,25 µl | P1 (10nmol) | 1,25 µl |
| L2 (10nmol) | 1,25 µl | L6 (10nmol) | 1,25 µl | P2 (10nmol) | 1,25 µl |
| Template (gDNA) | 1 µl | Template (gDNA) | 1 µl | Template (Plasmid) | 1 µl |
| Q5 Polymerase | 0,5 µl | Q5 Polymerase | 0,5 µl | Q5 Polymerase | 0,5 µl |
| | 25 µl | | 25 µl | | 25 µl |

The template for this 1st-step PCR is YPLV144(WT) gDNA and plasmid DNA with respective tagging cassette which is used for truncation (BLV). The PCR was performed in a thermocycler with the following conditions:

| | temperature | time | |
|---|---|---|---|
| predenaturation | 95 °C | 120 sec. | |
| denaturation | 95 °C | 10 sec. | 36x |
| annealing | 60 °C | 10 sec. | |
| elongation | 72 °C | 30 sec./kb | |
| final elongation | 72 °C | 300 sec. | |
| hold | 10 °C | ∞ | |

Afterwards, PCR products are loaded on 1% mini agarose gel with 0.004% HDgreen besides 1kB DNA ladder and 100V is applied for 30min. Hereafter, PCR products are checked for correct size by comparing them with DNA ladder height. The gel parts are cut on the UV table and cleaned up with an "MN PCR and agarose cleanup kit". DNA concentration is measured by nanodrop and is diluted to 25ng/µl with water.

For 2nd step PCR, the following reaction mix is used:

| | **2nd step A** | | **2nd step B** |
|---|---|---|---|
| $H_2O$ | 12,5 µl | $H_2O$ | 12,5 µl |
| 5x Q5 reaction buffer | 5 µl | 5x Q5 reaction buffer | 5 µl |
| dNTP (2mM) | 2,5 µl | dNTP (2mM) | 2,5 µl |

| | | | |
|---|---|---|---|
| L3 (10nmol) | 1,25 µl | P3 (10nmol) | 1,25 µl |
| P4 (10nmol) | 1,25 µl | L6 (10nmol) | 1,25 µl |
| LF PCR product (25ng/µl) | 1 µl | RF PCR product (25ng/µl) | 1 µl |
| TC PCR product (25ng/µl) | 1 µl | TC PCR product (25ng/µl) | 1 µl |
| Q5 Polymerase | 0,5 µl | Q5 Polymerase | 0,5 µl |
| | 25 µl | | 25 µl |

The conditions for the thermocycler are similar to the conditions of the 1st step PCR. After finishing off the 2nd step PCR, 4µl are mixed with 6x agarose LD load on 1% mini agarose gel with 0.004% HDgreen besides 1kB DNA ladder and 100V is applied for 30min. Hereafter, 2nd step PCR product A/B are checked for the correct size and the product leftover is used in the transformation process.

### 3.6.2 Lithium acetate transformation

The slightly adapted protocol for the transformation procedure is published from Hyun Soo Kim, Keogh lab, AECOM and can be viewed accordingly [Hyun Soo Kim].

In short, start by growing cells in YES to reach an OD600 of 0.5, which is approximately 0.5 x $10^7$ cells/ml. Next, take 5 ml of cells and pellet them by spinning at 3000 rpm for 2 minutes. Wash the cells in 1ml of $H_2O$ and centrifuge them at 3000rpm for 1min in 1.5ml reaction tube. Repeat the washing with 1ml of LiTE. Afterwards, the cell pellet is resuspended in 100µl of LiTE. Carrier DNA is heated at 95°C for 10min, placed on ice and 20µg of carrier DNA is add to the mixture (4 µl of 5 µg/µl ssDNA) and 4µl of 2nd step PCR product A and B. Mix gently by snipping the reaction tube and incubate the mixture at room temperature for 10 minutes. Next, add 260µl of PLATE and mix gently by pipetting. Incubate for 30-60 minutes at 30°C. 43µl of DMSO is add after incubation and mix gently by snipping of the reaction tube. Perform a heat shock by incubating at 42°C for 5 minutes. Allow the samples to cool down for 1-2 minutes to return to room temperature. Pellet by brief centrifugation ("short spin" function of 5425 centrifuges for 5 sec) and discard the supernatant. The cells are then resuspended in 1 ml of YES or appropriate medium for >90 min up to 6h at 30°C. Pellet the cells again and resuspend in 200µl of ddH2O. Plate on appropriate selection plates and incubate at 30°C until colonies arise, which should take about 3 days. Occurring colonies are further analysed for correct insertion by colony PCR.

### 3.6.3 Colony PCR

After transformation, the successful integration of transformed DNA fragments is verified by performing a PCR directly on colony material. The colony is picked with a sterile 10µl pipette tip and dissolved in a PCR reaction tube filled with 10µl of sterile water. Additionally, cells with a wild-type genotype are prepared in the same fashion and serve as a negative control. The colony PCR MM is prepared as follows:

| | **For each reaction** |
|---|---|
| $H_2O$ | 15 µl |
| 5x Phire reaction buffer | 5 µl |
| dNTP (2mM) | 2,5 µl |
| L1 (10nmol) | 0,5 µl |
| L6 (10nmol) | 0,5 µl |
| colony suspension | 1 µl |
| Phire polymerase | 0,5 µl |
| | 25 µl |

While 1µl of suspension is used as a template, the primer pair L1 / L6 is picked for the modified gene of interest by the performed transformation. The colony PCR was performed in a thermocycler with the following conditions with reduced temperature ramping speed (ΔR = 0.2°C / sec) to achieve the best results:

| | temperature | time |
|---|---|---|
| predenaturation | 95 °C | 120 sec. |
| denaturation | 95 °C | 10 sec. |
| annealing | 60 °C | 15 sec. |
| elongation | 72 °C | 30 sec./kb |
| final elongation | 72 °C | 300 sec. |
| hold | 10 °C | ∞ |

Afterwards, samples were mixed with 6x agarose-LD and 15µl of the mix is loaded on 1% agarose gel, beside a 1kB DNA ladder. 100V is then applied for 30min. The product length is verified by the expected length of the modified fragment. The PCR product should appear at different height compared to WT negative control. From these positive clones, 5µl of original colony suspension is spotted on a YES plate and grown at 30°C. Cryostocking of these strains is described in 4.6.5.

### 3.6.4 Crossing/Mating

To combine two created phenotypes, the crossing of two strains with different sexus (h+/h-) is performed. If two different strains are patched on a ME agar plate, the process of genomic recombination is induced which leads to meiotic recombination between the independent sets of chromatins into 4 individual spores. Three potential outcomes are possible for each spore: 1. The genome contains modified gen A, and wild type gen B, 2. The genome contains modified gen B, and wild-type gen A, 3. The genome contains modified gen A and gen B.

#### 3.6.4.1 Iodine staining

Iodine staining of *S.pombe* tetrade is due by a staining of the α-1,4-glucan polymer by iodine [Yamashita et al. 2017] which is an integral component of the ascospores [Ohtsuka et al. 2022]. Therefore, Iodine staining is used to detect presence of ascospores in grown cells.
Cell which needs to be tested are grown on YES-agar plate and ME-agar plate with dot spot methode (chapter 3.8). If the undiluted spot is fully grown, small amount of iodine crystals are distributed in a disposable dish under a chemicals fume hood. The lid of the respective agar plate is removed, and the cells are exposed to the iodine fume by flipping the plate top down over the iodine crystals. The plate is incubated for 5min up to 10min max. For final documentation, the plate is photographed or scanned (the cells are inviable after iodine exposure, so no follow up experiments are possible). Strains which generating ascospore show a dark violet staining, while mitotic grown cells appear in ocher.

### 3.6.5 Preparation of cryostocks

Successfully transformed strain colony is stroked on YES agar plate with resistance agent (g418, NAT). The plate is afterwards incubated for 48h at 30°C. A single colony is then patched at a YES plate centre and therefore grown for 24h at 30°C. 200µl autoclaved water is added on top of the grown colonies and cells are spread by a sterile inoculation loop over the area. The plate is then closed, parafilm sealed and grown at 30 °C for additional 24h. Cells are scratched off from the plate and resuspended in cryovials filled with 800µl sterile glycerol (25% v/v).

## 3.7 Growth conditions of liquid cultures

The growth condition of *S.pombe* is described in [Petersen and Russell 2016]. *S. pombe* cells were grown on shaker at a temperature of 30°C at 150-180rpm in YES, EMM-G and EMM-N

in an Erlenmeyer flask with corresponding size. Flasks up to 1L are incubated in "Ika KS 4000" shaker on sticky mat, while larger flask are incubated in incubation shaker ("Multitron Pro", "Innova 44"). The replication time for WT growth in YES is measured with 2.5h, in EMM-G the replication time is empirical determined as 4h which is used as fundament for overnight calculation.

## 3.8 Dotspots growth assay

For the dot spot assays, cells must handle below bunsen burner flame to keep all solutions sterile to prevent contamination of dilutions.

### 3.8.1 Temperature stress dotspots

cells are grown to 0.5OD/ml and two milliliters are pelleted in 1.5ml reaction tube with 3000rpm for 2min. The pellet is washed in sterile water and resuspended in 1ml of sterile $H_2O$. Dilutions is performed in sterile 96-well microtiter plate with a 1:10 ratio in a total volume of 200µl. YES agarplate is labeled and warmed up to RT. 5µl of the respective cell dilution is carefully pressed out of the tip and is positioned on the plate as drop. The cell dilution spots need to stay separate to prevent overlap of cellspots. The spot which are positioned on plate are dried under flame, closed and sealed with parafilm. The plate is then incubated at the respective temperature till the first spot is fully outgrown.

### 3.8.2 pH stress dotspots

Dot spots are made in the similar fashion as the temperature stress dot spots (chapter 3.8.1). Instead of spotting the cell dilutions only on YES agar, a comparable YES agar plate with adjusted pH (pH 11 plate) is used.

## 3.9 Mating efficiency comparison

The mating efficiency is tested in a h90 background, which changes its replication behavior from asexual mitotic fission to sexual meiotic reproduction when exposed to ME media which lacks a nitrogen source [Egel 1971]. The h90 strains are grown in 5ml YES preculture at 30°C at 160rpm. When OD reached 0.5 OD/ml, 1ml of cells are pelleted and wash once in EMM-N. The cells are spotted on ME media. The occurrence of ascospore formation is checked at various time points by microscopy (3.2.1) and iodine staining (3.6.4.1)

## 3.10 Oligo d(T) comparative interactome captures

oligo d(T) comparative interactome captures in *S.pombe* was essentially performed as described beforehand [Birot et al. 2022] while the protocol is founded on research in *S.cerevisiae* [Beckmann et al. 2015] and mammalian cell [Castello et al. 2013] .

7

### 3.10.1 Cell growth, crosslinking and lysing

To test the optimal 4tU amount, cells were grown in 1 L EMMG with limited amounts of uracil (10 mg/L) and labelled with 4sU (0-100 mg/L) for 4h. Cells are then harvested by centrifugation (4500rpm, 4°C) and UV-crosslinked at 365 nm at 3J/cm2 in 50 mL PBS while cooled on an ice-cold aluminium block. The cells are washed once, resuspended in 800µl lysis buffer and dropped with a pipette into LN to snap-freeze and the created beads are then stored at -80°C.

Lysing of the cells was done by adding pellets and 1ml of lysis buffer with PIC (1:10000) and PMSF (2mM) into a mortar filled with LN. Cells were crushed in a mortar for 0-30min and lysate, was poured into a falcon. Additional lysing methods which are investigated were the FastPrep (2 cycles, 120sec, 6 m/sec, QuickPrep) and the Cryomill (8 cycles, 5 min precool, 3 min run, 2 min cool, 8 CPS). The grindade is poured back into falcon and freeze at -80°C till further use.

### 3.10.2 Oligo(dT) capture

The oligo d(T) capture was performed in all essential points according to the previously described protocol and can be viewed in detail [Birot et al. 2022] while proteinase K treatment is not performed.

1ml of oligo d(T) beads is used per 1L grindate and cell lysate is rotate for 2 h at 4°C. The beads are washed two times with washbuffer 1, washbuffer 2 and low salt buffer in this order. The elution is performed with 330µl elution buffer at 55°C for 10min. The RNase treatment is performed by addition of 4µl 1:500 dilution of RNaseMix. This mix consisting of RNase A (10 mg/ml) and RNase T1 (100 U/µl) stock and the sample is incubated for 1 h at 37°C, then 15 min at 55°C. Sample volume is reduced by amicon filter (3kD cutoff), by centrifugation at full speed for 30min and subsequent wash with 500µl 50mM NaCl. The residual volume of 25µl is recovered and stored.

### 3.10.3 Mass spectrometry

Mass spectrometry data were supplied by Dr C. Kilchert, raw data is published in 2020 [Kilchert et al. 2020]. MS experiment was carried out with two sets of triplicate experiments (WT1 + mtl1-1; WT2 + rrp6Δ + dis3-54). WT1 and 2 data sets were merged for analysis of the WT interactome, and comparative interactomes were analyzed relative to the corresponding WT. A "no crosslink" control was included in the first experiment (WT1 + mtl1-1).

## 3.11 RNA sequencing

For RNA sequencing, three individual EMM-G cultures per investigated strain (YPLV144: WT, YPCK306: *Δfft2*, YPCK349: *Δfft1)* are prepared (3x50ml), separately inoculated and incubated at standard conditions to an OD of 0,5 OD/ml. Also, *S. cerevisiae* (YF336) is inoculated in YES and grown at same conditions to an OD of 0.5 OD/ml (total volume = pombe precultures * 5ml) as a spike in.

When the optical density reaches 0.5 OD/ml, 50ml of *S. pombe* culture and 5ml of *S. cerevisiae* culture is harvested at 4°C, 3000rpm, 5min centrifugation. The 50ml pellet is resuspended in 500µl AE-buffer and mixed with the spike in pellet. The total RNA is extracted as described in chapter 3.5.2 with eye mark on the constant cooling of fractions.

After successful pelting of total RNA, pellet is resuspended in DMPC $H_2O$ and measured in nanodrop. Digestion of DNA is performed by RQ1 DNase treatment by the following mixture:

| | **For each reaction** |
|---|---|
| 4µg RNA | X µl |
| 10x RQ1 DNase buffer | 4 µl |
| RQ1 DNase | 2 µl |
| DMPC $H_2O$ | Ad 40µl |

The volume of RNA to reach 4µg needs to be calculated from nanodrop measurement. After the mix is pipetted in 1.5ml reaction tube and incubated at 37°C for 40min. After enzyme reaction is done, volume is filled up to 500µl by AE-buffer and RNA extraction is repeated as described before in chapter 3.5.2.

The pelleted RNA is recovered in 40µl DMPC $H_2O$, measured and checked for a 260nm/280nm ratio > 2. If first quality check is passed, an additional degradation check is performed by Agilent RNA 6000 Pico chip in bioanalyzer. The protocol is described by the manual which is

supplied by agilent. The RNA is then aliquoted and hand over to the lab of Dr. Stefan Günther (MPI, Bad Nauheim), which performed the library preparation and sequencing procedure.

## 3.12 Chromatin immunoprecipitation (ChIP)

The ChIP protocol is supplied by Dr Cornelia Kilchert and modified in the process of the underlying work. In general, the protocol is lasting for 4 days which mainly depending on the time of the bead incubation of the immunoprecipitation.

### 3.12.1 Crosslinked ChIP and analysis in qPCR

day1:

200 ml of YES is inoculated from overnight culture and grown to OD600 of 0.5. After 0.5 OD/ml is reached, 20 ml of 11% HCHO is added, and culture is incubated for 20min on shaker. 30ml of 3M glycine is added to quench the crosslinking reaction, followed by additional 5 min of incubation. The full volume is pelleted in one 50ml centrifugation tube (5 rounds at 4°C) and washed once with 25ml of TBS and afterwards with ice cold FA lysis buffer/0.1% SDS, freshly mixed with 1mM PMSF and stored at -80°C.

day2:

Resuspend the pellet in 1.6 ml ice cold FA lysis buffer/0.5% SDS, freshly mixed with 1:10.000 PIC. The suspension is split into two screw vials with ~300µl unsterile glass beads on ice. The vial is screwed tightly, and the cells are lysed in the FastPrep with (2 cycles, 120sec, 6 m/sec, QuickPrep) at 4°C. Isolation ring of UZ-tube is placed on top of a sterile 15ml centrifugation tube. A 0.7mm diameter cannula is then heated to red heat in a bunsen burner flame and bottom and lid of the screw vial is pierced. The vial is placed inside of the isolation ring, centrifuged at 800 rpm and washed four times with FA lysis buffer/0.1% SDS. This procedure is repeated also for the second screw vial. The whole lysate is then transferred into a quick seal UZ-tube and tared with a counterweight. For ultracentrifugation, the UZ is precooled and 70Ti rotor is positioned inside the chamber on the magnetic motor spindle. The break and the acceleration speed are set on maximum strength (10) and centrifugation of the sample is done for 30min at 22.000rpm (38,759g [Beckmann Coulter]) at 4°C.

After centrifugation is over, the remaining supernatant is decanted, the UZ tube is placed on ice. Now the chromatin which surrounds the debris pellet as clear viscous halo is resuspended. Therefore, a wooden stick is used to briefly release the clear chromatin halo from the tube wall and afterwards roughly mashed with the debris part and the residual liquid. 750µl of ice-cold FA lysis buffer/0.1% SDS is add and mixed with wooden stick till the lysate is completely homogenized. The homogenate is thereafter transferred by a piston pipette into a 15ml

polycarbonate tube, which is placed on ice. UZ tube and wooden stick are then washed with additional 750µl FA lysis buffer/0.1% SDS and added into the same polycarbonate tube. The tube adapter for the "bioruptor standard" (sonicator) with metal spacer is inserted into the tube so that it covers the full depth of the homogenate. The tube holder is placed in the bioruptor water bath, which is filled with ice water (80% water, 20%ice). Sonicate in the Diagenode Bioruptor (Nasmyth lab) on high power for 80 min, 15" on, 45" off permanent. Check every 20min for ice level and exchange if necessary. After sonication is finished, the sheared chromatin is split into two 2 ml reaction tubes. 750µl of FA lysis buffer/0.1% SDS is added and centrifuged at 25.000g for 20min at 4°C in cooling centrifuge 5425 R. Supernatant is pooled, measured in nanodrop for broad DNA concentration (best >800 ng/µl) and aliquoted in 400µl fractions in 1.5ml reaction tube. 50µl is stored separately as input control and 400µl are used for IP, while the other aliquots are stored at -80°C.

IgG agarose beads are used in precipitation of HTP tagged proteins and 30 µl of slurry for each sample and can be used directly from factory container. Protein G magnetic beads are used in H3/H3K9me2 precipitation to control methylation status of chromatin region. To couple beads with antibody, 20µl of slurry is washed on the magnetic rack three times with TE. The washed magnetic beads are resuspended in 200µl of TE and 5µl of antibody. The bead suspension is then incubated on a rotation wheel for 2 h at 4°C. Afterwards, beads are washed twice in TE and once in FA lysis buffer/0.1% SDS and resuspended in 30 µl FA lysis buffer/0.1% SDS per sample.

For immunoprecipitation, 400µl of chromatin aliquot is mixed with 380µl FA lysis buffer/0.1% SDS, 20µl 5M NaCl and 30µl of bead slurry. The reaction tube is closed and incubated on rotation wheel at 4°C o.n.

<u>day 3:</u>

The beads are pelleted with respective methods (magnetic beads: magnetic rack, agarose beads: 2000rpm, 2min, RT) and wash twice with 1 ml of each buffer in the following order: buffer I, buffer II, buffer III and buffer IV. To get rid of wash solution in agarose beads precipitation double stack pipette tip is used to minimize the bead loss. To elute the purified protein of the beads, last wash solution is tossed, and the remaining beads are heated for 20 min at 65 °C with 2000 rpm in 200 µl ChIP elution buffer. Beads are afterwards precipitated, and supernatant is transferred to a fresh 1.5ml reaction tube. The residual beads are washed with 200µl TE, shaked with 2000 rpm for 5min and supernatant is pooled in the same reaction tube. The 50µl input aliquot is prepared for decrosslinking by adding 150 µl of FA lysis buffer/0.1% SDS and 200 µl of TE to the 50 µl chromatin. To the input and the IP sample 30 µl of 20 mg/ml pronase solution, incubate for 1 h at 42°C and then decrosslink at 65 °C o.n.

day 4:

At the next day, 50 µl of 4M LiCl is added and vortexed. The DNA is isolated with the phenole/chloroform methode (3.5.1). The received IP DNA pellet is resuspended in 200µl $H_2O$ and the input pellet in 500µl $H_2O$ respectively and analyzed in qPCR (3.1.1)

### 3.12.2 Crosslinked ChIPseq preparation and bioinformatical analysis

sample preparation of crosslinked ChIPseq is performed like ChIP analysis (3.13.1) by Dr. Birte Keil. The samples are prepped in triplicates. The library preparation and sequencing procedure is done by the lab of Dr. Stefan Günther (MPI, Bad Nauheim).

For bioinformatical analysis, the webpage of galaxy is used (https://usegalaxy.org/). Supplied FASTQ files trimmed for adapter sequence by "Trim Galore!" [Krueger 2021] single-end, default conditions. Trimmed FASTQ are therefore aligned to build in reference genome of *S. pombe*, supplied by usegalaxy (version 1.1), by the tool "bowtie2" [Langmead and Salzberg 2012] with default conditions for single-end reads. The aligned read file (BAM) is then analyzed in multiple ways:

1. The coverage of BAM on the reference genome is calculated by "bamCoverage" [Ramírez et al. 2016] to verify ChIPseq signal visually in integrated genome as a bedgraph or bigwig file. The bin size was set to 10.
2. Metagene plots are generated by firstly by preparing a datamtarix of bigwig file with the tool "computeMatrix" [Ramírez et al. 2016]. Reference annotation supplied in GTF format. Scale of region, as well as up- and downstream region size is set to 1000kB. With "plotProfile" [Ramírez et al. 2016] the data matrix is transformed into metagene plot. Plot type is set as "line", the "mean" is used as statistic.
3. To quantify the ChIPseq data, the sum of counts over a single annotation is analysed by the tool "featurecount" [Liao et al. 2014]. The created BAM file and an annotation file in GTF format is used for this step. Strand specificity was set to "unstranded" in ChIPseq experiments, output format was unchanged, and a gene length file is created to calculate RPKM for each gene. The scatterplot, boxplots and violine plots are modulated in excel and the graphs and statistics are generated in OriginPro 2023.

## 3.13 Native glycerol gradient centrifugation

### 3.13.1 Estimation of size selectivity of gradient by protein standard

size selectivity of Superdex 6 column is investigated by test run of 4 different protein mixes with 1.5mg/ml of respective protein and 200µl of suspension is mixed with 5% glycerole:

| | |
|---|---|
| Mix1 | Apoferritin + BSA |
| Mix 2 | ß-amylase + carboanhydrate |
| Mix 3 | Alcohol dehydrogenease + cytochrome c |
| Mix 4 | Blue dextran + thyroglobuline |

The superose 6 column is equilibrated with 1 CV (25ml) of degassed 20% ethanol and 2 CV (50ml) of degassed water at 0.5ml/min flowrate before first use. Column is washed with 1 CV of sample buffer (5% glycerol). 500µl of each diluted protein mix is load by syringe and sample is eluted with a flowrate of 0.3ml/min for 80min (1 CV). Protein peaks are detected by UV-vis and peak maximum is take into calculation with respective protein weight.

### 3.13.2 Gradient centrifugation of native lysates

continuous gradients are made by gradient master 108 in polypropylene tubes fitting SW32Ti rotor. Half volume of tube is filled with degassed 10% glycerol and is underfilled by identical volume of 40% glycerol. Tubes are closed by long caps, placed in magnetic wielder and run with gradient master "10%-40% glycerol long cap" program.

The freshly harvest pellet from 150ml media (1 OD/ml) is lysed in lysis buffer by Djik [van Dijk et al. 2007]. Lysing is processed in FastPrep (2 cycles, 120sec, 6 m/sec, QuickPrep) at 4°C with addition of glasbeads. Lysate is centrifuged on max speed for preclearance and 500µl of supernatant is load on top of gradient. The gradient is then tared and centrifuged in ultracentrifuge with SW32Ti swingbucket rotor with 25,500 RPM for 18h at 4°C, importantly set break on 5!

The gradient is fractionated with äkta start. The tube is punctured by needle applicator on bottom and fractionation is processed with a flowrate of 2ml/min in clean prelabeled 1.5ml reaction tubes which results in 40 fractions of 1ml. The fractions are precipitated with 250µl of E-TCA, inverted and incubated 10min at -20°C. After centrifugation for 5min at maximum speed, supernatant is tossed, and pellet is washed two times with 200µl ice cold acetone. The pellet is dried resolved in 50µl SDS-loading buffer and cooked for 10min at 95°C. 20µl is load on large SDS-PAGE (chapter 3.3) and signal evaluated by western blot (chapter 3.4).

## 3.14 Crosslinked immunoprecipitation (CLIP)

Grow *S. pombe* strain in a 20ml YES culture overnight. Then, inoculate 2x1L EMMG low Ura (5L flask) with 30 OD of preculture cells suspended in 10ml YES. Incubate the flasks at 30°C with 150-200 rpm for 16-18 hours until the OD/ml reaches 0.5-0.7. Add 50mg/L of 4tU (in 10ml DMSO) to each flask and incubate for an additional 4 hours at 30°C.

Centrifuge the cells at 4500 rpm and 4°C for 5 minutes, resuspend the pellet in 25ml cold 1x TBS + 2mM PMSF, then fill the suspension in 50ml falcon and centrifuge for 5 minutes at 5000 rpm and 4°C. Resuspend the pellet in 50ml 1x TBS + 2mM PMSF and crosslink one cell pellet at 365 nm with 3J constant in petri dish on ice cold metal block.
Wash the cells with 25ml 1x FA 0.1% SDS + 2mM PMSF, then centrifuge and store the pellet on ice. Puncture the lid of a 50ml Falcon, place it on ice and fill it with liquid nitrogen. The cell pellet is resuspended in 800 µl 1x FA 0.5% SDS + 2mM PMSF + PIC (1:10000), dropped slowly into the liquid nitrogen. Centrifuge tube with beads is stored at -80°C.
Grind the cells with 1ml 1x FA 0.5% SDS + 2mM PMSF + PIC (1:10000) in a mortar filled with liquid nitrogen, then pour the mixture into the original Falcon and store at -80°C. Add 5ml RIPA + 2mM PMSF + PIC, rotate at 4°C for 10 minutes, then centrifuge and pool the supernatants. Aliquot 500 µl of the supernatants in 2ml 1.5ml reaction tubes and store at -80°C.

Before partial RNA digestion, take 13µl of lysate and add 2 volumes of RQ1-buffer (40mM Tris/HCl pH 8, 10mM MgSO4, 1mM CaCl2). Then add 3.0µl RQ1 (2 U/µl) and 1.5µl RNAsin. To degrade RNA, prepare "high" and "low" RNase I dilutions, add 15µl of the dilution to the lysate, and incubate for 3' at 37°C, shaking at 800 rpm. For Immunoprecipitation, add 30µl of IGG-agarose slurry and 20µl of 5M NaCl to the RNase-treated lysate, rotate for 2 hours at 4°C. Wash 4 times with TBS800-T and 2 times with PNK buffer.
Prepare the PNK-mix with radioactive ATP in radionucleotide lab (SCP801;12,33pmol/µl) and add 20µl of the mix to washed beads. Incubate at 37°C for 20 minutes while shaking at 800 rpm. Wash with cold TBS-T and PNK buffer. Add 20 µL of LDS loading buffer to beads, denature for 10 minutes at 70°C while shaking, and run on a 4-12% Bis-Tris Gel in the NuPAGE system for 3.5 hours at 200V. Transfer the gel to a nitrocellulose membrane and blot overnight at 15V at 4°C. Label membrane with a radioactive pen and expose the membrane to X-ray film in a metal cassette to detect the signal using the Typhoon.

# 4 Results

## 4.1 Fft2 accumulates on RNA in exosome deficiency mutants

### 4.1.1 Fft2 is accumulating on RNA in exosome deficiency mutants

Comparative RNA interactome capture (comp. RIC) was performed in different mutants of exosome components [Birot et al. 2022]. The performed experiment gives conclusion about altered association of proteins to polyadenylated RNA in these mutants. This experimental approach reveals, which proteins are more strongly associated with RNA molecules that accumulate within exosome mutants. These proteins could be part of the RNA-binding complexes that have already been described as RNA-guiding, like MTREC (chapter 1.4).

Proteins that show accumulation on RNA in comp. RIC analysis of the exosome deficiency mutants *Δrrp6*, *mtl1-1* and *dis3-54* (exemplary *Δrrp6* comp. RIC is shown in Figure 7a) were pre-screened to identify potential regulators of the exosomal pathway.

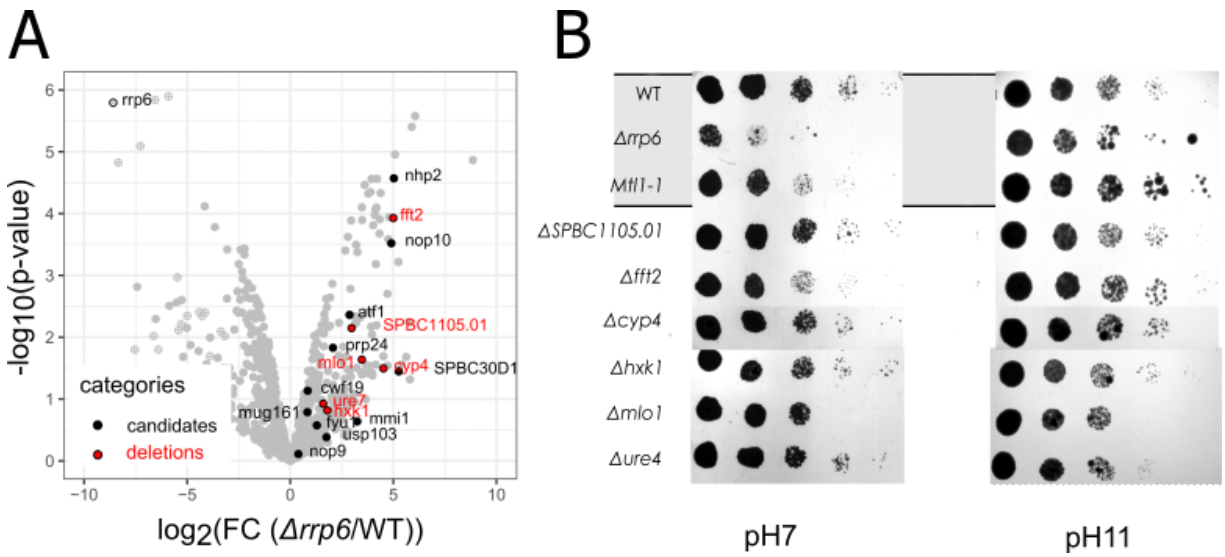


*Figure 7 deletion of selected candidates reveals enhanced growth in Δfft2 under pH stress*

A) volcano plot of exemplary comparative RNA interactome capture (comp. RIC) [Kilchert et al. 2020; Birot et al. 2022] between *Δrrp6* and WT control, in which proteins that accumulate more strongly on RNA in the wild type are located on the left, and proteins with stronger accumulation in the *Δrrp6* background are found on the right half. The x-axis indicates the accumulation of the proteins as foldchange, the y-axis the significance of this accumulation, indicated by the p-value. Proteins whose deletions were tested for a growth defect at high pH are highlighted in red, all other potential candidates are highlighted in black. B) growth of highlighted deletion mutants is compared between YES-agar media with native pH (pH 7) and with NaOH adjusted pH 11 at ambient temperature (25°C). The growth of exosome deficiency mutants (*Δrrp6* and *mtl1-1*) is enhanced at pH11 as it was expected from published data [Mukherjee et al. 2016; Higuchi et al. 2018]. By comparison with WT (WT) a strong growth reduction between pH7 and pH11 is detectable for all deletions, beside of *Δfft2,* which shows enhanced growth like EDM.

Possible targets of this pre-screen are proteins with a classical canonical RNA binding domain, proteins that are directly or indirectly involved in the binding of different RNA classes or proteins that show interactions with already known EAC proteins and also accumulation in all three tested exosome deficiency mutants. Potentially interesting proteins are shown in Table 1.

Table 1 list of pre-screened candidates, study deletions highlighted in red [Harris et al. 2022]

| ID | Name | RNA | Exosome interaction | Meiosis involvement |
|---|---|---|---|---|
| SPAC1782.10c | Nhp2 | snoRNA, rRNA | YES | no |
| SPCC1235.05c | Fft2 | no | no | no |
| SPAP27G11.13c | Nop10 | snoRNA, rRNA | yes | no |
| SPBC29B5.01 | Atf1 | RNA | No | yes |
| SPBC1105.01 | SPBC1105.01 | rRNA | no | no |
| SPBC1861.04c | Prp24 | snRNA | no | yes |
| SPCC31H12.03c | Mlo1 | mRNA | yes | yes |
| SPBP8B7.25 | Cyp4 | no | no | no |
| SPBC30D10.07c | bpl1 | no | no | no |
| SPAC30D11.09 | Cwf19 | mRNA | yes | yes |
| SPCPB16A4.05c | Ure7 | no | no | no |
| SPAC24H6.04 | Hxk1 | no | no | no |
| SPCC1322.04 | Fyu1 | no | no | no |
| SPCC736.12c | Mmi1 | meiotic RNA | yes | yes |
| SPAC1F3.09 | Mug161 | mRNA | no | yes |
| SPBP35G2.09 | Usp103 | mRNA | yes | no |
| SPAC6G9.02c | Nop9 | RNA | yes | no |

Research from 2016 reveal an accumulation of iron homeostasis transcripts (e.g. *fip1,fio1* and *str1*) in a *Δrrp6* background [Mukherjee et al. 2016]. The iron metabolism proteins plays a role in pH resistance growth [Higuchi et al. 2018] and it could be shown that cells with lack of these iron homeostasis transcripts shows an reduced growth at higher pH value than supplied at standard conditions.

The hypothesis is, that the growth of EDM is enhanced on high pH growth conditions, because accumulation of iron homeostasis transcripts should positively affect the growth on high pH when compared to a respective WT. To establish the link between the tested candidates and the exosome, a selection of candidates is deleted in individual strains (Figure 7 A and Table 1, red labelled) and tested for growth under pH stress condition on rich media (Figure 7 B).
As hypothesised, the exosome mutants *Δrrp6* and *mtl1-1* show increased growth when compared with standard pH conditions, due to the enhanced amount of iron homeostasis transcripts. A respective wild-type strain shows reduced growth when plated on high pH YES agar. In contrast to the pH conditions described in [Higuchi et al. 2018] (YES standard: pH 5.3, high pH conditions: pH 6.6), the standard YES agar pH in this study shows already a value of 6.9-7.2 and the observed high pH phenotype is only reached at pH 11 at RT.
Besides of the known exosome related mutations *Δrrp6* and *mtl1-1*, Fft2 is the only protein which shows an enhanced growth at high pH in contrast to standard pH conditions, in a comparable fashion like the exosome mutants. The growth of all other tested deletion strains is slightly impaired at high pH conditions and comparable to the growth of WT (Figure 7 B).
Fft2 accumulated on poly(A)+ RNA in all three exosome mutants tested; in contrast, this was not the case for Fft3, a paralogue of Fft2 (Figure 8). Fft1 could not be detected in the comp. inter. capture at all, which gives a hint for a diversified effect among the Fft-family members. The relative accumulation of Mmi1, an MTREC component and known regulator of the exosome complex, on poly(A)+ RNA is shown for reference. While EDM *mtl1-1* and *Δrrp6* show clear reduction for poly(A)+ RNA accumulation, *dis3-54* is enhancing its occurrence on RNA. This is due to the block of exonuclease activity which leads to a stalling of the short-lived RNA in the exosome channel, which consequently enhances the purification quantity a lot.

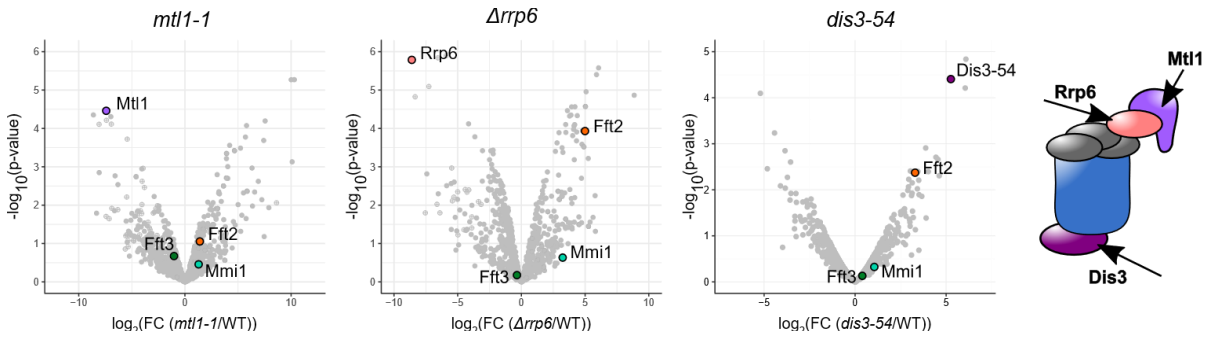


*Figure 8 oligo-d(T) RIC shows that RNA association of Fft2 is strongly increased in mutants of the exosome complex*

Comp. RIC is illustrated for exosome deficiency mutants *mtl1-1, Δrrp6* and *dis3-54 [Kilchert et al. 2020; Birot et al. 2022]* whose interaction is illustrated in the right cartoon. Highlighted SMARCAD1-family member Fft3 (green) and Fft2 (orange) show a strong accumulation of Fft2 while Fft3 is not affected by exosome deficiency mutants. As positive control for RNA accumulation serves

meiotic RNA binding protein Mmi1 (light blue). The respective exosome deficiency mutant is indicated by scheme fitting colour. Axis label similar to Figure 8.

Because the diversified RNA accumulating of Fft2 and Fft3 suggests a diversified function of the Fft-family member in *S. pombe,* a growth assay on YES standard media was carried out at different temperatures to further analyse the response to temperature stress (Figure 9). *Δfft3* has a severe growth defect, in cold- (16°C) as well as elevated temperature (37°C) conditions. On the other hand, it just has a minor growth defect at standard conditions (30°C). While growth of *Δfft2* and *Δfft1* is not affected at 37°C, the growth is surprisingly enhanced at cold temperatures, when compared to a wild-type strain. A functional understanding cannot be presented yet, but this observation strengthens the hypothesis of functional diversification in the Fft-family.

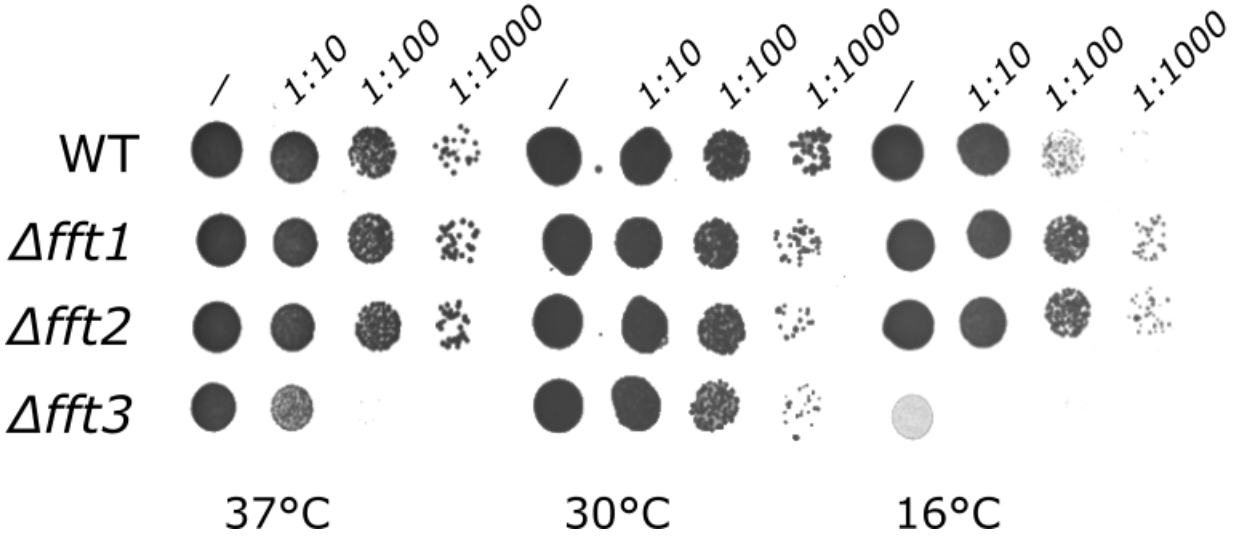


*Figure 9 response in growth of the Fft-family on temperature stress*

Growth defects of Fft paralogues is revealed on YES-agar plate at respective temperature. Dot spots are diluted with sterile water at a 1:10 ratio in a sterile 96well plate. Volume of 5µl is spotted and first spot of WT (WT) grown to saturation. While *Δfft3* shows a strong growth defect at elevated temperature (37°C) and cold temperatures (16°C), just a minor growth defect for standard temperature conditions (30°C) can be detected. *Δfft3* and *Δfft3* interestingly show enhanced growth at cold 16°C, while at other temperatures not affecting growth when compared to WT. Altered growth for all paralogues links

## 4.2 Structural analysis of Fft-family

However, after Fft2 was identified as a potential exosome interacting protein, the population phenotype was also shown to diverge significantly between the 3 family members. Therefore, SMARCAD1 orthologues from different species were analysed by their sequence conservations and structure prediction to unravel differences between the Fft2 orthologues.

Especially for Fft2 and Fft3 it could already demonstrate that their function is not completely equivalent [Ait-Saada et al. 2019]. Organisms with one SMARCAD1 orthologue (*H. sapiens:* SMARCAD1, *S. cerevisiae:* FUN30, *D. melanogaster:* Etl1) shows multifunctional activity like histone modifications, heterochromatin maintenance and DNA damage response as recently reviewed [Tong et al. 2020]. Other functions of Fft3 are the enhancement of RNAPII transcription by nucleosome disassembly [Lee et al. 2017], which is not a described characteristics for SMARCAD1 and FUN30. On the other hand, SMARCAD1 seems to *de novo* assemble heterochromatin [Rowbotham et al. 2011] while FUN30 and Fft3 could just be connected in the maintenance and inheritance of heterochromatin [Taneja et al. 2017] which demonstrate that function in the Fft-family diversifies from SMARCAD1.

### 4.2.1 SMARCAD1-family interspecies amino acid conservation

To compare the overall structure, alphafold2 predictions of six orthologues are aligned and compared for their structural conservation between species and Fft paralogues in *S. pombe* (Figure 10). It can clearly be observe that the prediction algorithm identifies a highly structured core with high confident score (blue and light blue), while the rest of the amino acid sequence shows no structure and therefore high alignment error (yellow and orange). The core contains the functional domains DEXDc and HELICc, which could be identified before [Tong et al. 2020], while no clear structural separation of both domains is observable. FUN30 is the only orthologue that holds a short α-helix motive of the highly structured domain which is exposed from the core by a short linker. No functionally described domains can be found at either the N-terminal or C-terminal end. Accordingly, these are present without specific structure as intrinsically disordered regions (IDR) with conserved intrinsically disordered domains (IDD) [van der Lee et al. 2014], which are associated with RNA/DNA binding [Chen et al. 2006]. While the N-terminus is significantly longer and "shields" the functional centre, only Fft2 and Etl1 have a significant C-terminus, which gives them a unique feature compared to the other orthologs. Also, the paralogues Fft1, Fft2 and Fft3 are distinguishable by their N-terminus length, which could play a unique role protein stability (Figure 23 western blot). Overall, the high flexibility of the N-terminal end could explain the diversified function.

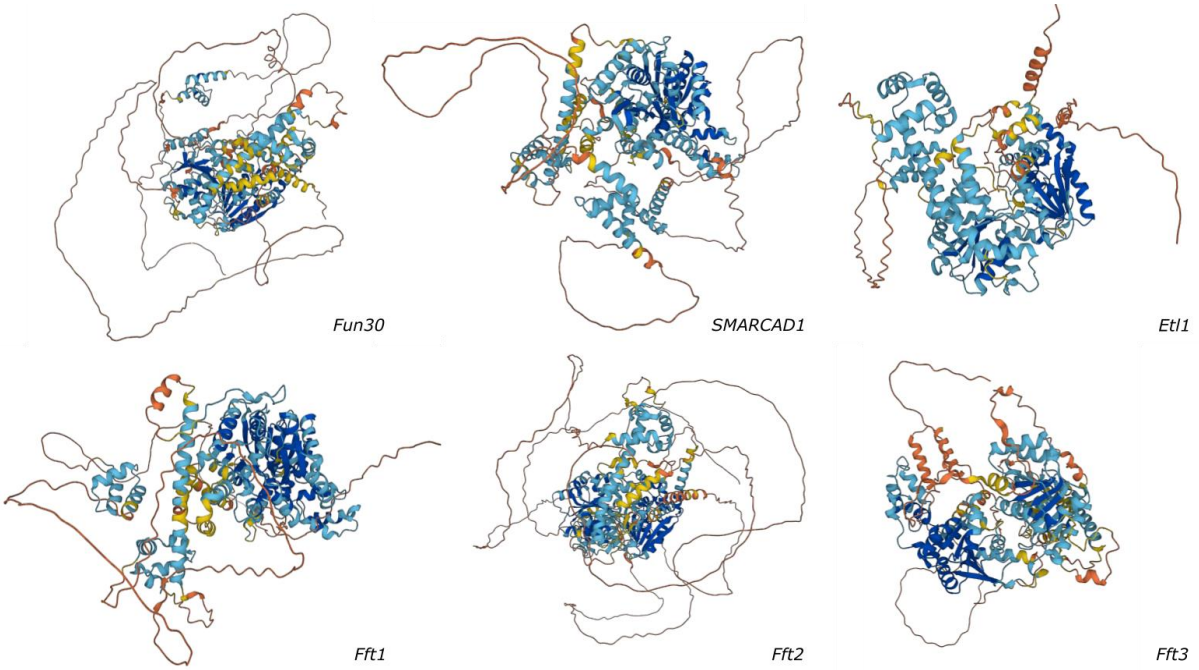


*Figure 10 tertiary structure of SMARCAD1-family show highly conserved core and variable IDR*

The tertiary structure of the SMARCAD1-family member is predicted by alphafold2 database [Varadi et al. 2022] on basis of the published amino acid sequence supplied by the database. While dark blue colour illustrates a low predicted alignment error (PAE) which conveys a high degree of certainty of the structure shown, orange colour indicates a high prediction error, which makes the predicted structure more unlikely. While the functional core show high similarities between the analysed orthologues, length and structure of N-terminal and C-terminal extension is highly variable. This is due to the varying length of these extensions and the lack of a predicted intrinsic structure (IDR) which differentiate the orthologues.

The amino acid conservation between members of the Fft-family in *S. pombe* (Fft1,2,3and their orthologues in *H. sapiens* (SMARCAD1), *D. melanogaster* (Etl1), *S. cerevisiae* (FUN30) and Fft-family in *S. japonicus* (Fft1,2,3) was analysed by CLUSTAL omega alignment.

The alignment of the nine orthologues demonstrates that the functional domains, namely DEXDc, HELICc and the intermediate linker show the highest conservation ( Figure 11 A). Moreover, the functional domain, which includes DEXDc a respective linker and the HELICc domain, has a very high conservation in between the analysed orthologues. The N-terminal and C-terminal parts show just minor conservation characteristics, which are potential IDR´s. The N- and C-terminal extensions outside the structured domains show much less sequence conservation, except for short sequences. This is probably due to the fact that the C-terminal protein structure is just present for Fft2 (*S. pombe, S. japonicus*) and Etl1.

Phylogenetic analysis of the orthologues reveals a sequence conservation which splits the phylogenetic tree in in three branches ( Figure 11 C). The first branch is represented by SMARCAD1 and ETL1, the second includes FUN30 and the third branch contains the *S. japonicus* and *S. pombe* Fft-family member. The

branches indicate that the Fft-family distinguish respective to the other orthologues in terms of amino acid conservation. Also, it is recognizable that FUN30 shows less conservation when compared to the Fft-family, which is probably due to the stretch at the N-terminal region of the structured domain.

For the two fission yeasts species that both have three different SMARCAD1 paralogues, sequence conservation is more prominent for Fft1 and Fft2 between organism (51,5% Fft1 *S. p./S. j.* and 59.7% Fft2 *S. p./S. j.*) and weakest for Fft3 (47,1%), with Fft3 of *S. j.* ( Figure 11 B). The orthologues FUN30, Etl1 and SMARCAD1 diverging most strongly from the Fft3 *S. j. (respective:* 34.9%, 28.4%, 33.1%), which suggest the least sequence conservation for Fft3, while FUN30 show weak sequence conservation to all probed orthologues which fits its unique predicted structure (Figure 10).

To compare the conservation of the structural motif interactions, the PAE-matrix supplied by alphafold is illustrated as heatmap, where dark green colour indicates low alignment error of the underlying amino acid, which is common in secondary structures, but also in functional domains (
Figure 11 A).

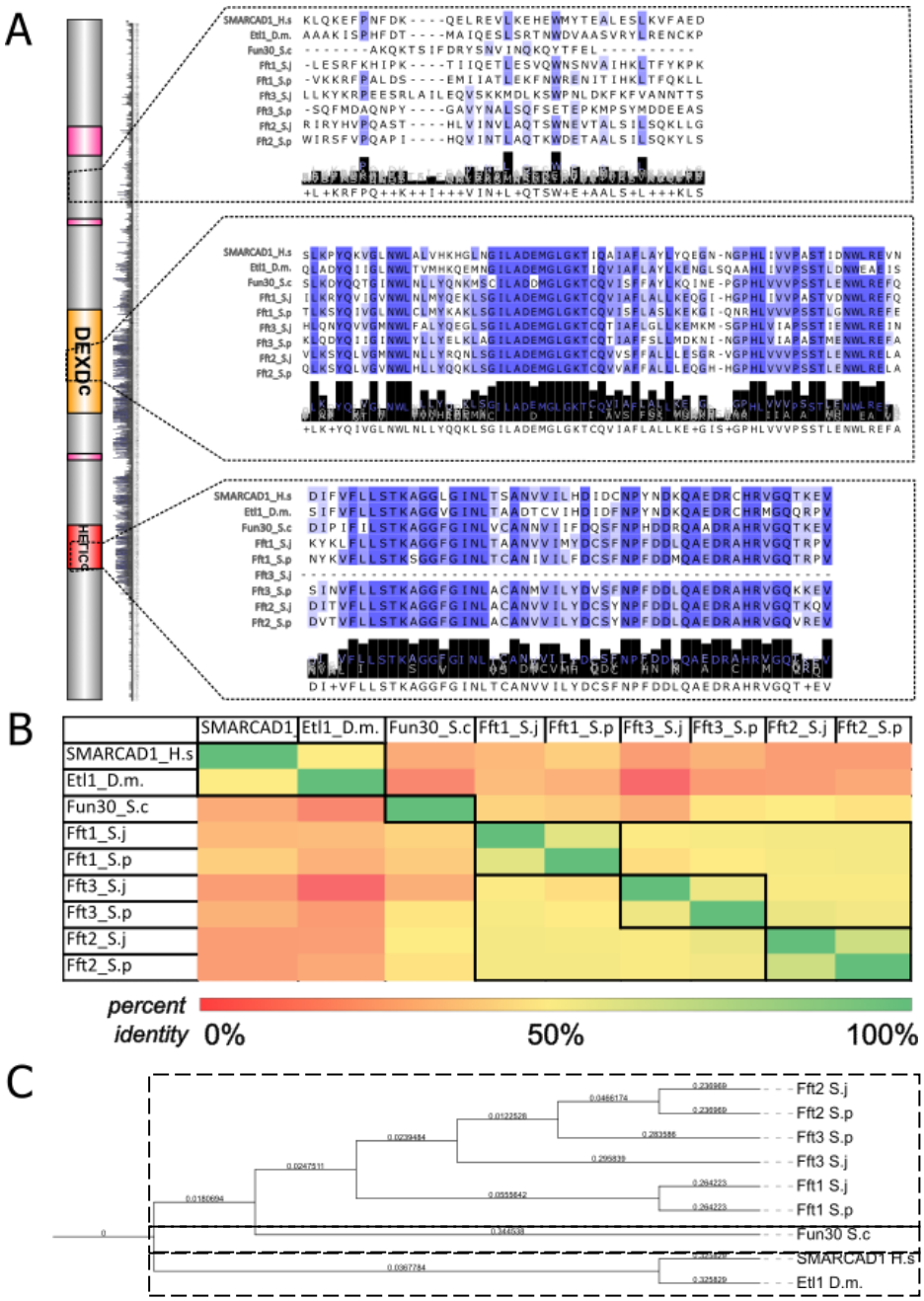


*Figure 11 protein sequences conservation between Fft-family member*

A) Amino acid sequence conservation between the 9 orthologs is analyzed by Clustal Omega alignment [Sievers et al. 2011]. A schematic representation of Fft2 *S. pombe* is next to the overall conservation value, while three exemplary regions are shown enlarged. Both functional domains show high amino acid conservation (blue) between all orthologs (HELICc and DEXDc), while the N-terminal extension shows high variability (white). The C-terminal extension is exclusive to Fft2 in *S. pombe* and S. japonicus and therefore does not show high conservation. B) The percent identity matrix (PIM) was calculated using Clustal Omega Alignment [Sievers et al. 2011] and is shown as a heatmap. As expected, the highest identity is shown for the Fft paralogues. As a second cluster, SMARCAD1 and Etl1 show high similarities, while FUN30 shows the lowest identity to all orthologs. C) The phylogenetic tree was calculated using the Clustal Omega alignment [Sievers et al. 2011] and reflects the categorization derived from the PIM.

The PAE-matrix from orthologues implicate a very high similarity between the functional domains of the compared orthologues DEXDc and HELICc, even when the amino acid conservation is below 50% (Figure 12 structural prediction by primary sequence reveals structured part with unknown function B), which suggest a strong functional conservation. DEXDc and HELICc domains can be separated into 2 independently folding parts (dark green squares), which are interacting with each other in all orthologues. In the analysis of FUN30 the DEXDc domain is separated by an unstructured linker, which fits the observation of the predicted structure (Figure 10) as well as the overall amino acid conservation ( Figure 11 B). Furthermore, the structure prediction reveals a major conservation area at the N-terminal end.

For most orthologues, a specific structure prediction of the not conserved N-terminal extension is mostly missing, but excluding Fft3, all orthologues hold a small motif consisting of 4 α-helixes with a total length of ~60 AA (Figure 12 B). For Fft3 this motif is not predicted. Fft3 from *S. japonicus* shows the most lose interaction between the DEXDc and HELICc domain, indicated by lighter green colour in the interaction region of these domains (Figure 12 A). The biggest change notable for Fft2 is the long C-terminal tail which is intrinsically disordered. Fft2 is the only member in the SMARCAD1-family which holds this characteristic, which could explain the RNA accumulation in EDM when compared with Fft3 (Figure 8).

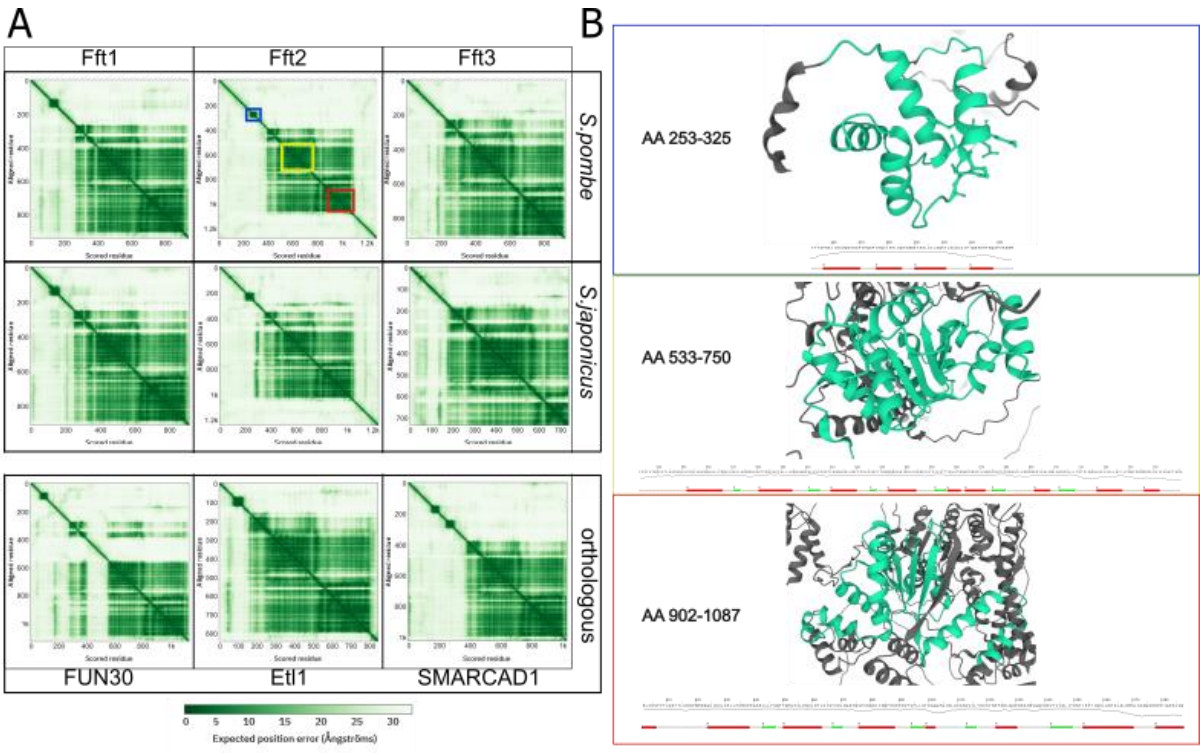

*Figure 12 structural prediction by primary sequence reveals structured part with unknown function*

A) The predicted alignment error (PAE) matrix provided by alphafold based on the alignment of the respective amino acid to each other in the primary sequence. Strongly structured regions tend to have alignment errors based on the secondary structure formed. *S. pombe* and *S. japonicus* Fft paralogues and orthologues from *S. cerevisiae* (FUN30), D. melanogaster (Etl1) and *H. sapiens* (SMARCAD1). All PAE matrices are generally very similar. The major changes are an unstructured section in FUN30, a weaker interaction between the DEXDc (yellow) and HELICc (red) domains in Fft3, a small, highly structured region in the N-terminal extension, and different lengths of the N/C-terminal extensions B) The zoomed structure is highlighted in light green for the corresponding region in the example of Fft2. The region outlined in blue consists of 4 α-helices that have no described functionality, while the yellow box represents the DEXDc domain and the red box the HELICc domain. Secondary structural elements found in these high interaction areas are α-helices (red bar) and β-sheets (green bar) and are shown below the respective 3D model.

The SMARCAD1-family is connected with overlapping functionality of the individual member [Tong et al. 2020], but also different functions for individual members are described [Lee et al. 2017; Taneja et al. 2017]. While the structure and the folding prediction of the DEXDc and HELICc domain is comparable (Figure 10, Figure 12), the amino acid composition of the terminal extensions widely differ, even between close related organisms like *S. pombe* and *S. japonicus* (Figure 11). Fft2 as largest member of the SMARCAD family contains a relative long C-terminal end where no structure is predicted. The unique N-terminal IDR, which includes a 4 x α-helix motive, makes the Fft2 structure unique, which could explain the functional differences towards Fft3.

## 4.3 Meiosis initiation is enhanced in Fft2 deletion strain

### 4.3.1 Microscopy evaluation in starvation time course

After the detailed evaluation of Fft2 in comp. RIC for exosome deficiency mutants (Figure 8), the question arose whether Fft2 has a direct influence on the meiosis process, which is a process that is heavily modulated by the nuclear RNA exosome [Kilchert et al. 2016]. To test this hypothesis, Fft2 is deleted in an h90 strain with a GFP-labelled lac operon system used to verify correct chromosome segregation (Figure 13). At the experiment starting point, only a few mitotic cells are visible, but after 24 hours the cell density is significantly higher, with no detectable cells in meiotic prophase or later (data not shown). After 48 hours, *Δfft2* strain already show cells in meiosis I/II (indicated by red arrow), while the corresponding wild-type strain shows only mitotic cells. After 72 hours, both the *Δfft2* strain and the corresponding WT strain show fully formed ascospores, with each spore containing a corresponding Lac1-GFP

signal. This suggest that at least chromosome segregation and spore formation are not impaired, while the initiation of meiosis seems to be accelerated in contrast to a Fft2-WT background.

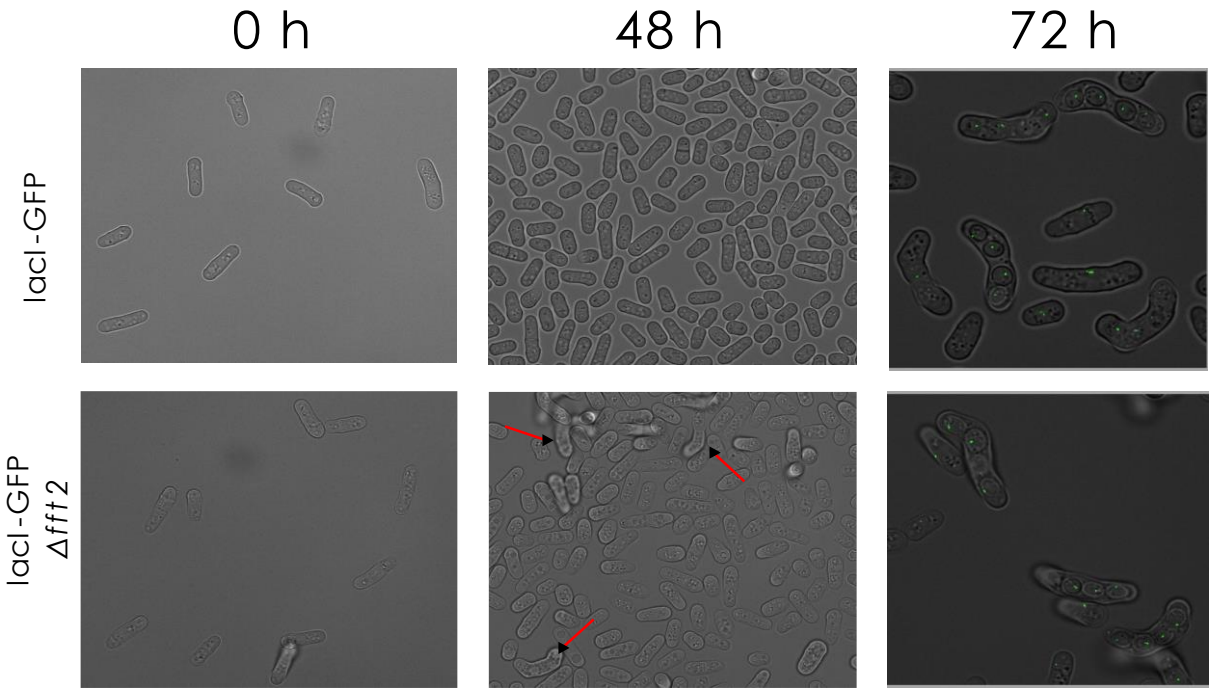


*Figure 13 Meiosis initiation is enhanced in Δfft2 background without failure in chromosome segregation*

The cells of Lac1-GFP () and Lac1-GFP *Δfft2* () are grown to a total OD of 0.5 OD/ml in YES, 2ml of culture is washed and resuspended in 1ml EMM-N. 10µl of cell suspension is microscope direct as 0h timepoint and the remaining volume is divided in half between one YES plate and ME plate. Growth of plate is performed at ambient temperature for 72h and every 24h cells are microscope by resuspending small amount of cells in EMM-N for live cell microscopy. At 48h, first cells in *Δfft2* passed the meiotic prophase and can be detected as "pre tetrads" (red arrow). The chromosome segregation, indicated by Lac1-GFP is not impaired in *Δfft2* strain background.

The onset of meiosis is also quantified by determining the ratio of ascospores/cell at each time point and plotted as a bar graph (Figure 14 B). An alternative method for quantifying sporulating cells is to stain the spore wall of cells grown on ME plates with iodine vapour, where a dark purple colour indicates a high number of ascospores, while growth on standard non-sporulating media results in a yellow colour (Figure 14 A). Quantification using both methods support the earlier observation that deletion of Fft2 promotes meiosis initiation but has no effect on the absolute number of ascospores or chromosome segregation. Meiosis is initiated in the process of zygotic meiosis by the response to mating pheromones, which is followed by the mating of two cells with opposite mating types [Nielsen and Davey 1995; Seike and Niki 2022]. This pairing process initiates meiosis, but how Fft2 might be involved in this process is not clear. As later experiments show, membrane channel transcripts are

dysregulated in the *Δfft2* background (Figure 19, App. table 1), which could lead to faster pheromone uptake. Chromatin recruitment could also potentially be related to chromatin condensation, causing cells to pass through meiotic prophase more rapidly, as evidenced by increased sporulation. To understand how Fft2 affects meiosis initiation, more meiosis initiation experiments need to be performed.

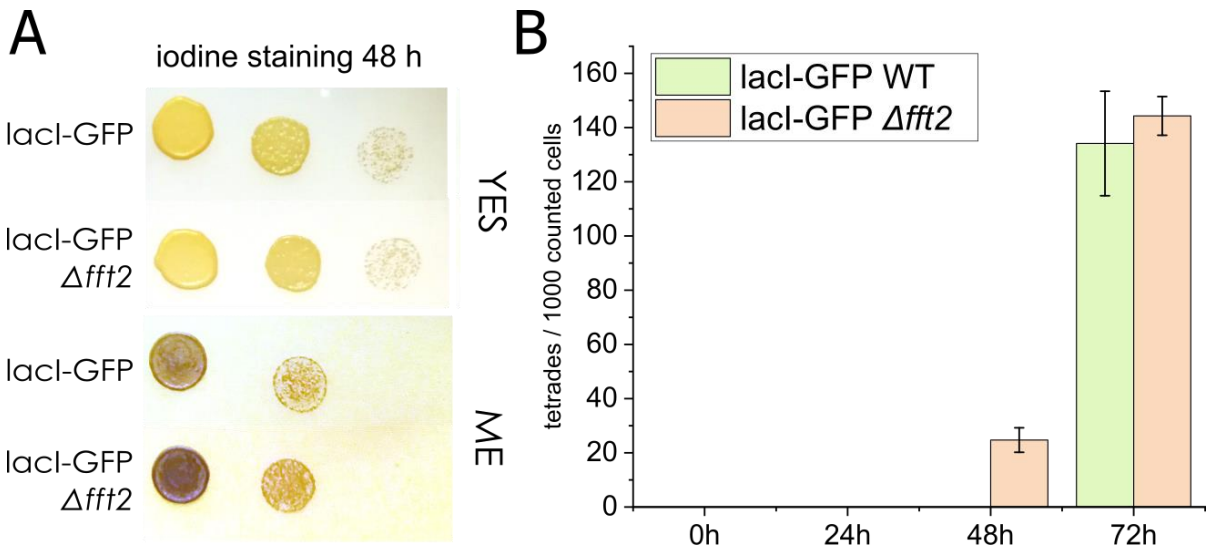


*Figure 14 quantification of sporulation suggest a meiosis start 24h earlier while absolute amount of ascospores remains constant*

A) cells for iodine staining originate from microscopy experiment (Figure 13) and are prepared the same way. Cells with 1 OD/ml are diluted 1:10 and 1:100, dot spotted on YES and ME and grow at ambient temperature for 48h and 5min exposed to iodine vapour before documenting. A clear, not quantified difference, in iodine staining is observed in *Δfft2* background. B) quantification of microscopy experiments (Figure 13) is performed by counting of 2 individual samples of similar plate. SEM is applied on bar charts. At each timepoint, the total amount of tetrads is plotted for 1000 total counted cells.

## 4.4 Size of Mtl1 dependent complexes is reduced in *Δfft2* background

The observed accumulation of Fft2 on RNA in exosome mutants and in the cell program of meiosis is compatible with an involvement of Fft2 in regulation of the exosome complex. While a functional involvement is suggested from previous meiosis experiments (chapter 4.3), a direct interaction of Fft2 with the exosome or exosome adaptor complexes like MTREC is not investigated yet. Density gradient centrifugation has been used previously to characterise exosome-associated protein complexes [Lubas et al. 2011] which leads to the hypothesis that if Fft2 directly interact with the exosome complex, the deletion of Fft2 should affect the relative positioning of the exosome complex in a native glycerol gradient. Because it is unknown by now where and how Fft2 interacts with the multi-layer exosome complex, Mtl1 as core component of MTREC is chosen for glycerol gradient investigation because it connects regulation of meiotic transcripts [Yang Zhou et al. 2015; Marayati et al. 2016], with formation

of facultative heterochromatin [Zofall et al. 2012] and degradation of cryptic unstable transcripts [Yang Zhou et al. 2015] and therefore qualified a potential complex formation with Fft2 is potentially possible and is investigated.

### 4.4.1 Establishing a glycerol gradient with adapted resolution limits by size exclusion chromatography

To calibrate the Superose 6 column for size exclusion chromatography, peptidase-digested protein standards were loaded by syringe and eluted with X buffer. The elution volume was monitored and plotted against the expected size of the protein standard (Figure 15). A linear fit was calculated with the corrected Pearson correlation coefficient (adj. $R^2$) of 0.894 and plotted for the observed elution volumes. The linear fit is therefore a good approximation of the measured elution volume to the expected protein size and the tested fit is used for estimating the protein size of a linear 10% to 40% glycerol gradient (Figure 16).

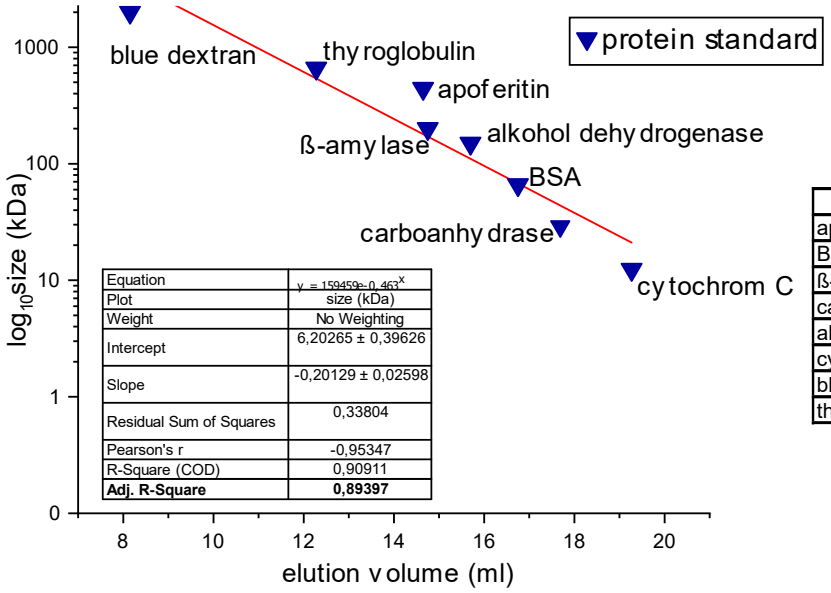


| | size (kDa) | elutionvolum |
|---|---|---|
| apoferitin | 443 | 14,65 |
| BSA | 66 | 16,75 |
| ß-amylase | 200 | 14,75 |
| carboanhydrase | 29 | 17,69 |
| alkohol dehydro | 150 | 15,7 |
| cytochrom C | 12,4 | 19,27 |
| blue dextran | 2000 | 8,15 |
| thyroglobulin | 660 | 12,28 |

*Figure 15 Determination of the Superose 6 10/300 GL resolution capability by protein standard*

Size exclusion chromatography of superose 6 column is determined with 4 separate protein mix containing 2 separate proteins with 1.5 mg/ml each. Column is equilibrated 1h by sample buffer with 0,5 ml/min and protein mix are load separately by syringe into the injection valve and eluted over column with a flowrate of 0.3 ml/min. Eluted volume of respective protein peak is detected and plotted against log transformed protein size ($log_{10}$ kDa). Linear correlation is calculated with an $R^2$ of 0.894, which represents a linear correlation between elution volume and protein size.

To estimate the relative size of complexes in glycerol gradient fraction, YPL144 (WT) native lysate was loaded on a gradient and fractionated via Äkta start. The fractions 1, 5, 12, 25, 33

and 38 were analysed by size exclusion chromatography via Superose 6 and a sigmoidal curve was fitted via the Boltzmann equation (

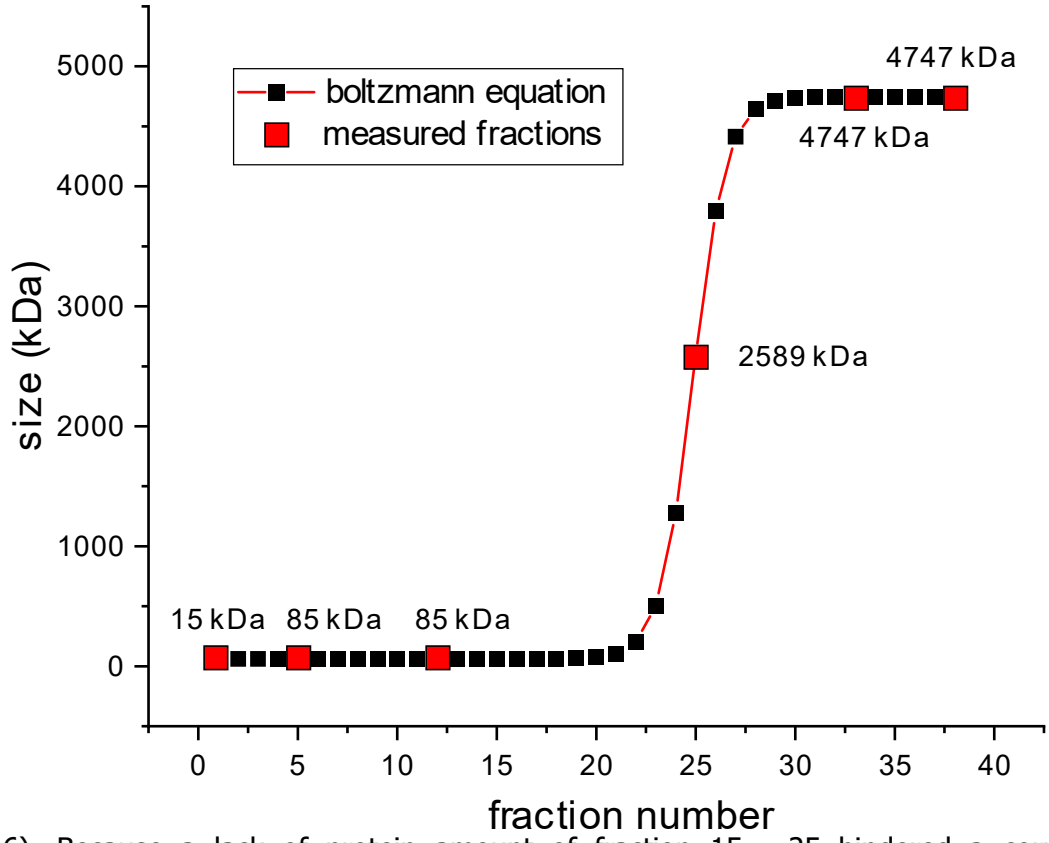


Figure 16). Because a lack of protein amount of fraction 15 - 25 hindered a correct measurement (Figure 17B UV), important measure points for the correct slope, is lacking in this analysis.

*Figure 16 Size selectivity of 10-40% glycerol gradient estimated by Superose 6 size exclusion chromatography*

The size of the gradient fractions was determined by Superose 6-column size exclusion chromatography for fractions 1, 5, 12, 25, 33 and 38. 200µl of the obtained äkta fraction was diluted (200µl in 300µl) and 500µl was added with a syringe at 0.3ml/min. The elution volume of the largest detected peak of each fraction is assumed to be representative of the protein size of the fraction, and the fractions tested are labelled as red squares with the calculated fraction size. The black squares represent the fraction weight calculated according to the Boltzmann equation based on the actual fractions measured. Fraction number 1 represents the lowest glycerol content of the gradient, while fraction 40 represents the highest glycerol content of the gradient.

As a result, the data is insufficient for reliable fitting and the calculated slope is likely too steep to represent the actual protein weight for the 10-40% glycerol gradient, especially in the lighter fractions. Nevertheless, fractions 1-19 were identified by sigmoidal boltzmann equation as the light plateau of the density gradient with an expected protein size of < 85 kDa and fractions 38-28 form the heavy plateau with a calculated weight of > 4715 kDa. Because of the unchanged elution volume for the tested fraction in the plateau area, size estimation of

complexes is difficult in these areas. Instead, complex size separation is mostly realised between fractions 19 and 28 in the range between 85kDa and 4642kDa of the linear glycerol gradient which fits the aimed experimental conditions.

### 4.4.2 Native density gradient centrifugation reveals Fft2 as interactor of Mtl1

To investigate the integrity of exosome targeting complexes, lysates of Mtl1-HTP strain (YPCK57) were compared with Mtl1-HTP, *Δfft2* lysates (YPCK217) to assess the effect of *Δfft2* on the complex size of MTREC, the *S. pombe* equivalent of *H.sapiens* PAXT complex (Figure 17).

In the Mtl1-HTP background the respective protein A western blot signal is distributed across the gradient, with two peaks visible in fractions 12-22 and 25-33. The signal shifts towards lighter fractions when Fft2 is deleted, peaking in fractions 8-18 instead. A representative western blot of YPCK57 and YPCK217 illustrate an observable shift (Figure 17A). While in YPCK57 two peaks are detectable (P1: fraction 15-20, P2: fraction 27-32), YPCK217 just show one broader peak (fraction 8-15), which at least suggest a loss of complex variability. Also, a strong enhancement of the Mtl1 signal in the lighter fractions, and reduction of signal in the heavy fractions demonstrate, that heavy complexes which contain Mtl1 vanish in an *Δfft2* background. Instead, the Mtl1 signal accumulates in the light complex weight area of the density gradient which suggest strong involvement of Fft2 in the Mtl1 complex forming, which is fitting with the presence of Fft2-3HF itself in the heavy fractions of the density gradient (App. figure 2). Also, Mtl1-HTP shifts in a *Δrrp6* background in a similar fashion (App. figure 2) which underlines the observed loss of Mtl1-dependent complexes.

Quantification of blots from multiple-density gradients supports this observation (Figure 17 B/C). Mtl1-HTP and Mtl1-HTP/*Δfft2* gradient is performed as triplicate, quantified and the relative intensities of each fraction is plotted as scatter (Figure 17 B) or as heatmap to estimate the protein shift in gradient(Figure 17 C). The measurement of relative protein concentration by constant UV-monitoring is performed, while the fractionation takes place. It is notable that most proteins can be found in the top fractions 1-10 and the bottom fraction 30 – 40. In the intermediate fraction just very low quantities of total protein are found, but the major amount of western blot signal shows up in these fractions (fraction 10-33). As detected in western blot (Figure 17 A), a shift of Mtl1-HTP signal is observed in a *Δfft2* background. While Mtl1-HTP show accumulation as double peak in gradient fraction 14-21 and 28-32, this pattern is abolished in *Δfft2* and the majority of Mtl1-HTP signal is detected at fraction 11-17. The results

indicate, that the distribution of Mtl-1 in glycerol gradient is more narrow when Fft2 is depleted. The signal is also visualised in a heatmap, where the colour is related to the fraction of highest intensity (Figure 17 C). It should be noted that the underpinning triplet shows high variations, which are indicated by a colour-matching area, which corresponds to the area in which the SEM was calculated.

Overall, a clear shift of Mtl1-HTP signal to lighter fractions is identified in a *Δfft2* background, which can be interpreted as a loss of heavy complexes that includes Mtl1. This shift is also observable in *Δrrp6* (App. figure 2) and the majority of these complexes can therefore be stated as exosome dependent. Loss of complexes in *Δfft2 in* a similar fashion suggest an important role of Fft2 in forming of these Mtl1 dependent complexes, which could explain the behaviour of *Δfft2* at pH stress (Figure 7) and the accumulation on polyadenylated RNA in exosome deficiency mutants, like other known exosome specificity factors (Figure 8).

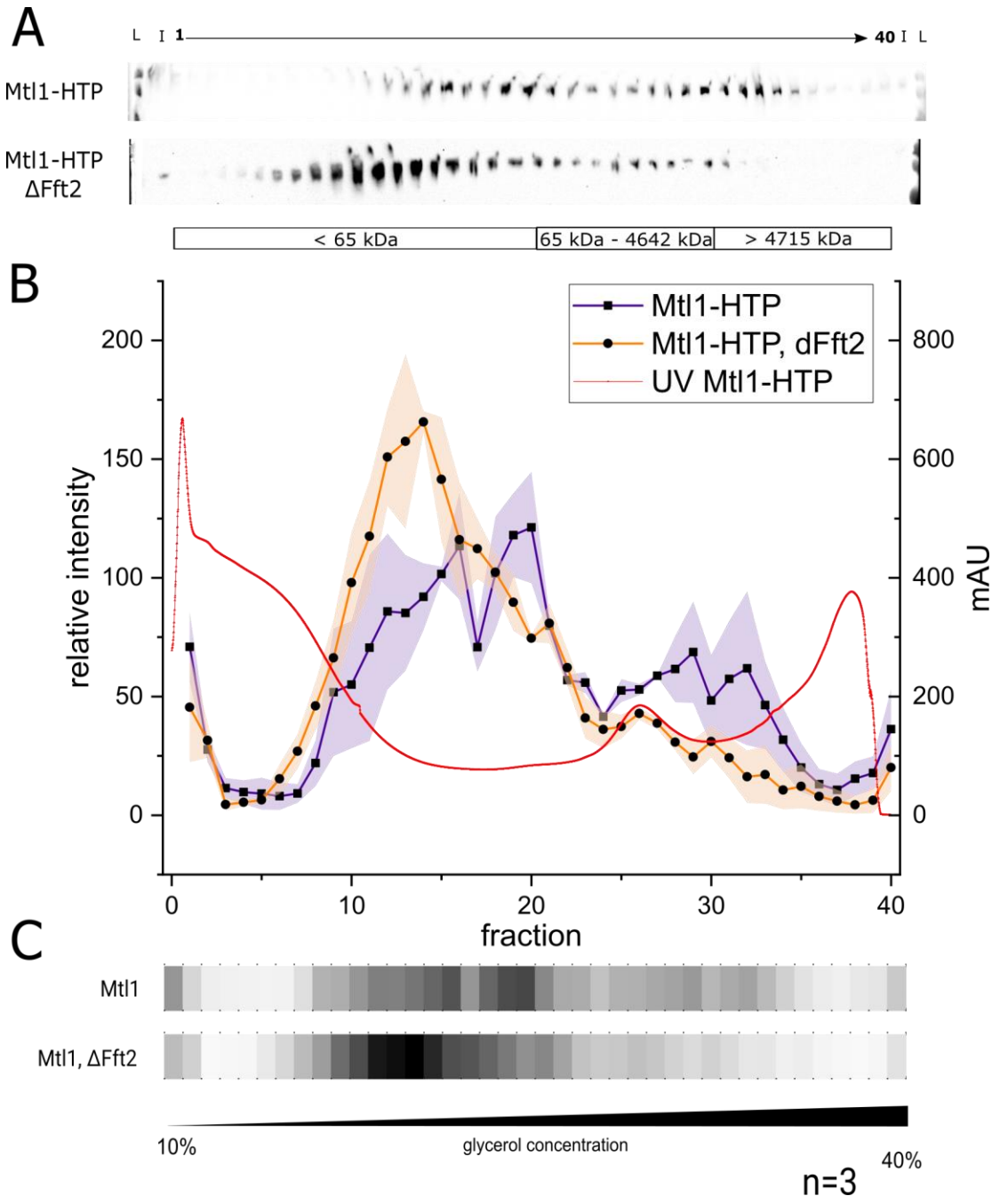


*Figure 17 lack of Fft2 leads to a shift of Mtl1 dependent complexes*

A) representative WB of 10%-40% glycerol gradient triplicate performed on Mtl1-HTP (YPCK57) and Mtl1-HTP *Δfft2* (YPCK217) in comparison. WB signal of MTl1-HTP is detected by PAP antibody. While in WT Mtl1-HTP is found in 2 distinct peaks, a clear shift of Mtl1-HTP into lighter fractions is observed in a *Δfft2* background, which is interpreted as loss of Mtl1 dependent complexes. B) Quantification of unrelated triplicate (n=3) show a robust loss of Mtl1 peak around fraction 30 and a corresponding shift from fraction 19/20 to fraction 15 in *Δfft2* background. SEM which represents the sample variation is plotted as colour fitting area. The total protein distribution is continuously measured by Äkta UV and obtained data is plotted as red line with corresponding mAU y-axis on the right. C) Relative density is calculated and transformed into a heatmap to determine centre of Mtl1-HTP protein weight within the gradient. Therefore, the fraction with highest relative intensity (fraction 15 of Mtl1-HTP *Δfft2*) is set to 100% intensity and the other values of colour scale is calculated with regard to this fraction. It is obvious that Mtl1 lose its appearance in higher glycerol concentrated fraction by *Δfft2* and centers between fraction 13-16.

### 4.4.3 Fft3 and SMARCAD1 do not show a significant shift under RNase treatment in density gradients

After I analysed the involvement of Fft2 in the complex formation of Mtl1, the question arose if the location of Fft2 in the gradient is exclusively protein dependent or the recruitment of Fft2 on RNA also facilitates larger complexes. To investigate this hypothesis, a native *S. pombe* WT lysate is loaded on a 5% to 50% sucrose gradient, treated with and without RNase mix. The sucrose gradient is fractionated, and the respective proteins of each fraction are then detected by mass spectrometry. This data was available in the lab, generated and illustrated by Dr. N. Wäber (Nadine Wäber, unpublished data, Figure 18 A). For comparison, human SMARCAD1 and Rrp6 from the R-DeeP database [Caudron-Herger et al. 2019] are also included (Figure 18 B). R-DeeP is described by its creators to "adapt the concept of RNA dependence, defining a protein as RNA dependent when its interactome depends on RNA" [Caudron-Herger et al. 2019], which differentiate the method from RIC that needs a direct protein-RNA interaction [Castello et al. 2012]. R-DeeP database focus on human proteins and by today around 5000 proteins are analysed for their RNA dependency by RNase treated sucrose step gradient centrifugation (5% to 50% sucrose) (available under [Diederichs Lab/Projects 2018]).

Besides Fft3 and Rrp6, no exosome components or Fft-family members are detected in the MS analysis experiment of *S. pombe* (Figure 18 A). RNase treatment of lysate leads to a significant shift of Rrp6 towards lighter fractions in *S. pombe* and *H. sapiens* which is in line with former RIC investigations [Castello et al. 2012; Bao et al. 2018]. The behaviour of Fft3 in the sucrose gradient distinguish from SMARCAD1 of R-DeeP databank with the appearance of 2 clear peaks, while SMARCAD1 shows only a solitary peak at a relative light fraction (Figure 18 A+B). For Fft3 and the orthologue SMARCAD1 the effect of RNase treatment on the protein localisation is much smaller when compared to Rrp6 of both organisms. Surprisingly, Fft3 changes the relative protein abundance of peaks to the heavier peak when the lysate was treated with RNase, while SMARCAD1 gradient localisation is completely unresponsive to RNase treatment. It is important to emphasize that SMARCAD1 is found only in light fractions and does not shift, while Fft3 has two peaks in heavier fractions, the heavier of which increases after a RNase treatment, which suggest functional differences in RNA dependent complex forming.

The results indicate a minor involvement of RNA in the gradient localisation of Fft3, the paralogue of Fft2. While no observable effect is detected in RNase treated fractions for the

SMARCAD1 protein, Fft3 shifts slightly after RNase treatment. Surprisingly the shift occurs counterintuitive to the heavier fractions and needs therefore deeper investigations. Nevertheless, the occurrence of two distinguishable peaks for Fft3, differentiates it from SMARCAD1, which is in line with the findings in this study so far.

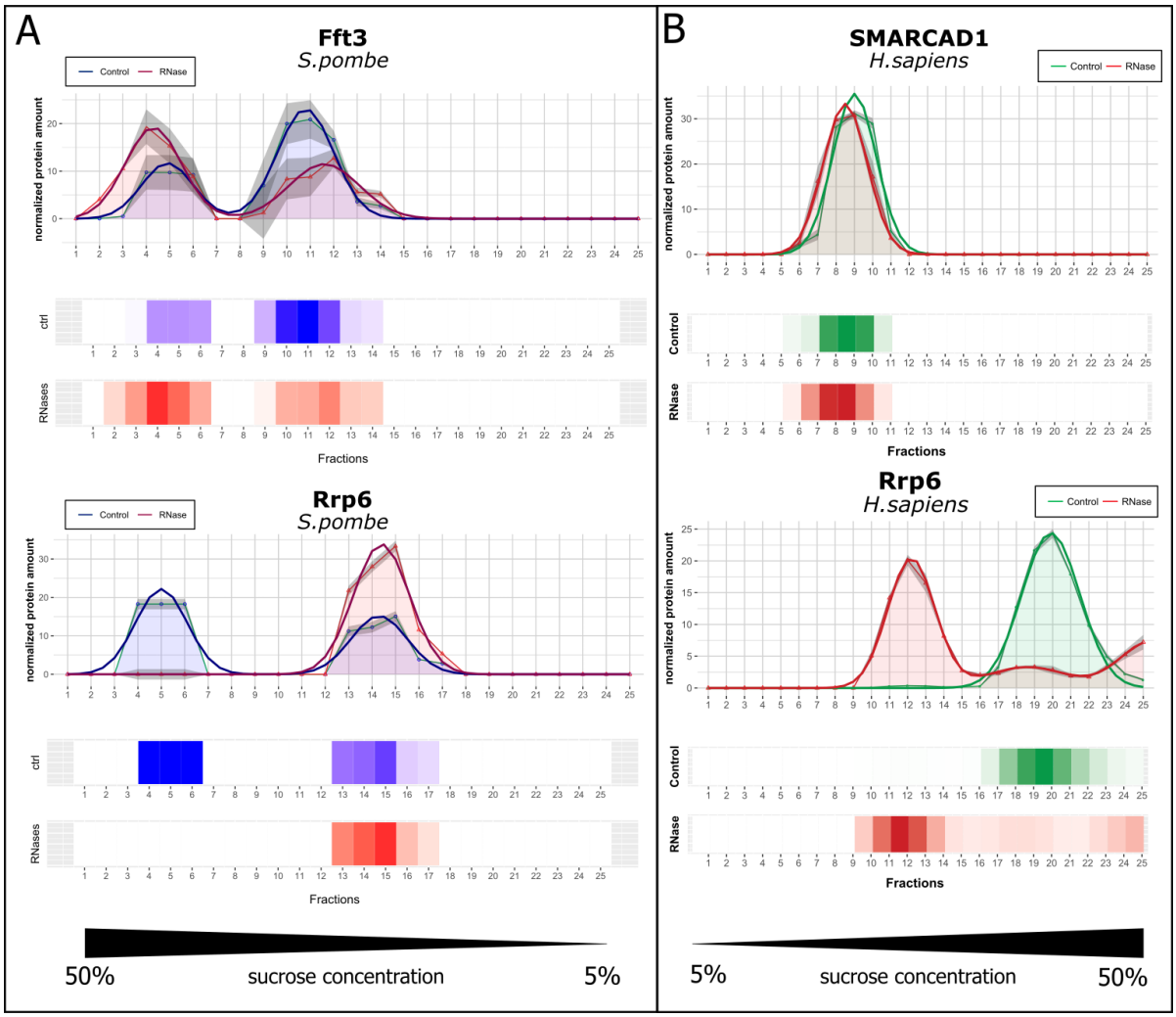


*Figure 18 Fft3 and SMARCAD1 show just minor changes in gradient localisation under RNase treatment*

A) unpublished data, supplied by Dr. Nadine Wäber, show that the sucrose gradient localisation of *S. pombe* Rrp6 based on the presence of RNA while Fft3 is not. The protein content of single fractions is analysed with mass spectrometry while one triplicate set of lysates is treated with RNase mix, the other is use without treatment as control. B) RNA dependent protein data of *H. sapiens* is obtained from R-DeeP databank [Caudron-Herger et al. 2019] which is obtained in a 5% to 50% sucrose gradient. Comparable to *S. pombe* Rrp6, Rrp6 shifts dramatically when lysate is treated RNase, but SMARCAD1 instead is not responsive. In comparison to Fft3, SMARCAD1 is located as a single peak, while Fft3 is found in2 distinguishable peaks.

To summarize, Fft2 affects the complex formation of Mtl1 and a deletion of Fft2 leads to a relocalisation of Mtl1 at light gradient fractions. This can be interpreted as a loss of high molecular exosome target complexes in a Fft2 deletion strain. While deletion of Fft2 results in a reduction of Mtl1 dependent complexes, the orthologues Fft3 and SMARCAD1 show that the

formation of high molecular complexes is not necessarily depending in its majority on RNA, as RNase treated sucrose gradients demonstrates.

## 4.5 Deletion of Fft2 has little impact on the transcriptome

After investigating the decrease of Mtl1 containing high molecular complexes in *Δfft2*, an infliction in exosome-dependent RNA degradation seems obvious. To test this hypothesis, a total RNaseq is performed for *Δfft2* (YPCK306) and also for *Δfft1* (YPCK349) because their growth behaviour on temperature stress is comparable (Figure 9) but they differ in RNA accumulation in exosome deficiency mutants (Figure 8).

### 4.5.1 Fft2 is minorly inflicting the transcriptome

To understand the cold-sensitive phenotype demonstrated in *Δfft1/2* (Figure 9), I tested the whole transcriptome level via total RNaseq and compared DEG (differentially expressed genes) of *Δfft2* with *Δfft1* (Figure 19).

It is observeable that both deletions just minorly affect the transcriptome. When loose conditions for significant differentially expressions are applied (FC: $Log_2$ +/- 0.6, p-value < 0.05), the analysis reveals just 133 DEG for *Δfft2* (up 54, down 79) and just 36 DEG for *Δfft1* (p: 6, down:30) when compared to WT expression. The effect on transcriptome is therefore relatively small and no significant overlaps in up- (2 transcripts) or downregulated transcripts (5 transcripts) are detected between *Δfft1* and *Δfft2*. Downregulated transcripts in both deletion strains were involved in cytoskeleton organisation and cellular detoxification, the only upregulated transcripts which encode for a protein, namely alr2, is involved in the alanine metabolism and a target of MTREC complex [Sugiyama et al. 2013].It is noteworthy, that the iron homeostasis transcript, which accumulates in *Δrrp6* background [Mukherjee et al. 2016] , is not accumulating in *Δfft2* or *Δfft1.* Therefor the observed growth behaviour of *Δfft2* at pH stress exposure (Figure 7) cannot directly linked to the described involvement of iron metabolism genes in pH stress resistance [Higuchi et al. 2018]. A full list of DEG is found in the appendix (App. table 1).

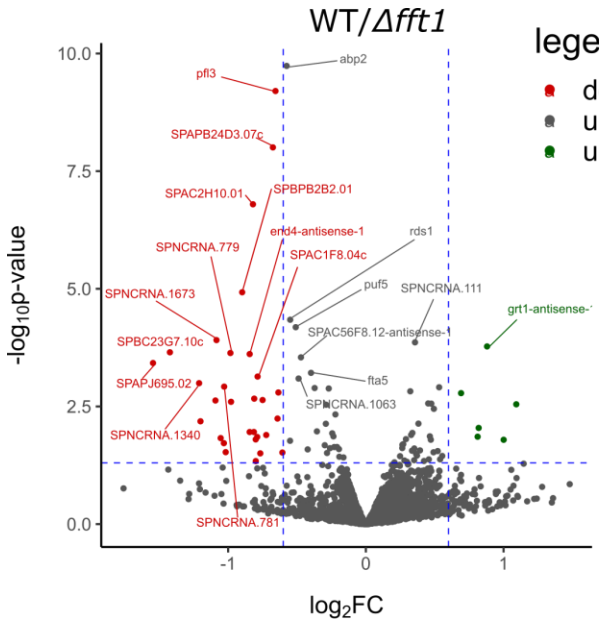


| downreg. overlap | | upregulation overlap | |
|---|---|---|---|
| **ckk2-antisense-1** | ncRNA | **alr2** | alanine racemase activity |
| **lid2-antisense-1** | ncRNA | **grt1-antisense-1** | ncRNA |
| **SPAC1F8.04c** | hydrolase, cell detox. | | |
| **SPBC1289.14** | aktin cytoskeleton organisation | | |
| **SPBC23G7.10c** | NADH-dependent flavin oxidoreductase, cell detox. | | |

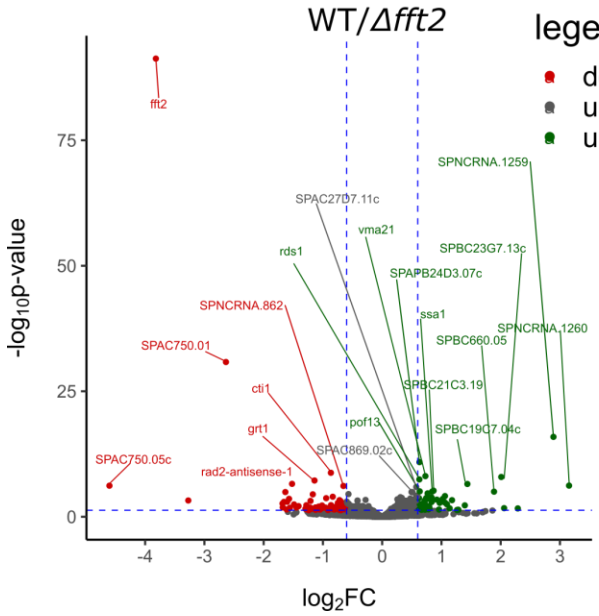


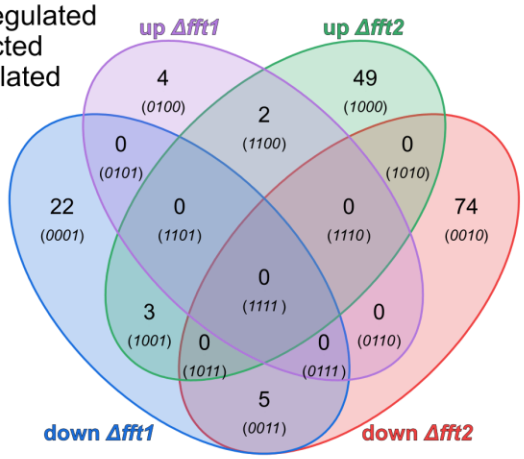


*Figure 19 DEG analysis of Δfft1 and Δfft2 strains reveals minor inflictions on transcriptome*

Differentially expressed gene (DEG) regulation is calculated between Δfft1/2 and a respective wild-type strain (YPCK144) which was performed by MPI Bad Nauheim. The fold change is plotted against p-value in a volcano plot by the use of R. Genes with FC >0.6 and p-value < 0.05 are labelled as up-regulated (green), genes with FC < -0.6 and p-value < 0.05 as down-regulated. The top 30 DEG hits for *Δfft2* and *Δfft1* are labelled with their transcript name. The DEGs are also analysed for their occurrence as up- or down-regulated DEGs in both deletion strains. 133 DEGs are classified for *Δfft2* and 36 DEGs for *Δfft1*, but only 2 genes are up-regulated and 5 down-regulated for both deletions as listed in the table and visualized in multi-Venn diagram.

### 4.5.2 GO term analysis of DEG in *Δfft2*

To identify, if specific families of protein-coding transcripts are differentially expressed in the Δ*fft2* strain, a GO-analysis was performed by PANTHER (Figure 20). The analysis displays that a large part of *Δfft2* DEGs are unmappable in GO analysis. This is because ncRNA or antisense transcripts lack a GO-family entry or various protein-coding transcripts are not classified by now and could therefore not be mapped. The most abundant protein class which appears for downregulated transcripts, as well as for upregulated transcripts is metabolite interconversion enzymes. While high similar protein classes are found, the second largest molecular function which is found in downregulated transcripts in *Δfft2* transcriptom, is binding (GO:0005488) and catalytic activity (GO: 0003824). For upregulated transcript, the abundance of these molecular functions is flipped.

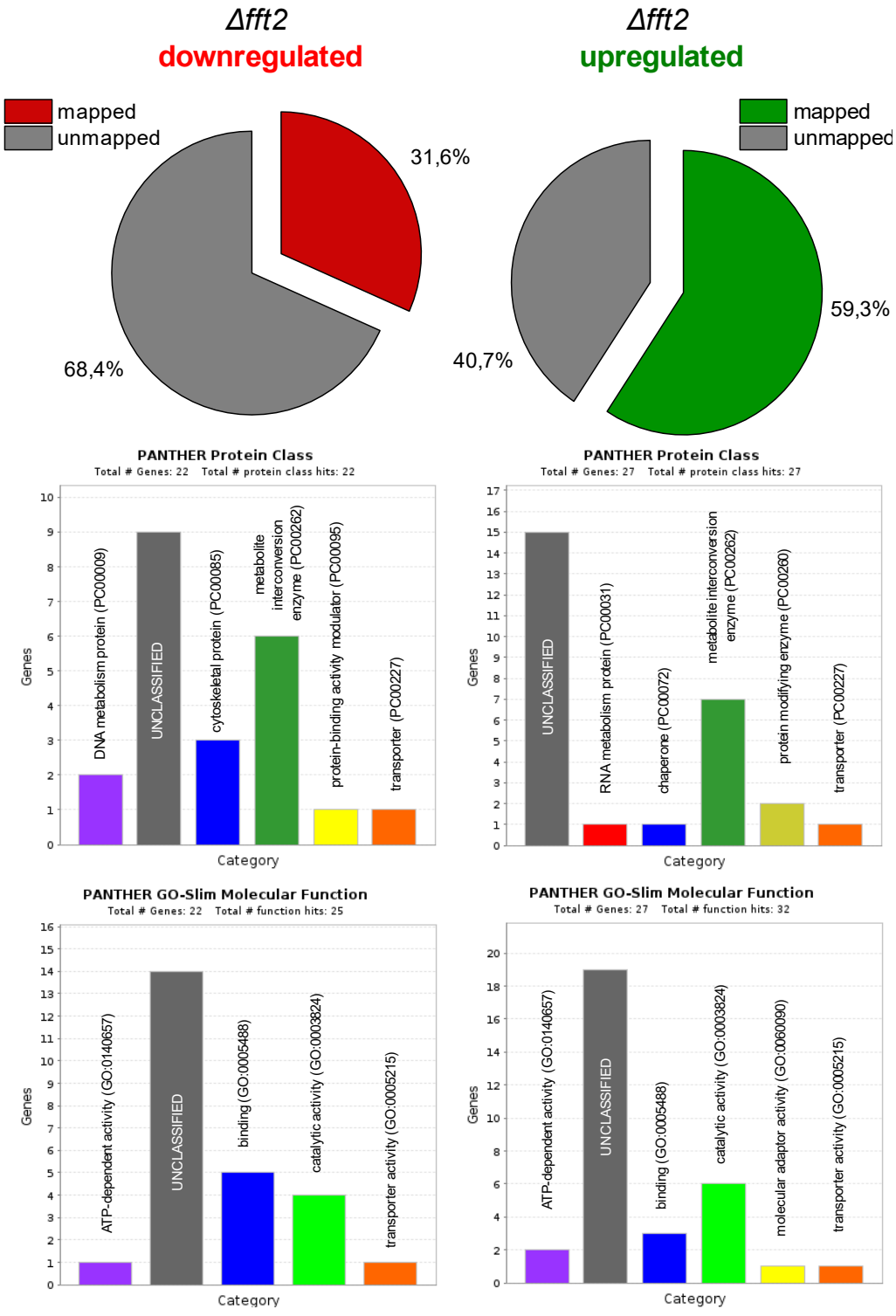


*Figure 20 GO-term analysis of Δfft2 shows that a large proportion of DEG consists of ncRNA transcripts.*

The 133 DEG transcripts are analysed according to PANTHER protein class and GO-Slim function [Thomas et al. 2022]. The pie charts were created by the author, while the bar charts were created as a result of the GO term analysis. The results show that only 31.6% of the down-regulated and 59.3% of the transcripts could be assigned to a protein class and a molecular function, which means that about half of the DEGs have no protein class or function. These transcripts are therefore listed as non-coding transcripts. Of the remaining transcripts, most are categorised as "unclassified" without specific functions. With only a few divergent transcripts, the up- and down-regulated genes are from similar classes or have a similar function.

### 4.5.3 RNaseq meiosis targets

To investigate the effect of *Δfft2* on exosome-dependent transcripts, the transcript level of meiotic RNAs, an exemplary exosome-controlled mechanism, are compared between *Δfft2* and various exosome deficiency mutants like *Δrrp6, mtl1-1* and *Δmmi1* (Figure 21). The data for the respective exosome deficiency mutants is supplied by [Kilchert et al. 2015] . While for all tested exosome mutants an increase of meiotic transcripts is observed, deletion of *fft2* does not change known meiotic transcript levels when compared with a respective WT. This finding suggest, that *Δfft2* does not broadly affect the exosome related homeostasis of important meiotic transcripts in mitotic cells. Single transcripts that are involved in meiosis are differentially expressed in *Δfft2* (*SPBC19C7.04c, mug108, mei3, rec7, spo4, omt3*) but just *SPBC19C7.04c, mug108* and *omt3* show a statistical significance change (App. table 1). This could indicate that Fft2 is involved in a separate pathway to regulate the level of meiotic transcript, with or without exosome involvement. The three transcripts (*SPBC19C7.04c, mug108* and *omt3*) show a differential expression in at least one exosome deficiency mutant as well (App. Table 2). The identified differentially expressed transcripts in *Δfft2* are therefore not necessarily affected by all tested exosome deficiency mutants. While *mei3* is affected in all exosome mutants, *omt3* is just differentially expressed in *Δrrp6* mutant. *mug108* is affected by *Δmmi1* mutation and *SPBC19C7.04c* by *mtl1-1* and *Δmmi1*. This data suggest that Fft2 is potentially involved in regulation of secondary meiotic RNA transcripts in an alternative exosome regulation pathway.

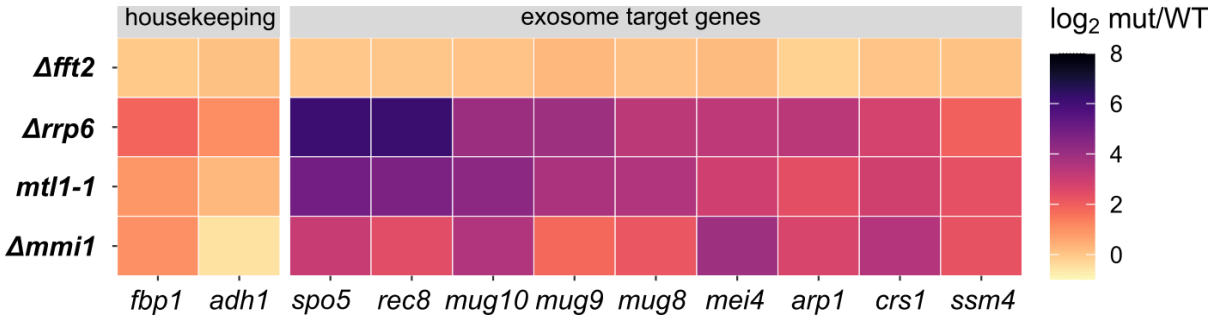


*Figure 21 Comparison of exosome deficiency mutants with Δfft2 level of common meiotic transcripts reveals*

Heatmap, supplied by Dr. Cornelia Kilchert of respective exosome mutants [Kilchert et al. 2015; Mukherjee et al. 2016; Birot et al. 2022] is calculated by the $\log_2$ fold change to the respective WT. For all exosome mutant's meiotic genes are strictly upregulated while housekeeping genes remain unresponsive. *Δfft2* in contrast shows no differential expression of the major exosome targets, but individual meiotic transcripts are found as differentially expressed in *Δfft2* (App. table 2).

## 4.6 Fft2 as novel RNA binding protein

Next, I wanted to identify RNAs that Fft2 interacts with as direct RNA binding was indicated from former RIC experiment (Figure 8)

For this purpose, Fft2 was analysed by Photoactivatable-Ribonucleoside-Enhanced Crosslinking and Immunoprecipitation (PAR-CLIP) which directly crosslinks RNA with interacting proteins by nucleotide resolution crosslinks [Danan et al. 2016].

Since Fft2 is found in comp. inter. capture as potential novel RNA binding proteins, HTP-tagged variants of Fft2 and its paralogue Fft3 (YPCK9: Fft2-HTP, YPCK416: Fft3-HTP) are therefore tested by PAR-CLIP for their RNA binding capability. An untagged WT (YPCK144 no tag), a strain including Mtl1-HTP (YPCK57 Mtl1) as a known RNA binder and a strain with SPAC3c7.04-HTP as a potential DNA binding transcription factor (YPLV742: TF) were included as controls (Figure 22).

Evaluation of phosphorscreen reveals signal of radioactively labelled RNA bound to protein. In the WT lanes, the signal background of the [γ-$^{32}$P] ATP labelling is visualized. For SPAC3c7.04 the observed signal is comparable to the detected background with 365nm UV crosslinking, which can be interpreted as no RNA binding for SPAC3c7.04-HTP, which was expected from the protein biology. In contrast, Mtl1 shows a relevant signal in low RNase treated lane ($10^{-5}$) at the expected protein size in blot with a characteristic smear of $^{32}$P signal [Stebel et al. 2022]. This signal was lost when the lysate was treated with high RNase concentration ($10^{-3}$), which demonstrates the specificity of the $^{32}$P signal for RNA and was also shown in other investigations before [Rio 2014]. Fft2-HTP shows a high radioactive signal signal under high RNase concentration ($10^{-3}$), but the signal is strongly decreased in low RNase concentration ($10^{-5}$), which is the opposite behaviour observed in MTl1-HTP. This pattern for Fft2-HTP can be inverted when the duration of RNase digest is increased (App. figure 1). Therefore, the result could be interpreted in a way that the amount of RNA bound by Fft2-HTP is much higher as it is the case for Mtl1-HTP, or that the bound RNA is less accessible, and the RNase treatment takes longer to partially degrade the bound RNA.

For Fft3-HTP in comparison, the detected radioactive signal pattern matches the pattern observed for Mtl1. The signal intensity after high RNase treatment is notably higher, which could also reflect in higher amounts of bound RNA or less accessibility. It must be mentioned that Fft2-HTP, as well as Fft3-HTP, show enhanced protein degradation when compared to Mtl1-HTP or SPAC3c7.04-HTP in similar conditions.

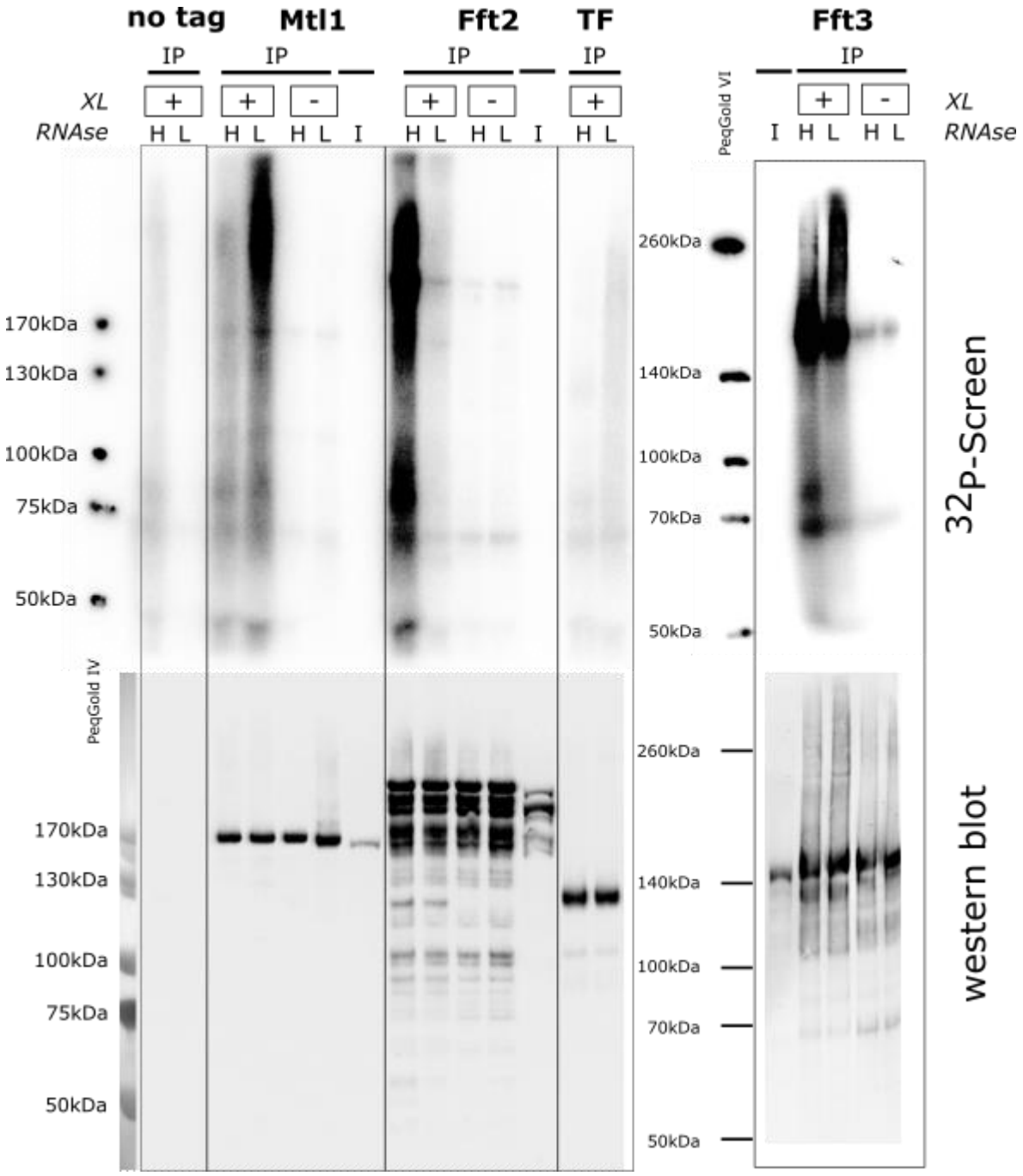


*Figure 22 Fft2 and Fft3 show de novo RNA binding in vivo*

The PAR-CLIP experiment was performed in EMMG with low uracil content (10 mg/L). 4tU was added to the medium at an OD of 0.5 OD/ml and incubated for 4 hours. Cells are lysed by crushing in LN and the lysate is incubated at 37°C for 3 minutes for DNA and different partial RNA digestion. IP is run for 2h at 4°C and washed 4 times with TBS800-T and 2 times with PNK buffer. Radiolabelling is done with T4-PNK and 25 pmol for SCP801 for 20min. Beads are then washed, protein eluted in LDS loading buffer and PAGE performed with WB in NuPAGE gel system (4-12%). The phosphor screening is performed with a Typhoon FLA 9500, while the Western blot signal is obtained by α-PAP. WT represents an untagged control showing a background signal. Mtl1-HTP shows a strong signal in the phosphor screening that disappears with high RNase treatment, indicating RNA specificity. Both Fft2-HTP and Fft3-HTP show strong binding to RNA, while SPAC3c7.04-HTP as a transcription factor control (TF) does not bind to RNA at all. Fft2 is strongly degraded in the WB, while Mtl1-HTP and TF appear to be stable. Fft3 also shows signs of destabilisation, but much weaker than Fft2.

The experiment validates that Fft2, as well as Fft3, binds RNA directly, which is a novel characteristic firstly described for both proteins in *S.pombe*. When compared with the similar tagged TF (SPAC3c7.04-HTP), contamination with DNA is very unlikely which makes the protein-RNA interaction specific. Which RNAs are bound by Ftt2/3 and if these correlate with transcripts that are differentially expressed (Figure 19) is currently under investigation.

### 4.6.1 Fft2 truncations show no effect on RNA binding but enhance protein stability

The PAR-CLIP analysis reveals the ability of Fft2, as well as Fft3, to bind RNA, but which part of the protein interacts with RNA is still unknown. To understand the mechanism for the novel RNA binding in Fft2-HTP, three C-terminal truncations with HTP tag were created: AA1-AA392 (T1), AA1-AA751 (T2), and AA1-AA1073 (T3) (Figure 23). The ability of the truncated proteins to bind RNA was also investigated in PAR-CLIP and compared with Fft2-HTP full length (FL) and SPAC3c7.04-HTP (TF).

While for Fft2-HTP, the previously investigated signal pattern could be reproduced and the T3 truncation show no effect on the RNA binding capability of Fft2. Remarkably, the stability of all three truncations is strongly enhanced, and hardly any degradation can be detected, which implies that the C-terminal end of Fft2 the cause of the observed instability of Fft2.

For the T1 truncation, the phospho-screen displays a pattern comparable to Mtl1-HTP (Figure 14). An improvement of RNA accessibility in T1 truncations could lead to an enhanced RNases digestion. Interestingly, the T2 truncation does not show any [γ-$^{32}$P] ATP signal that exceeds the background signal set by TF. Based on the observed RNA binding of T3, it can be assumed that not the RNA-binding domain was truncated, but a secondary effect of this protein truncation could explain the lack of RNA binding, like a misfolding in the secondary structure of T2.

To summarize, T1 as the shortest truncation, maintains its RNA binding ability, while the detected signal pattern is inverted, comparable to the pattern seen for Mtl1 (Figure 22). This result implies that the binding of RNA takes place in the unstructured N-terminal end of Fft2. This interpretation fits our structure analysis (Figure 12). Fft3 does not contain a C-terminal end with unstructured regions (IDR) unlike Fft2 but is also able to bind RNA (Figure 22). In addition, the experimental data show that the presence of unstructured C-terminal end weakens the integrity of the Fft2 protein.

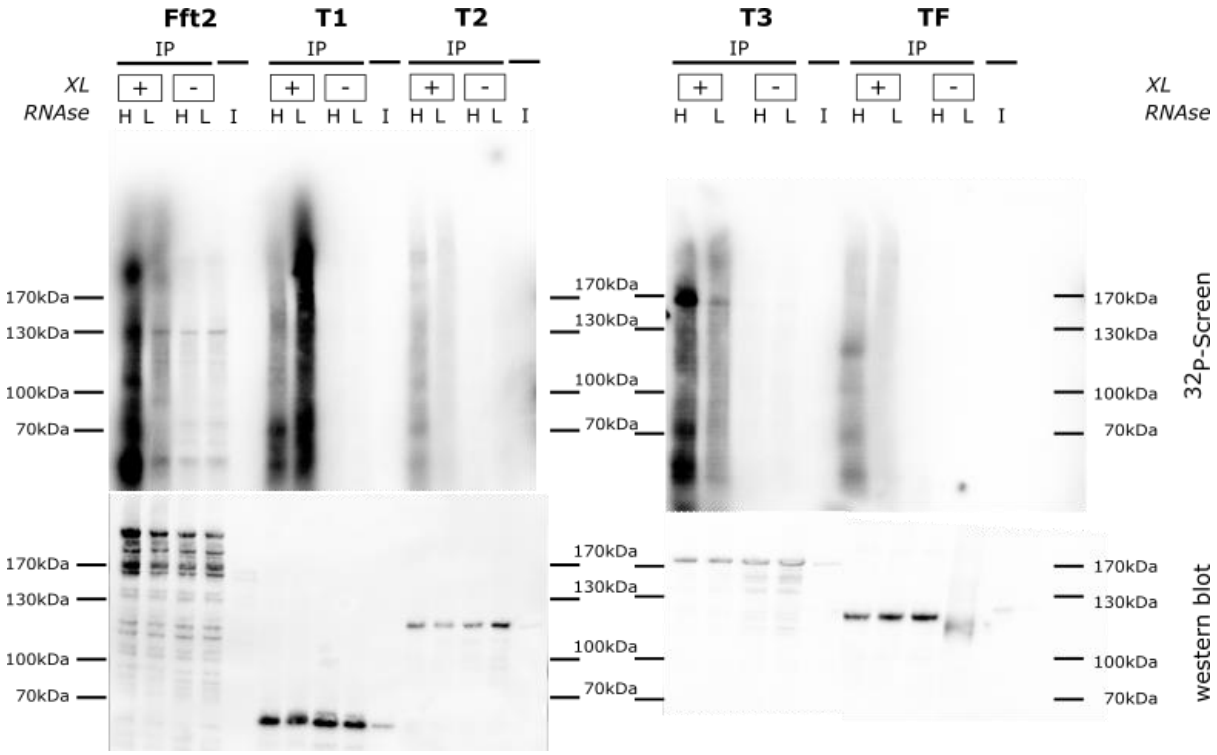


*Figure 23 c-terminal truncation of Fft2 maintains RNA binding ability*

The PAR-CLIP experiment was performed in EMMG with low uracil content (10 mg/L). 4tU was added to the medium at an OD of 0.5 OD/ml and incubated for 4 hours. Cells are lysed by crushing into LN and the lysate is incubated at 37 °C for 3 minutes for DNA and various RNA partial digests. IP is run at 4°C for 2 hours and washed 4 times with TBS800-T and 2 times in PNK buffer. Radiolabelling is done with T4-PNK and 25 pmol SCP801 for 20 minutes. Beads are then washed, protein eluted in LDS loading buffer and PAGE is performed with WB in NuPAGE gel system (4-12%). The phospo-screening is performed with the Typhoon FLA 9500, while the Western blot signal is obtained by α-PAP. Fft2 represents the full-length protein, while T1-T3 represent the respective C-terminal truncations. Both T1 and T3 retain their RNA-binding ability, while T2 lacks this characteristic compared to the non-RNA-binding TF control (SPAC3c7.04-HTP). This is probably due to misfolding, as T1 regains binding ability as a shorter truncation. While Fft2 is strongly degraded, as demonstrated by WB, all three truncations show increased protein stability, suggesting involvement of the C-terminal extension in protein stability.

## 4.7 Chromatin recruitment of Fft2 depends on nuclear RNA exosome components

To better understand Fft2 function, various genotypes were analysed in ChIPseq to determine the global pattern of Fft2 recruitment to chromatin (experiment performed by Dr. B. Keil AG Kilchert, library prep and sequencing performed by Dr. S. Günther at MPI Bad Nauheim). The respective level of Fft2 is not affected by different deletion mutants as verified by western blot (App. figure 3).

### 4.7.1 Global reduction of Fft2 recruitment in a *Δrrp6* strain background

The alignment profile of performed ChIPseq experiments shows the flattest profile for Fft2-HTP, which suggest the best peak detection over the background (Figure 24 A). Fft3-HTP and Fft2-HTP *Δrrp6* show just minor differences from untagged control, which indicates less aligned reads in fewer bins and therefore a weaker peak detection in these datasets. A spearman correlation test demonstrates that the closest relation of datasets is identified between Fft2-HTP and Fft2-HTP *Δrrp6,* which was expected (Figure 24 B). Fft3 instead shows a weak correlation with both Fft2 datasets, which indicates that Fft3 is differently recruited to chromatin than Fft2 itself. A surprising finding is a relatively strong correlation between Fft2-HTP *Δrrp6* and the untagged control, which is the strongest correlation for the untagged control overall and is probably due to the low overall read count of ChIPseq experiments.

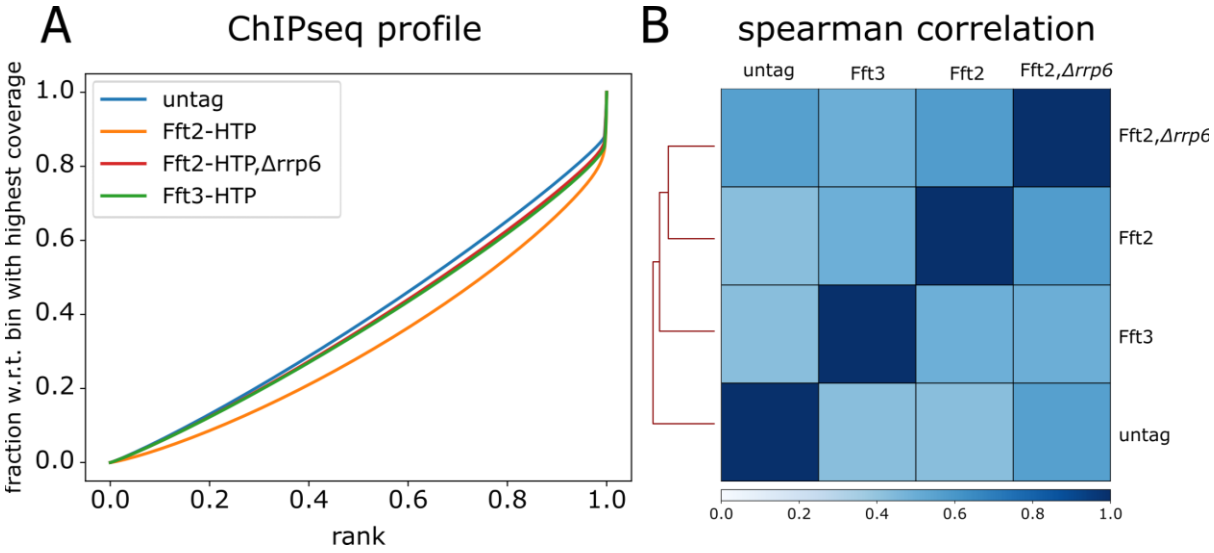


*Figure 24 genome-wide quality screening of ChIPseq datasets*

A) The quality of the obtained ChIPseq peak detection is tested with the ChIPseq profile "plotFingerprint" [Ramírez et al. 2016]. A very specific and strong ChIP enrichment would lead to a large part of the reads being accumulated in only a few bins and the resulting graph showing a steep slope towards the right edge. Here it is visible that Fft2 ChIPseq is slightly different from Fft2-HTP Δrrp6, Fft3-HTP and the untagged control, but the peak detection is not very strong. B) A Spearman correlation [Ramírez et al. 2016] is calculated between untagged, Fft3, Fft2 and Fft2-HTP Δrrp6 to show the similarity between the data sets. As expected, Fft2 and Fft2-HTP Δrrp6 show the highest correlation of the tested datasets, but surprisingly, the untagged control Fft2 shows the highest correlation also with Fft2-HTP Δrrp6, again indicating the relative low peak height in Fft2-HTP.

To identify where Fft2 is recruited on the gene body, a metagene plot profile was calculated based on gene coordinates supplied by pombase.org [Harris et al. 2022]. Hence, a metagene plot between all annotated transcripts is performed (Figure 25) to analyse the global recruitment pattern of Fft2 and the impact of exosome absence.

After normalisation of read count the most striking effect is, that the signal of Fft2-HTP is reduced when compared with the signal level of Fft2-HTP obtained for *Δrrp6* background. Also, the strongest recruitment reduction of Fft2-HTP in *Δrrp6* background is not detected over the tested class of transcript annotations (TSS to TES), but it is recruited upstream and downstream of those annotated regions. This can be interpreted as a possible involvement of Fft2 in promotor and terminator regulation and that Fft2 is not directly involved with the transcription machinery. The plotted class of "transcripts" not just includes protein coding genes but also annotations like ncRNA, protein-coding, LTR, antisense RNA and many more. This suggests that Fft2 is recruited potentially also to non-protein coding transcripts like ncRNA or miRNA, which are included in the class of "transcripts" for which a prominent signal is detected. Finally, it must be emphasized that Fft2-HTP is more likely to be recruited to the 3' end of transcripts, but the general trend, to obtain more reads in 3' direction, is also observed for the untagged control and needs to be critically interpreted.

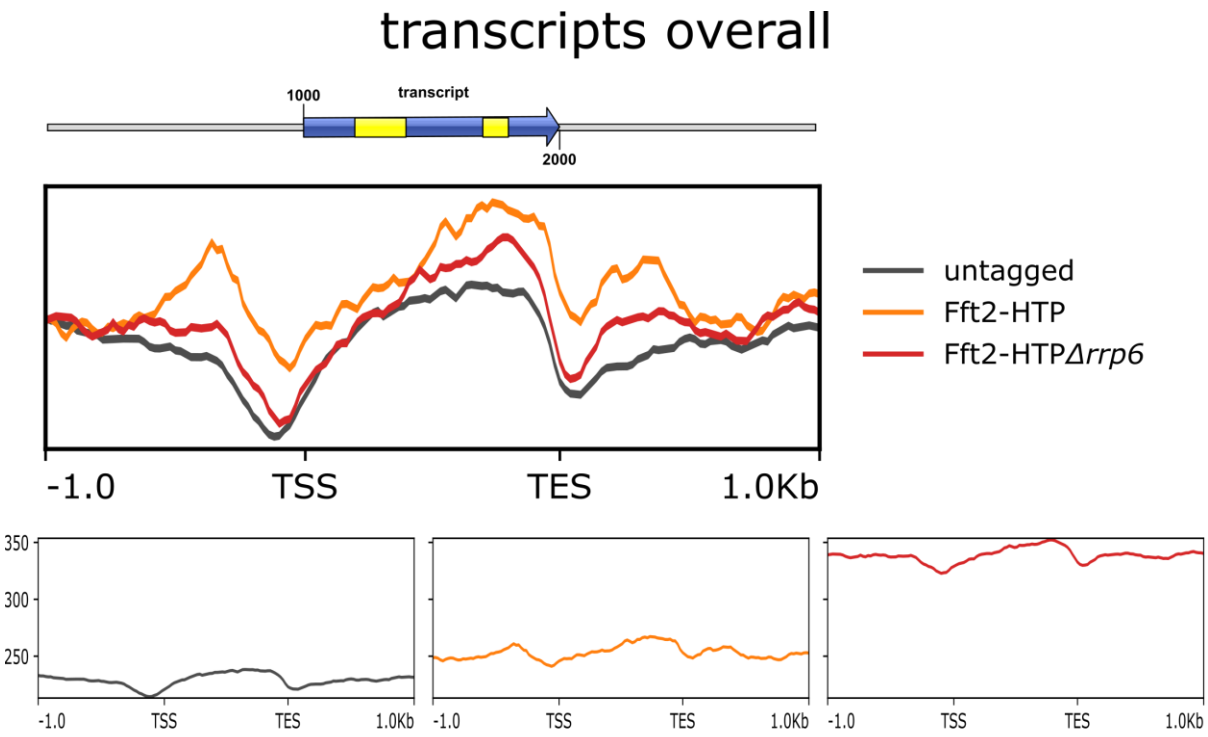


*Figure 25 global repression of Fft2 recruitment to transcript regions*

The representation global Fft2 recruitment is illustrated as metagene plot, processed in galaxy [The galaxy community 2022]. Annotation of transcripts is provided by pombase [Harris et al. 2022] and written in gtf file. Each annotated region is scaled to 1kB, and the upstream and downstream regions of each annotation are analysed. For the combined graph, the individual signal level is normalised to its -1.0kb position. Interestingly, Fft2 is recruited to transcript regions with a 3' skew. Deletion of Rrp6 reduces the overall signal of Fft2-HTP recruitment to chromatin. In addition, Fft2-HTP also recruits to the promoter and terminator of annotated regions (up- and downstream), which also links to the transcriptional machinery.

### 4.7.2 Chromatin enrichment of Fft2 is observed for specific non-coding regions

For a deeper understanding of Fft2 chromatin recruitment at non-coding regions, another superclass of ncRNA is investigated, namely the long terminal repeats (LTR). This class of transcripts are known to be regulated by the Fft2 and Fft3 protein by direct recruitment to chromatin [Persson et al. 2016]. Also, the transcript class of unstable transcripts (XUT, DUT, CUT) that have been detected in RNA metabolism mutants [Atkinson et al. 2018] and the cryptic unstable transcripts are known to be degraded by the nuclear exosome [Zhou et al. 2015] which is the reason for selective analysis of this transcript class.

#### 4.7.2.1 Fft2 is selectively recruited to LTR regions

To analyse Fft2 recruitment over all 251 annotated LTR regions, a metagene plot is used to evaluate the recruitment pattern, while a feature count analysis reveals a more detailed screening of individual LTRs (Figure 26). The feature count analysis accumulates the reads which occurs over a region on chromatin and is compared afterwards between two ChIPseq datasets to analyse possible signal differences. The metagene plot is performed in reference point mode, which plots the signal that surrounds the beginning of each LTR annotation (+1 position) upstream, as well as downstream of the respective start position. Most of the detected reads are located at the LTR start site and flattened at the upstream and downstream regions (Figure 26 Fft2 is recruited to selected LTR regions and is affected negatively in the Δrrp6 backgroundA). A signal reduction is observed in Fft2-HTP *Δrrp6*, which reflects the overall binding loss of Fft2 in *Δrrp6* background (Figure 25). In Fft2-HTP an additional peak around 500bp upstream (-0.5Kb) occurs but is lacking in Fft2-HTP *Δrrp6* background.

While in metagene analysis, a clear enrichment of reads over LTR regions is observed, counting of reads for a specific LTR reveals a split in positively and negatively affected LTRs in *Δrrp6* background (Figure 26 Fft2 is recruited to selected LTR regions and is affected negatively in the Δrrp6 backgroundB). Data points below the black line show higher FC in Fft2-HTP *Δrrp6* strain than for Fft2-HTP and vice versa. 26 LTRs reads are not detected and those are excluded from further analysis. It is noticeable that LTR with an overall count of < 1640 are negatively affected by *Δrrp6,* while LTR with a measured count of > 1640 correlates with a positive feature count tendency. This positive correlation could be due to read normalisation in Fft2-HTP *Δrrp6,* which raises the background level and therefore affects the Fft2-HTP / Fft2-HTP *Δrrp6* ratio of low counted LTR stronger. It´s likely that LTR below a certain feature count level do not recruit Fft2 at all. Nevertheless, when a paired t-test was applied for Fft2-HTP /Fft2-HTP *Δrrp6* datasets, no significant change is observed ($p = 0.058$). A power analysis for the same matrix reveals a level of 0.47, which indicate a lack of data points to observe an

effect as significant (Figure 26 Fft2 is recruited to selected LTR regions and is affected negatively in the Δrrp6 background).

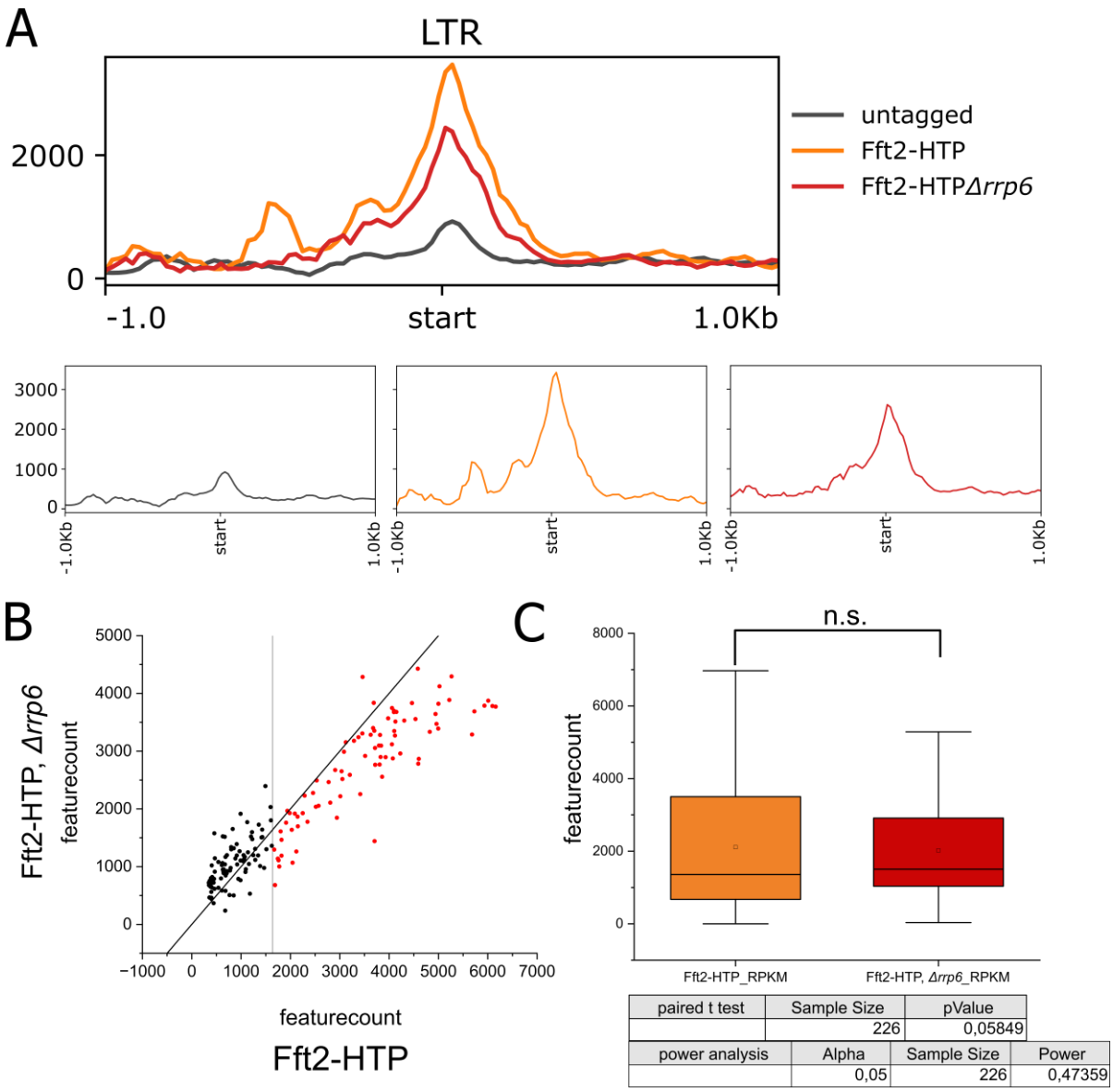


| paired t test | Sample Size | pValue |
|---|---|---|
| | 226 | 0,05849 |

| power analysis | Alpha | Sample Size | Power |
|---|---|---|---|
| | 0,05 | 226 | 0,47359 |

*Figure 26 Fft2 is recruited to selected LTR regions and is affected negatively in the Δrrp6 background*

A) Fft2 recruitment of LTR regions is presented as a metagene plot processed in galaxy [The galaxy community 2022]. The labels of all 251 LTRs were manually written into a gtf file. The metagene plot was processed using the "reference point" method, which reflects the +/- 1kB ChIPseq signal around the annotation start point. Fft2 is strongly recruited to the LTR start site, which is reduced in the Δrrp6 background. In addition, Fft2 is recruited in a very sharp peak upstream of LTR regions, which is lost in the Δrrp6 background. Both suggest an effect of Rrp6 deletion on the efficiency of Fft2 recruitment. B) Feature count comparison of LTR recruitment shows a split into two subpopulations, as shown by the dispersion of the Fft2-HTP and Fft2-HTP Δrrp6 trait enumeration. The intense black line shows the same number of FC between the two strains as a reference. LTRs detected above the black line are analysed with higher feature counts in Fft2-HTP Δrrp6 than in Fft2-HTP, below vice versa. Above a detected feature count of 1641 (vertical black line), most LTRs show reduced Fft2 recruitment in Δrrp6, while a lower feature number

leads to the opposite. This is interpreted as a Δrrp6 normalisation artefact, which is clearly seen in LTRs with reduced or absent Fft2-HTP recruitment. C) The statistical difference between both strains is probed by a paired t-test which reveals no significant change in Fft2-HTP recruitment in the Δrrp6 background (p =0.058). This lack of significance is likely due to the Δrrp6 normalisation artefact visible in the scatter plot. The power analysis provides a result of 0.47, which means a 53% chance of missing a significant effect (false negative).

In summary, Fft2 is recruited to LTR regions, and this recruitment is negatively affected by *Δrrp6.* While the recruitment to LTR regions is merely reduced in Fft2-HTP *Δrrp6,* a smaller peak signal in the upstream region is completely lost. It is also demonstrated that deletion of Rrp6 affect the Fft2-HTP recruitment on bound LTR´s negatively, but in this experimental setup, no significant effect of *Δrrp6* on Fft2 recruitment is found.

#### 4.7.2.2 Regions of DUT and CUT transcripts recruit Fft2 which is impaired by *Δrrp6*

Besides LTR, unstable transcripts are another class of ncRNA, which are targeted by various RNA degradation pathways in *S. pombe* [Atkinson et al. 2018]. Like the performed analysis for genomic transcript annotations and LTRs, the binding pattern of Fft2-HTP is analysed for DUT (dicer unstable transcript), CUT (cryptic unstable transcripts) and XUT (Xrn1 unstable transcripts) is verified by metagene analysis (App. figure 4). The metagene plot is calculated for the centre of the respective region with 1Kb upstream/downstream to catch binding patterns in the direct region of unstable transcripts. In comparison with LTR, much fewer reads are counted for unstable transcripts overall. Additionally, a clear recruitment pattern is missing for Fft2-HTP, as well as for Fft2-HTP in *Δrrp6* background and obtained signal mimics a "random walk". Therefore, no global recruitment of Fft2 to regions unstable transcripts is detected, but for individual annotations recruitment of Fft2 is evaluated (App. figure 4).

As no recruitment pattern is recognisable by metagene analysis, the number of reads over the respective annotations is analysed in a similar way to the LTR analysis. Calculated feature counts evaluated for the Fft2-HTP strain are plotted against Fft2-HTP *Δrrp6* background for each class of unstable transcript and, as well, in respective violin plots (Figure 27). It is to state that the most annotated transcripts are found for CUTs (2732) when compared with DUT (1392) or XUT (1116), which is reflected by smaller datapoint clouds. The colour of the data points is determined according to the ratio between the number of features of Fft2-HTP and Fft2-HTP *Δrrp6.* The overall feature count ratio calculated for XUTs is lower, than for CUTs and DUTs (Figure 27 A). Interestingly, the feature counts of annotated CUTs and DUTs show a lot more regions with high feature counts in the Fft2-HTP strain in contrast to XUT

annotations, which was not expected on basis of the performed metagene analysis (App. figure 4).

A student's t-test is applied to the entirety of dataset of feature counts and the distribution is displayed in violin plots (Figure 27). As a result, very significant differences between untagged control and Fft2-HTP are calculated for CUT (p-value=$5.1*10^{-37}$) and DUT (p-value=$1.6*10^{-13}$) but not for XUT (p-value=0,72). These very significant p-values must be related to the absence of an applied relative normalisation. As a result, these significance levels may not represent the actual signal differences between WT, Fft2-HTP and Fft2-HTP *Δrrp6* samples. When the Fft2-HTP feature counts are compared for each individual annotation with Fft2-HTP *Δrrp6*, a very significant effect of Rrp6 deletion is monitored for CUT (p-value=$1,7*10^{-41}$) and as well for DUT (p-value=$4,2*10^{-12}$). The feature count ratio of XUT annotations between Fft2-HTP with Fft2-HTP *Δrrp6* show no significant difference between both data sets (p-value=0,81).

The analysis of unstable transcripts reveals that Fft2 is recruited at selected cryptic unstable transcripts (CUT) and dicer unstable transcript (DUT) sites, while for Xrn1 unstable transcripts (XUT) no recruitment of Fft2 could be verified. Also, *Δrrp6* reduces the recruitment of Fft2 significantly at these genome regions.

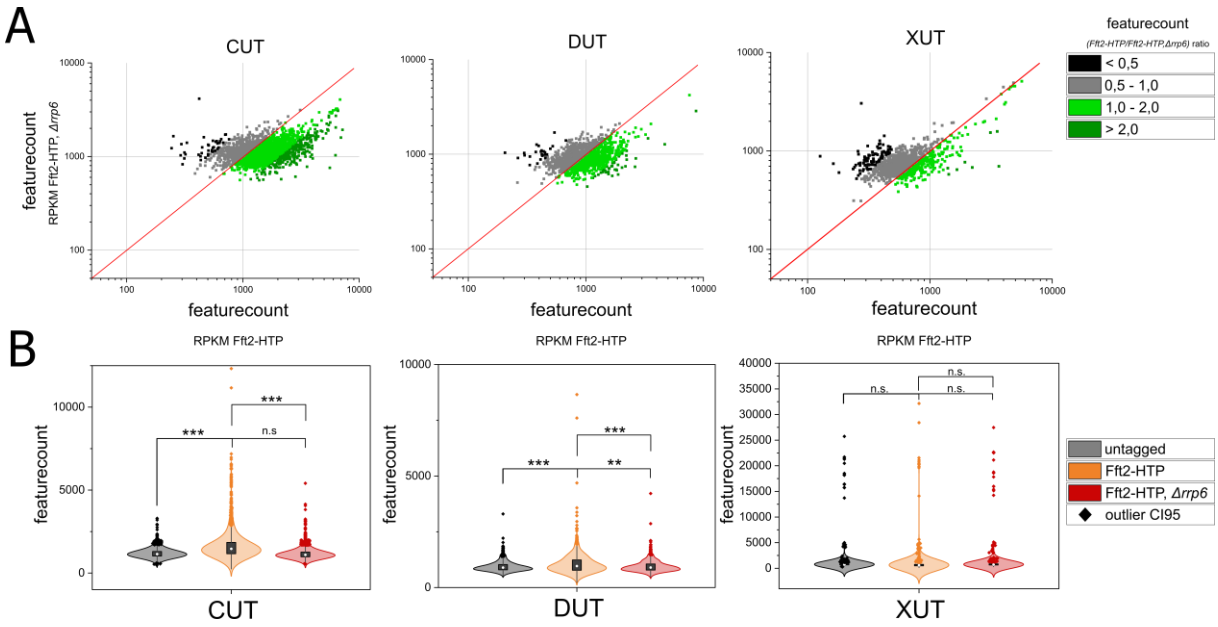


*Figure 27 feature count analysis demonstrates significant enrichment of Fft2 for DUT and CUT*

A) feature count scatter plot of individual unstable transcripts annotations of LTR recruitment unravel different recruitment between the Fft2-HTP and Fft2-HTP Δrrp6 strain. The red line shows the same number of features between the two strains for a single transcript annotation. The colour indicates the respective ratio calculated between Fft2-HTP and Fft2-HTP *Δrrp6* while green shows higher detected counts in Fft2-HTP, black and grey represent higher detected count in Fft2-HTP *Δrrp6*. While for CUT, the majority of annotations feature count is higher in Fft2-HTP, DUT feature count shows equal amounts of positive and

negative affected annotations in *Δrrp6* background. XUT transcripts show more higher abundancy for higher detected counts in Fft2-HTP than *Δrrp6*. B) violin plot of detected counts for respective unstable transcript class illustrates the variation between untagged, Fft2-HTP and Fft2-HTP *Δrrp6*. The significance of variation is analysed by student t-test (* < 0.05, ** < 0.01, *** < 0.001). For CUT very significant effects are observed for Fft2-HTP over untagged (p-value: $5.09*10^{-37}$) and Fft2-HTP over Fft2-HTP *Δrrp6* (p-value: $1.67*10^{-41}$). For DUT significant difference is calculated between untagged and Fft2-HTP (p-value: $1.61*10^{-13}$ ) as well as Fft2-HTP *Δrrp6* (p-value: 0.0027), but also between Fft2-HTP and Fft2-HTP *Δrrp6* (p-value: $4.24*10^{-12}$ ). For XUT no significant change is observed.

### 4.7.3 Recruitment to chromatin is affected in Mtl1-1 mutant in LTR regions

While I could prove that Fft2 is recruited to ncRNA regions of chromatin, especially DUT, CUT and LTR, and in addition this recruitment is negatively affected by *Δrrp6*, the principle of its recruitment remains unclear.

To unravel the mechanism of chromatin recruitment, Fft2 binding is analysed for LTR regions (exemplary *LTRC.50*) and classic exosome-regulated transcript regions (exemplary *mei4*) in a background of MTREC mutants *mtl1-1* and *Δmmi1* (Figure 28 A). As previously demonstrated by ChIPseq analysis, Fft2-HTP is highly recruited at the LTR region, while MTREC components are not present. As expected, deletion of the DSR-binding protein Mmi1 is not affecting Fft2-HTP recruitment at a significant level. Instead, *mtl1-1* mutation shows a strong effect on Fft2-HTP recruitment at the *LTRC.50* region, which demonstrates the involvement of the MTREC complex in the process of Fft2 recruitment, while no significant recruitment of the MTREC components itself could be observed in this experimental setup.

To illustrate if Fft2 deletion influence the recruitment of MTREC complex at exosome target genes vice versa, Mmi1-HTP and Mtl1-HTP recruitment to *mei4* is compared with *Δfft2* background (Figure 28 B). Interestingly, *Δfft2* is not affecting Mmi1 or Mtl1 recruitment at *mei4*, while *Δmmi1* and *mtl1-1* in Fft2-HTP background significantly reduced Fft2-HTP recruitment at exosome-regulated gene regions.

Overall, the comparison of deletion mutants reveals that *mtl1-1* leads to a loss of Fft2 recruitment on its specific target sites, while *Δmmi1* just affects Fft2-HTP recruitment at exosome target genes. The loss of Fft2 binding over LTR regions in an *mtl1-1* strain background is not depending on a direct recruitment of the MTREC complex, which suggest a recruitment impairment via MTREC which does not require interaction at the chromatin site. On the other hand, Fft2 deletion doesn't affect the recruitment of MTREC complex on exosome target sites like *mei4* but the occurrence of MTREC is necessary for Fft2 detection by ChIP experiment.

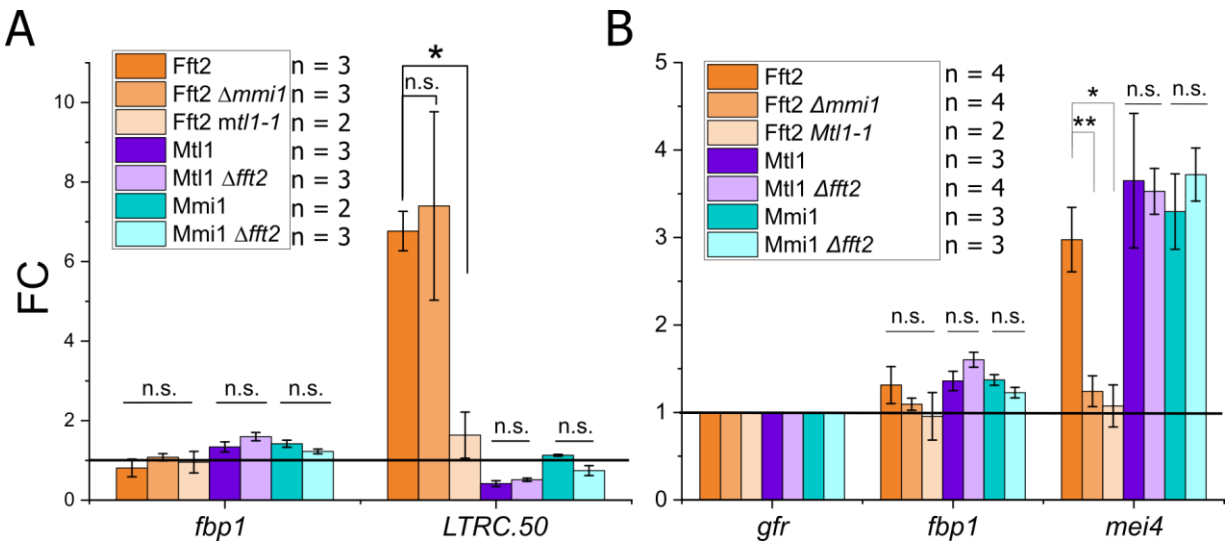


*Figure 28 Impairment of Fft2 recruitment is driven by MTREC core protein Mtl1*

The ChIP signal of HTP tagged strain is detected by qPCR with region-specific primers. The ΔΔcT signal is calculated by normalising the ChIP signal to the respective input, and the foldchange (FC) is calculated via a gene-free region (GFR = FC 1). Fbp1 as a metabolic gene (fructose-1,6-bisphosphatase) serves as a control region. Statistical significance is calculated using Student's t-test (* < 0.05, ** < 0.01), and SEM is shown as error bars. Fft2-HTP, Mtl1-HTP and Mmi1-HTP are tested for their recruitment to A) LTRC.50 and B) mei4 with corresponding deletions and *fbp1* normalisation. In general, *Δfft2* does not affect the recruitment of Mtl1 or Mmi1 at all. Instead, Δmmi1 and mtl1-1 mutants significantly impair Fft2 recruitment at *mei4*, while at the LTR region only mtl1-1 shows a reduction in Fft2-HTP recruitment. Remarkably, this effect occurs without recruitment of Mtl1-HTP to LTR regions. A) general n=3, Fft2-HTP Mtl1-1 and Mmi1-HTP n=2; B) Fft2-HTP, Mtl1-HTP *Δfft2*, Fft2-HTP *Δmmi1* , n=4; Mtl1-HTP, Mmi1-HTP, Mmi1-HTP *Δfft2*, n=3; Fft2-HTP *Δmtl1-1*, n=2

### 4.7.4 RNase-reduces Fft2 chromatin recruitment on specific target regions

While a novel RNA binding activity of Fft2 and Fft3 is demonstrated before (Figure 22), a systematic analysis of this function is still lacking for the Fft paralogues. To validate whether the RNA binding activity of Fft2 is affecting its chromatin recruitment ability, chromatin immunoprecipitation is performed with and without RNase treatment and the recruitment is compared to untreated ChIP sample (Figure 29). In regions where the Fft2 binding is strongly reduced in a *Δrrp6* background, for example LTRC.50 (Figure 28 A) and ncRNA.5066 (Figure 28 B), which is annotated as DUT [Atkinson et al. 2018]. In regions with low Fft2-HTP ChIP signal, where *Δrrp6* has a mild (*mei4*) or no measurable effect on Fft2 recruitment (*ssa2*), no significant change in recruitment could be observed after RNAse treatment. One possible interpretation from this experiment is, that RNA as well as the exosome are relevant for the recruitment of Fft2. It must be stated, that the experiment is not able to unravel the question if RNA and the exosome are both necessary to maintain the Fft2 recruitment *in vivo*.

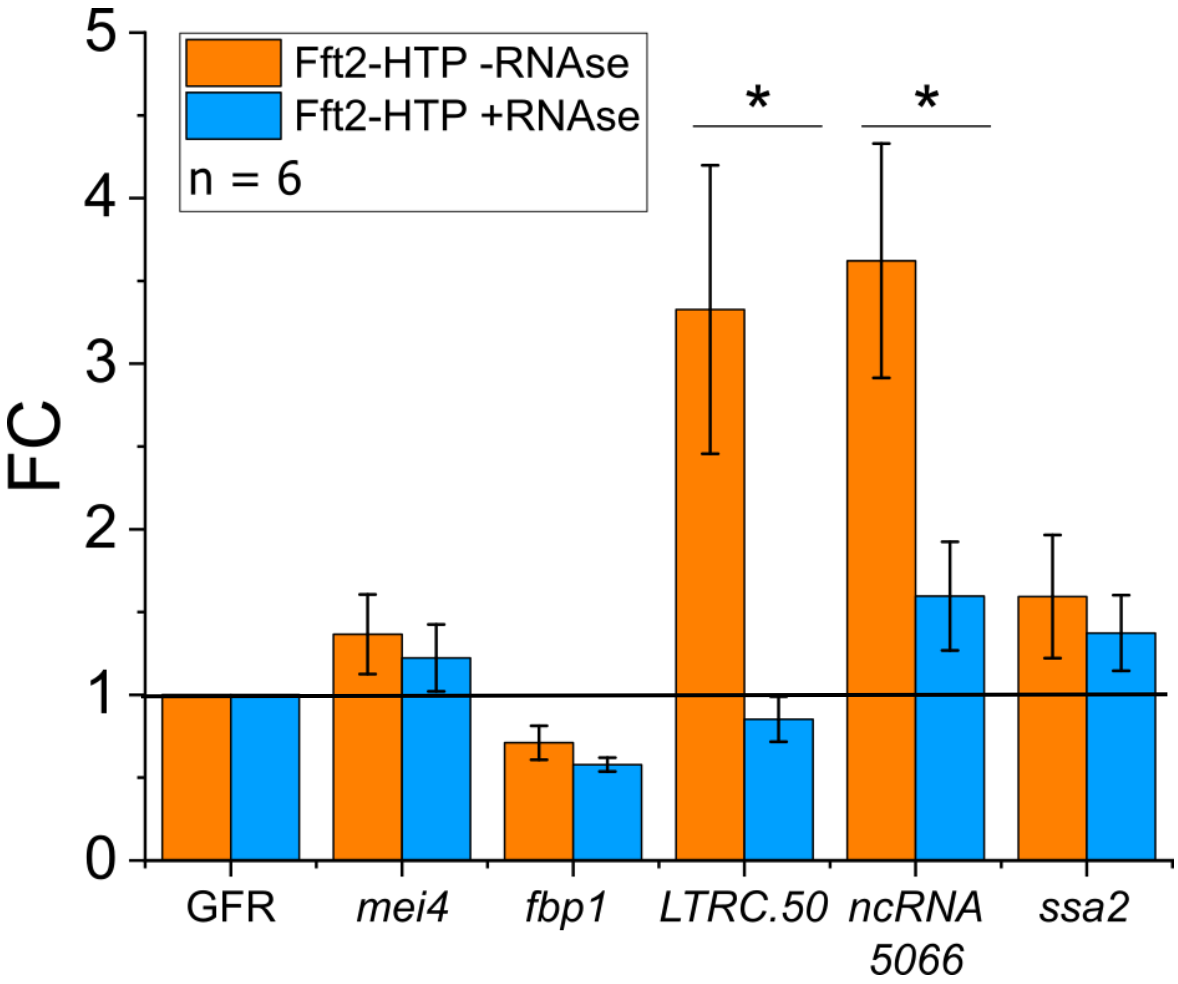


*Figure 29 chromatin recruitment of Fft2-HTP relies on RNA presence*

The ChIP signal is detected by qPCR with region-specific primers. The tested regions are manually selected from ChIPseq with high peak signal for Fft2-HTP, while Ssa2 shows unaffected Fft2 recruitment in the Δrrp6 background. The ChIP signal ΔΔcT is calculated by normalising cT to the respective input, followed by foldchange (FC) calculation over a gene-free region (GFR = FC 1). Fbp1 as metabolic gene (fructose-1,6-bisphosphatase) serves as control region. Statistical significance is calculated using Student's t-test (* < 0.05), and SEM is shown as error bars. Fft2-HTP ChIP lysate is treated with 2 µl RNase mix for 30min at 37°C prior to immunoprecipitation. The -RNase sample is incubated under same conditions without RNase mix. A significant effect is observed only for LTRC.50 and ncRNA.5066, while the overall signal of Fft2-HTP is reduced compared with Figure 28. n = 6

### 4.7.5 Truncation of Fft2 protein does not impair chromatin recruitment

The Fft2 recruitment to chromatin is investigated in this study, but a model for recruitment is still missing. The C-terminal truncations, which maintain their RNA binding characteristics (Figure 23) are therefore tested for their chromatin recruitment (Figure 30). Surprisingly, all three tested truncations maintain their recruitment at LTRC.50 region, as verified by ChIPseq. It is to conclude, that the N-terminal extension is still recruited to the chromatin, without a known DNA binding domain. The hypothesis that the N-terminal extension is bound by the exosome complex must be rejected, since the central exosome components have a significant

influence on the recruitment of Fft2 but are not recruited to the LTR regions at all. (Figure 25,Figure 28).

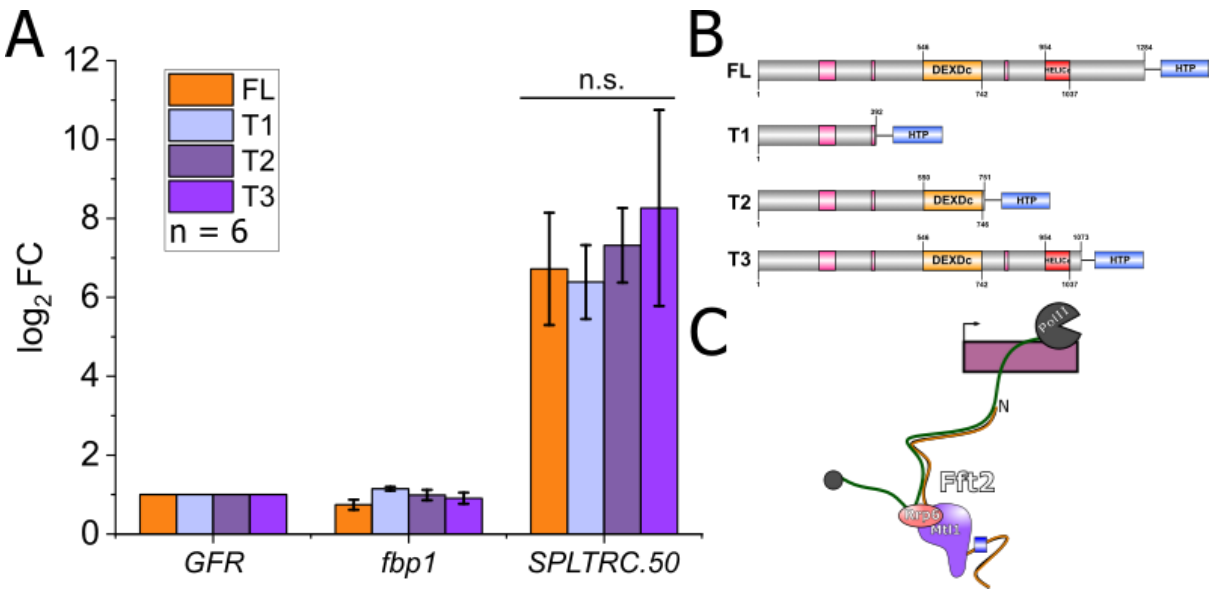


*Figure 30 Fft2 truncations maintain chromatin recruitment*

A) The ChIP signal is detected by qPCR with region-specific primers. The ΔΔcT signal is calculated by normalising the ChIP signal to the respective input, and the foldchange (FC) is calculated via a gene-free region (GFR = FC 1). Fbp1 as a metabolic gene (fructose-1,6-bisphosphatase) serves as a control region. Statistical significance is calculated using Student's t-test (* < 0.05), and SEM is shown as error bars. Full length Fft2 (FL) recruitment is compared against the C-terminal truncations and probed for their recruitment at LTRC.50 chromatin region. In general truncations of Fft2 remain their chromatin recruitment ability at LTR regions. n = 6 B) schematic overview of truncations (T1-T3) in contrast to full length (FL) Fft2 C) The hypothetical model of Fft2 recruitment is therefore that Mtl1 forms a complex with exosome and the N-terminal region of Fft2 which leads to the recruitment at chromatin region.

## 4.8 Deletion of Fft2 is not affecting heterochromatinization or histone variants

Fft2 and Fft3 are known to function as ATP-dependent heterochromatin remodeler and have been shown to negatively regulate retrotransposon activity by being recruited to long terminal repeats (LTR) [Persson et al. 2016]. Because of the known function, the involvement of Fft2 in heterochromatin maintenance and nucleosome assembly is analysed in the following section.

### 4.8.1 Fft2 is not involved in heterochromatin maintenance

Some exosome target genes, including the meiotic genes *ssm4* and *mei4*, are subject to facultative heterochromatinization [Zofall et al. 2012] as part of exosome-dependent gene regulation. Additionally the SMARCAD1-family member SMARCAD1 and Fft3 are known to establish and maintain heterochromatin [Rowbotham et al. 2011; Strålfors et al. 2011; Steglich

et al. 2015] , so a functional link of Fft2 to heterochromatin maintenance is possible, but is not experimentally demonstrated so far (inferred from sequence ontology [Harris et al. 2022]).
To analyse the methylation status of different chromatin regions, chromatin immunoprecipitation (ChIP) with α-H3 and α-H3K9me2 is performed (Figure 31 A). The calculated ratio between H3/H3K9me2 indicates the percentage of demethylated H3 that is presented in heterochromatin. In a WT strain (YPLV144), highly transcribed genes like *adh1* do not contain heterochromatin, *dg* repeats as part of centromeric repeat regions instead are highly methylated. Selected exosome target genes *mei4* and *ssm4* show H3K9me2 modification which considers facultative heterochromatin. To evaluate the specificity of the signal, *Δclr4* strain (YPCK520) is included. Clr4 is part of the CLRC complex and the only H3K9 methyltransferase present in *S. pombe*. It´s deletion leads to complete absence of H3K9 methylation. However, H3/HeK9me2 ChIP of *Δfft2* strain does not show a change of steady state methylation pattern. This is true for euchromatin (*adh1*), constitutive (*dg*) and facultative (*mei4*|*ssm4*) heterochromatin regions. Deletion of fft2 has no observable effect on H3K9 dimethylation of chromatin regions, neither positive nor negative (Figure 31 A).
To validate, if the chromatin recruitment of Fft2 does rely on the presence of the CLRC complex, a ChIP with IgG-agarose beads is performed for Fft2-HTP (YPCK9) and Fft2-HTP *Δclr4* (YPCK520) (Figure 31 B). *Fbp1* as a metabolic control gene is tested and shows no enrichment of Fft2-HTP over its gene region. *Mei4* is an exosome target gene that contains facultative heterochromatin and is bound by Fft2-HTP when compared with *fbp1.* In addition, this recruitment is not affected by *Δclr4* and therefore Fft2 chromatin recruitment is not impaired by *Δclr4* and the missing H3K9me2 modification is also not repelling Fft2-HTP from its target genes.

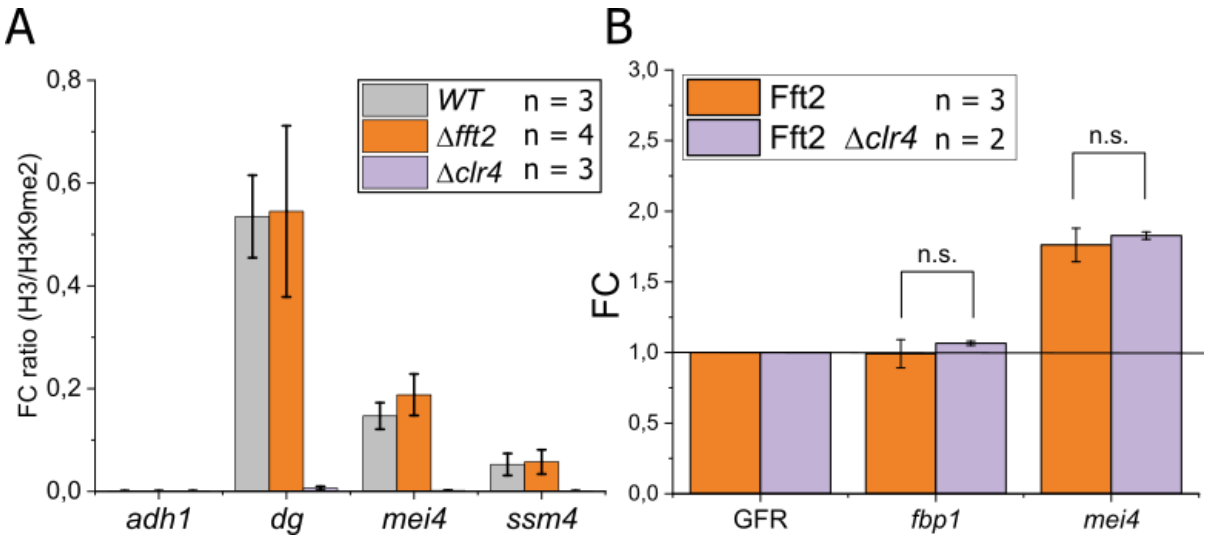


*Figure 31 Fft2 is not involved in facultative and constitutive heterochromatin maintenance and its recruitment is not affected by the heterochromatin machinery*

A) The methylation status of gene regions detected by qPCR of H3 and H3K9me2 antibody ChIP with region-specific primers The experiment is performed by Dr. Birte Keil. The fold change is calculated by normalising the ChIP signal to the respective input, and the fold change ratio (FC ratio) is calculated by dividing H3 by the obtained H3K9me2 cT. A ratio of 1 means that 100% of the H3 contains the heterochromatin tag H3K9me2 in a given region. adh1 as a metabolic gene (alcohol dehydrogenase) serves as an unmethylated control region. The SEM is shown as an error bar. The absence of Δclr4 leads to a complete loss of heterochromatin, as shown. The deletion of Fft2 itself has no effect on the formation and maintenance of facultative and constitutive heterochromatin. WT (YPLV144), *Δclr4*, n = 3; Δ*fft2,* n = 4

B) The ΔΔcT signal is calculated by normalising the ChIP signal to the respective input, and the foldchange (FC) is calculated over a gene-free region (GFR = FC 1). *Fbp1* as a metabolic gene (fructose-1,6-bisphosphatase) serves as a control region. Statistical significance is calculated using Student's t-test (* < 0.05), and SEM is shown as an error bar. Recruitment of Fft2 is unchanged in facultative heterochromatin regions by *Δclr4*. Fft2-HTP, n = 3; Fft2-HTP *Δclr4*, n=2

### 4.8.2 Occurrence of histone variant Pht1 mildly effects Fft2 recruitment

Beside of the described involvement of Fft2 orthologues in the heterochromatin maintenance, a nucleosome assembly activity for SMARCAD1 was described recently [Markert et al. 2021]. While *S.pombe* does not contain a lot of histone variants, Pht1 (H2A.Z orthologue [Carr et al. 1994]) is known to be involved in heterochromatin restriction and chromatin stability in the meiosis process [Kim et al. 2009]. Because Fft2 shows links to meiosis affection in *S. pombe* (Figure 13, Figure 14) the hypothesis arose that Fft2 is needed for histone exchange process like it is described for its paralogue Fft3 [Taneja et al. 2017]. The incorporation of the histone variant H2A.Z (*S. pombe* orthologue: Pht1) is also relevant to control antisense transcript level and is connected to the exosome subunit Rrp6 [Zofall et. al., 2009]. To verify if Fft2 is involved in histone exchange between Pht1 and H2A, ChIP experiment are performed for Fft2-HTP (YPCK9) and Pht1-HTP (YPCK552) which are then compared with respective deletions *Δfft2*/Pht1-HTP (YPCK543) and *Δpht1*/Fft2-HTP (YPCK551) (Figure 32). While over *fbp1* region no relevant enrichment is detected, analysis of *mei4* level reveals a weak enrichment of Fft2

as well as Pht1. The regions which are additionally analysed, are detected in ChIPseq by manual screening with eye mark on regions with high Fft2-HTP enrichment (discussed in chapter 4.7). A selection of chromatin regions for coding transcripts (*SPBC32H8.15*), non-coding transcripts (*nc-tgp1*) and long terminal repeat (*LTRB.35*) are displayed. Despite previous screening, *SPBC32H8.15* shows only weak Fft2-HTP recruitment, whereas clear Fft2-HTP recruitment is evident for *nc-tgp1* and *LTRB.35* which is implied from other experiments in this study. Pht1 is instead just found in low amounts at *mei4* gene site and mediocre recruitment at the region of *nc-tgp1*. Cautious interpretation of these results suggests no correlation between Fft2 presence at a given region and the H2A variant Pht1. However, when the regular strains are compared with the corresponding deletions *Δfft2* and *Δpht1*, it is evident that a deletion of Fft2 has no effect on the occurrence of Pht1 at the tested regions. However, a deletion of Pht1 has an observable effect on the Fft2 recruitment at the given regions. At *mei4* and *nc-tgp1* sites, *Δpht1* reduces the Fft2 recruitment while the deletion enhances the Fft2 recruitment for *SPBC32H8.15* and *LTRB.35*. Interestingly, the underlying data suggest that a *Δpht1* background results in enhanced Fft2 enrichment at regions with low Pht1 presence, while deletion of Pht1 reduces the Fft2 recruitment at sites which holds a relevant amount of Pht1. However, the sparse data do not allow further speculation on the effect of *Δpht1* on the chromatin recruitment of Fft2, but deeper investigations are indicated to reveal the connection between Pht1 and Fft2.

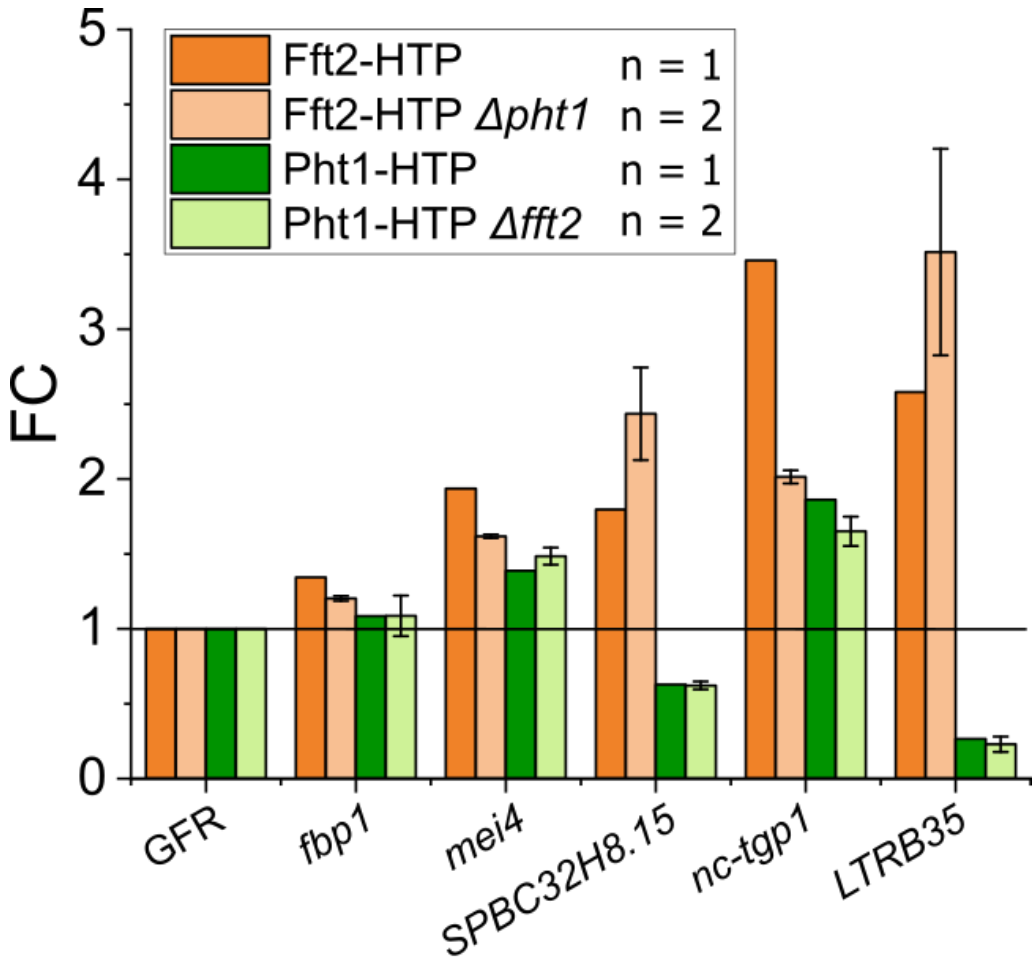


*Figure 32 Deletion of histone variant Pht1 inconsistently affects Fft2 recruitment*

The ChIP signal is detected by qPCR with region-specific primers. The tested regions are manually selected from ChIPseq with high peak signal for Fft2-HTP. The ΔΔcT of signal is calculated by normalising the ChIP signal to the respective input, and the foldchange (FC) is calculated via a gene-free region (GFR = FC 1). Fbp1 as a metabolic gene (fructose-1,6-bisphosphatase) serves as a control region. Because of lacking sample size for Fft2-HTP and Pht1-HTP, no statistical significance is calculated. Occurrence of Fft2 is not correlating with Pht1 (compare *mei4* with *LTRB.35*). While deletion of Fft2 in a Pht1-HTP background (light green) doesn't affect its recruitment, a vice versa strain (light orange) instead seems to affect Fft2 recruitment. With low relative Pht1 abundancy at region, Fft2-HTP in *Δpht1* background tends to increase its recruitment ability, while in regions with high Pht1 occurrence, Fft2 recruitment to chromatin is reduced. Fft2-HTP, Pht1-HTP, n = 1; Fft2-HTP *Δpht1*, Pht1-HTP *Δfft2*, n = 2

# 5 Discussion

The primary objective of this study was to investigate the functional characteristics of Fft2 as member of the SMARCAD1 family in *S. pombe*. Through a combination of comp. RIC, RNAseq, ChIP and ChIPseq, as well as CLIP experiments it has been demonstrated that Fft2 and Fft3 are novel direct RNA binding proteins (Figure 22), which has not been shown before for the *S.pombe* orthologues of the human SMARCAD1 protein. Also, the deletion of Fft2 enhances spore formation (Figure 13) and shows involvement in Mtl1-dependent complex formation (Figure 17).

Deletion of Fft1 or Fft2 results in minor changes of the transcriptome (Figure 19), but without a direct effect on transcript level of typical meiotic RNA transcripts, whose steady state expression is prevented by exosomal degradation. This could suggest a potential non-transcript wise regulation of meiosis by *Δfft2* (Figure 21).

A chromatin recruitment of Fft2 is observed at non-coding chromatin sites and this characteristic is affected by the RNA exosome, MTREC and RNA occurence (Figure 25, Figure 26, Figure 28).On the other hand, the deletion of Fft2 does not affect the recruitment of the exosome target complex to its specific targets (Figure 28 B), whereas on the contrary *Δrrp6* and *mtl1-1* but not *Δmmi1* impair the recruitment of Fft2 to its LTR and unstable transcript regions, while the function of Fft2 at these sites is still unclear (Figure 31, Figure 32, Figure 19).

Nevertheless, Fft2 and Fft3 seem to have different functions in stress response (Figure 9) and their accumulation on RNA in exosome mutant backgrounds (Figure 8) is clearly different, which implies a functional divergence between Fft3 and Fft2 which has not yet been determined. Surprisingly the N-terminal end is capable to maintain the newly found RNA binding activity (Figure 23, Figure 30) which implies that the N-terminal domain, which weakly conserved between the orthologues ( Figure 11), could be the main factor of the functional differentiation within the SMARCAD1-family.

## 5.1 Orthologues of the Fft – family response differently to environmental stress

The SNF-ATPase superfamily is widely known to be involved in the cell stress response. SMARCAD1 is involved in DNA double-strand resection following DNA damage [Chakraborty et al. 2018; Bantele and Pfander 2019] and promotes metastasis in breast cancer cells [Al Kubaisy et al. 2016]. While various forms of DNA damage response in the SMARCAD1 family

have been widely described, including FUN30 [Maurya et al. 2022], environmental stress factors such as hypoxia, heat stress, or malnutrition have not been investigated.

As hypothesized from published data [Mukherjee et al. 2016; Higuchi et al. 2018], an increased pH resistance in exosome mutants should correlate with upregulation of iron metabolism transcripts [Mukherjee et al. 2016]. Interestingly, *Δfft2* show comparable pH resistance (Figure 7), but does not affect transcript levels of iron metabolism transcripts (Figure 19, App. table 1), suggesting that pH resistance is likely due to other regulatory mechanisms. The largest transcriptional changes in *Δfft2* are often associated with cellular detoxification (e.g., SPAC750.01, FC: -2.46; SPAC186.07c, FC: +2.29) (App. table 1), suggesting the deletion of Fft2 is associated to a change in cellular stress response. Whereas pH stress, unlike other environmental stress, does not affect transcription rates but provides stabilization of the corresponding mRNAs [Canadell et al. 2015]. Enhanced growth of exosome mutants is likely due to impaired RNA degradation and therefore results in RNA stabilization before cells were exposed to the toxic environment. Whether increased RNA stabilization for corresponding RNAs under high pH conditions is the reason for the higher resistance of Fft2 is difficult to say from the transcriptomic data, as these are generated at neutral pH. Another explanation for the enhanced growth of *Δfft2* strains at high pH could be the adapted expression of transcripts involved in cellular detoxification, leading to better overall cell survival. The direct involvement of Fft2 in the complex formation of Mtl1 (Figure 17) is another hypothesis where Fft2 possibly alters the exosome through protein-protein interaction, which needs more evidence of Fft2/MTREC interaction under environmental stress response.

Another common environmental stress is exposure to extreme temperatures (Figure 9). Thermal stress management is studied in *S. pombe* in a variety of fields [Glatz et al. 2016] and is used to screen for temperature-sensitive phenotypes that are characterised by reduced cell population growth at high or low temperatures. For example, the exosome mutant *dis3-54* shows reduced growth at low temperature compared to wildtype Dis3 [Kinoshita et al. 1991] and the Rrp6 mutant *rrp6-ts32* shows impaired growth at high temperature [Shichino et al. 2018]. Based on this established screening method, deletions of Fft1, Fft2, and Fft3 are compared at low (16°C) and elevated temperature (37°C) to compare the cellular response of these three deletion strains (Figure 9). Growth at various temperatures shows different phenotypes of the three paralogs. The enhanced growth compared to the corresponding WT strain at 16 °C is observed only for *Δfft1* and *Δfft2* strains, while *Δfft3* shows a severe growth defect at cold and elevated temperatures. This growth characteristic stands out, as most temperature-sensitive *S. pombe* mutants show an overweighting of growth-reduced strains at cold temperatures [Harris et al. 2022]. A heat stress investigation, published in 2003 [Chen

et al. 2003], demonstrate that for the gene expression of Fft1, Fft2 and Fft3 no remarkable change is observed. This could imply a downstream alteration of the translated Fft3 protein in the response to heat stress (39° in [Chen et al. 2003]). While decreased cell population growth at low temperatures (FYPO:0000080) is widely investigated in *S. pombe*, increased cell population growth at low temperatures (FYPO:0005260) is a uncommon characteristics of protein deletions in *S. pombe* [Harris et al. 2022]. Especially for the SMARCAD1 family, Fft2 and Fft1 show this unique characteristic compared to Fft3. This difference in growth demonstrates a functional distinction between the Fft family members present in *S. pombe*, clearly showing that it is not a matter of gene duplication but that they apparently serve different functions within the cell.

## 5.2 Spore formation is enhanced in a *Δfft2* strain

The process of meiosis is triggered in *S. pombe* upon nitrogen starvation [Egel 1971] and leads to genetic recombination and eventually to the formation of ascospores [Tanaka and Hirata 1982]. Meiotic transcripts are negatively regulated by the nuclear RNA exosome [Zhou et al. 2015; Shichino et al. 2020], and it is already known that exosome deficiency leads to altered meiosis progression (e.g. [Harigaya et al. 2006; Yamashita et al. 2013]). Since Fft2 accumulates on RNA in exosome mutants (Figure 8), the effect of *Δfft2* on ascospores formation and chromosome segregation in meiosis was tested (Figure 13, Figure 14). Surprisingly, sporulation is enhanced in the *Δfft2* background compared to a corresponding h90 WT. This result was also confirmed by iodine staining indicating a higher number of ascospores in Δfft2 after 48 hours (Figure 14). The initiation of meiosis is controlled by the recruitment of several proteins to the meiotic outer plug [Ohtsuka et al. 2022]. Spo15 mainly drives this process, which is essential for spindle pole formation. Spo15 is indeed affected by Fft3 [Lee et al. 2017], suggesting that Fft2 could also act as an interacting partner or is involved in the regulation of other spindle pole body proteins, such as the Rab-like GTPase Ytp2 and Ytp3 [Imada and Nakamura 2016], which may cause the enhanced meiosis initiation. Whether Fft3 also affects meiosis initiation was not investigated in this work but given the enhanced growth of Fft2 at cold temperatures (Figure 9), diversified overall cell growth can be considered, because meiosis progression experiments was performed at 25°C on ME plate. Nevertheless, accelerated spore formation in *Δfft2* does not lead to increased miss-segregation of chromosomes (Figure 13), suggesting that Fft2 is involved in meiosis initiation but not in its later stages and in the formation of ascospores. This result is consistent with the non-overlapping RNAseq targets between nuclear RNA exosome mutants and *Δfft2* (Figure 21). Interestingly, transcripts involved in meiosis are both upregulated (*SPBC19C7.04c,*

*mug108, mei3*) and downregulated (*rec7, spo4, omt3*), suggesting that Fft2 has no clear influence on the overall meiosis transcript level. Mei3 indeed is known to inactivate Mei2 through PAT1 regulation [Yamashita et al. 2017] and dephosphorylated Mei2 hinders the activity of the Mmi1 exosome complex [Harigaya et al. 2006]. Therefore, upregulation of Mei3 in a *Δfft2* strain should increase sporulation activity in theory. On the other hand, Rec7 is described as an early phase meiosis protein that strongly influences meiosis progression [Molnar et al. 2001], and it´s downregulation in *Δfft2* background should negatively affect meiosis. Therefore, the enhanced meiosis initiation cannot be explained by the obtained total RNAseq data. It should be mentioned that these results depend on an RNAseq experiment in which mitotically grown cells were analyzed and therefore a *Δfft2* effect observed in meiotic cells could be missing. Also, other regulatory mechanisms could affect the translational rate of these of DEG, whose effects cannot be discussed here.

Based on the observed nuclear exosome connection for chromatin recruitment of Fft2 (Figure 30) as well as its involvement in the MTREC exosome targeting complex (Figure 17), it is likely that regulation of Fft2 is only relevant in cells undergoing the meiosis transition.

## 5.3 N-terminal extension of Fft2 is sufficient for RNA binding

While direct histone and DNA binding ability has been described for the SMARCAD1 family [Tong et al. 2020; Markert et al. 2021], the results of this work prove direct binding of RNA (Figure 22). This new function was already indicated by RIC in exosome mutants (Figure 8) [Kilchert et al. 2020] and could now be validated by CLIP experiments. It should be noted that these experiments were performed on cells in mitotic phase, where the full functional potential of Fft2 cannot be captured. Following the indication of Fft2 as a repressor of sporulation, the RNA binding ability could be an interesting anchor for further experiments in meiosis stage.

So far, it is still unclear whether Fft2 modulates exosome activity through its RNA-binding property. The MTREC component Mmi1 [Harigaya et al. 2006; Shichino et al. 2014; Kilchert et al. 2015] is a well-known transcript specific [Yamashita et al. 2012] RNA-binding protein, which is essential for targeting the exosome complex to meiotic RNA. In addition, my experimental data provide direct evidence for the RNA-binding ability of Mtl1 (Figure 22), which is consistent with the findings of the well-studied *S. cerevisiae* orthologue MTR4 (tRNA binding capability) [Wang et al. 2008; Harris et al. 2022].

No functional involvement of this RNA-binding activity in exosome-dependent regulation could be observed in this work. While Fft2 accumulates on RNA in exosome mutants (Figure 8), deletion of Fft2 does not lead to an increase in specific exosome target genes, which are

mostly meiotic transcripts (Figure 21). Instead, DEG in RNAseq analysis reveals a mild differential expression in multiple meiotic transcripts is observed *(SPBC19C7.04c, mug108, mei3, rec7, spo4, omt3*), with only *omt3* being directly regulated by all exosome deficiency mutants [Kilchert et al. 2015; Birot et al. 2022]. Here, it appears that Fft2 is not involved in the master regulation of meiotic transcripts but is itself capable interfere expression of selected transcripts, with or without exosome involvement. Whether the RNA-binding activity is necessary for the regulation of individual transcripts has not been assessed. It is also possible that Fft2 fine-tunes the exosome response, particularly in meiosis and under environmental stress conditions, which were not tested separately in this work. It would also be interesting to test if deletion of Fft2 alters the RNA binding of exosome components, which can detect by *in vitro* studies. The nature of ClIP just reveal direct RNA binding [Kilchert et al. 2020; Stebel et al. 2022] which could be improper to test for protein-protein impairment in RNA binding. However, what could be shown is that RNA is important for the proper recruitment of Fft2 at ncRNA regions and long terminal repeats (Figure 29). If this is due to an RNA-dependent Fft2 recruitment complex, or if Fft2 directly binds transcripts at this region is not clear, but it has been shown in published studies that *S. pombe* LTRs are partially transcriptional active and the LTR transcription is altered in meiosis, which is detected by HybMap method [Mourier and Willerslev 2010]. LTR and retrotransposon activity is an additional target to validate the effect of Fft2 in the progression of meiosis.

Interestingly, Fft3 is able to bind RNA in a similar manner as Fft2 (Figure 22), but does not accumulate on RNA in exosome mutants (Figure 8). Considering the different effects under environmental stress, it can be assumed that Fft3 has a different function potentially reflecting different binding partners. Because the RNA-binding ability of Fft2 is located in the unstructured region of the N-terminal extension, verified by RNA binding activity in Fft2 C-terminal truncation variants (Figure 23), it is likely that RNA binding of Fft3 is localised in the same region. Because all orthologues contain a weakly conserved and unstructured N-terminal extension (Figure 10,Figure 12), it is possible that all members of the SMARCAD1 family have RNA-binding activity. What also stands out is higher stability of Fft3 compared to Fft2, which degrades rapidly in lysates (Figure 22). The stability of Fft2 is increased in all C-terminal truncations, including T3, which only lacks the Fft2-specific unstructured C-terminal extension (Figure 23). Therefore, it can be stated that the C-terminal extension of Fft2 is linked to the observed instability and functional truncations can be used in further experiments to enhance experimental quality by a more stable protein. Based on the high conservation of the DEXDc and HELICc domains with associated functional diversification among Fft family members, it

can be speculated whether the non-conserved N-terminal extension is a key element of functional diversification among SMARCAD1 family members in *S. pombe*.

## 5.4 Fft2 is recruited to noncoding chromatin regions in an exosome-dependent manner

Fft2 is a member of the SNF-ATPase with a specific DNA-binding domain (DEXDc). Specific functions were described for its orthologue in previous studies like nucleosome exchange activity [Markert et al. 2021], meiotic recombination [Storey et al. 2018] heterochromatin maintenance [Strålfors et al. 2011; Steglich et al. 2015] as well as retrotransposon regulation [Persson et al. 2016]. For deeper understanding of Fft2 function *in vivo*, ChIPseq experiments were carried out to resolve the global recruitment of Fft2 to the chromatin.

### 5.4.1 Fft2 is recruited in an exosome-dependent manner to transcript regions

The statistical analysis shows that Fft2-HTP ChIPseq is different from both a corresponding unlabelled control and Fft2-HTP *Δrrp6* (Figure 24). This statement is supported by detectable difference in ChIPseq profile and a calculated spearman correlation between control and Fft2-HTP of 0.5, indicating fewer concentrated reads per bin and thus a smaller absolute alignment differences for each bin of Fft2-HTP compared with control. What could be evaluated in addition is, that Fft2-HTP, *Δrrp6* clearly differs from the Fft2-HTP signal and show high similarities with the untagged control, which is already a good implication for a negative global effect of *Δrrp6* on Fft2 recruitment.

The Metagene analysis reveal a recruitment of Fft2 to transcripts regions on chromatin (Figure 25) and LTR (Figure 26 A) but not broadly at unstable transcripts (App. figure 4). The plot reveals a binding of Fft2 at full annotated transcripts with an identifiable recruitment skew to the 3' end, which is reduced in a *Δrrp6* background (Figure 25), but it must be mentioned that this skew is observed for the signal of untagged control. But what is more remarkably is that Fft2-HTP is recruited upstream and downstream of transcript regions, which not observed in a *Δrrp6* background. This can be interpreted as an indication of Fft2 having a role in the regulation of the transcription promotor and transcription terminator but without a direct involvement of the transcription machinery. In *S.cerevisiea* it was published that a repression of transcription is processed by sliding of nucleosomes in promoter regions by FUN30 [Byeon et al. 2013] which demonstrates a functional link to the observed binding pattern. The investigated Fft2 recruitment fit with the published data and suggest a similar function of Fft2 in *S.pombe*, which needs to be verified by further investigations.

Another possible explanation for the recruitment of Fft2 to upstream and downstream regions is the potential presence of non-coding regions near genes. ncRNA generally has important functions in meiosis, such as chromosome pairing [Ding et al. 2013] and gametogenesis [Andric and Rougemaille 2021] and the deletion of non-coding RNA *SPNCRNA1669* is described as missregulating of mating in *S. pombe* [Ono et al. 2022]. The proximity of ncRNA to transcripts regions could interfere with potential signals received from promotor and terminator recruitment found for Fft2-HTP. The high abundancy of differentially expressed ncRNA in a *Δfft2* background, investigated by GO term analysis (Figure 20), could link the recruitment of Fft2 to non-coding chromatin regions with their expression. Besides of LTR, the class of unstable transcripts could not show a clear global recruitment of Fft2 (Figure 27) but interestingly, Fft2 recruits to selected CUT und DUT regions and this recruitment seems to be repressed by *Δrrp6,* which suggest an involvement of the exosome core module for the entirety of the observed Fft2 recruitment in *S.pombe*. The prominent recruitment to LTR regions is also negatively affected by deletion of Rrp6. This specific recruitment of Fft2 was published by [Persson et al. 2016] and regulation of LTR´s at least partly regulated by the exosome complex, indicated by these experiments. It has to be mentioned that not all LTR regions recruit Fft2 (Figure 26 B) which left the questions open of how the recruitment specificity of Fft2 is coordinated.

### 5.4.2 Recruitment of Fft2 depending on exosome components Rrp6 and Mtl1

A metagene plot of Fft2 recruitment at the annotated 251 LTR regions clearly shows strong Fft2 recruitment that is negatively affected upon Rrp6 deletion (Figure 26 A). Comparable to the observed recruitment in transcript regions, a strong enrichment of Fft2 upstream of LTR regions is detected, which completely vanished in *Δrrp6* strains, but a peak in the downstream region, as in illustrated for transcript annotation (Figure 25), is not detectable. Surprisingly, only one RNA belonging to LTR regions is identified as differentially expressed in the *Δfft2*-RNAseq analysis, but without significance (Tf2-11, p = 0.3,App. table 1). On the one hand, this could indicate that the existing expression of LTR [Mourier and Willerslev 2010] is not influenced by Fft2, and a possible regulation, depends on other factors. Fft2 fulfils a different function at LTR sites. On the other hand it might be that the repression of the LTR region is affected by *Δfft2* but compensated by its paralogues (Fft1/Fft3), as a cumulative effect has been shown previously [Persson et al. 2016].

#### 5.4.2.1 Fft2 recruitment to selected LTR regions depends on Rrp6

In addition to the purely graphical analysis, a feature count analysis is performed in which all read counts are summed over a given feature (Figure 26 B). The analysed LTR cluster into two subpopulations. One population shows a positive recruitment effect of Fft2-HTP in a *Δrrp6* background when plotted against the number of Fft2-HTP features. The other population shows a negatively affected Fft2-HTP recruitment in a *Δrrp6* background. These cluster of population are clear distinguished from each other. While positively influenced LTRs almost exclusively show low normalised trait counts (RPKM <1641), negatively influenced LTRs in contrast show high trait counts (RPKM >1641). Instead of interpreting this as two separate effects of rrp6 deletion, it is reasonable to assume deletion of Rrp6 leads to negative effects of Fft2-HTP recruitment. This is because the Fft2-HTP*, Δrrp6* strain shows high correlation with the untag control, as discussed previously (Figure 25, Section 5.4) and therefore the signals obtained in Fft2-HTP*, Δrrp6* strain are probably a normalisation artifact, resulting in a specific threshold for feature count analysis. Since the effect of *Δrrp6* changes in LTR with enriched feature count level, LTR with an RPKM < 1641 are interpreted as "non-Fft2 recruiting", but this statement needs to be further verified by ChIP experiments with spike in.

To determine statistical significance, a paired t-test is performed for the entire group of LTRs (Figure 26 C). The obtained p-value of 0.058 indicates that there is no significant difference of Fft2-HTP recruitment between the two strains. It should be mentioned that increased Fft2 recruitment as a result of *Δrrp6* is probably an artefact but affects the result of the statistical test. In addition, a power analysis was performed indicating a chance for a missed significant result of 53%. This high probability of false-negative correlation is most likely due to poor peak separation from the unlabelled control of the underlying data set (Figure 24).

#### 5.4.2.2 Mtl1 but not Mmi1 recruits N-terminal domain of Fft2 to LTR regions and exosome targets

Beside of Rrp6, Mtl1 is also involved in the Fft2 recruitment to LTRC.50 (Figure 28 A) and exosome target genes (Figure 28 B). Deletion of Mtl1 as core component of MTREC and other exosome target complexes [Yang Zhou et al. 2015; Ogami 2018], negatively affects Fft2 recruitment for LTR regions, while Mmi1 as DSR specific RNA binding protein [Yamashita et al. 2012; Kilchert et al. 2015] has no impact on Fft2 recruitment. Both proteins are part of MTREC, but Mmi1 is exclusively recruited to meiotic genes like *mei4* with DSR motive. This result implies that Fft2 assembles in Mtl1-dependent complexes that do not contain Mmi1 and that this assembly is necessary for Fft2 recruitment. Surprisingly, both Mmi1 and Mtl1 are

found on the exemplary LTR, which could be due to a too large distance between the protein and the DNA to be cross-linked.

When the Fft2 recruitment signal on LTRC.50 region is compared to ChIP experiments at *mei4* gene site, *Δmmi1* as well as *mtl1-1* background lead to a severe recruitment defect of Fft2 (Figure 28 B). This experiment demonstrates that a prior recruitment of Mtl1 is needed at the respective chromatin region to initiate the Fft2 recruitment as a follow up. In a *vice versa* experiment it is illustrated that Fft2 is not needed for the Mtl1 and Mmi1 recruitment at *mei4* site. The presented recruitment pathway for LTRC.50 could be as representative for all LTR but cannot be conclusively clarified. Considering the loss of Fft2 recruitment after Rrp6 deletion, based on ChIPseq data (Figure 26) a comparable recruitment mechanism for Fft2 at LTR regions can be assumed as likely. To verify the observed relation between Fft2, Mmi1 and Mtl1, more genes need to be tested homologue ChIP experiments, to see if the correlation is substantially present on other Fft2 target regions.

The complex forming of Fft2 with Mtl1 is further accomplished by the formation of large protein-protein complex as demonstrated by gradient centrifugation (Figure 17). Despite a lack of size estimation of the detected fractions due to methodological restrictions (chapter 4.4.1), the absence of Fft2 (*Δfft2)* results in an obvious shift of Mtl1-HTP in the size selective gradient fraction, which surpass the absolute size of Fft2 by far. Hence, it can be assumed that this is due to other proteins interacting with Mtl1, which depends on Fft2. This hypothetical "super complex" shift is comparable to Mtl1-HTP *Δrrp6* and Mtl1-1-FLAG shifts that are known to loss MTREC and/or exosome interconnection of Mtl1 (App. figure 2). Considering this remarkable shift, Fft2 seems to play an important role in the complex formation of Mtl1. The Mtl1-HTP shift in a *Δfft2* background is also quantifiable and connects Fft2 to the large area of exosome target factors.

ChIP experiments carried out with Fft2 truncation, which all maintained their original RNA binding activity (Figure 23), illustrate an unchanged recruitment at LTR region which can observed for all truncations (Figure 30). According to the argumentation before, the N-terminal extension of the Fft2 protein is needed to maintain its chromatin recruitment ability, at least for LTR regions. It is likely that beside of RNA binding (Figure 23) and chromatin recruitment (Figure 30) the N-terminal extension is at least partial responsible for the Mtl1 complex formation (Figure 17). When take into account that the N-terminal domain is heavily modified by phosphorylation in SMARCAD1 [Markert et al. 2021] and that phosphorylation on the other hand is connected to protein-protein interaction [Nishi et al. 2011] this hypothesis seems likely. To validate this hypothesis, glycerol density gradients must be carried out for

the C-terminal truncations in a Mtl1-HTP background and a respective N-terminal truncation which lacks the sequence of the T1 truncation (YPCK560).

How the molecular function of Fft2 proceeds the recruitment to LTR cannot be fully determined, but the obtained data lead to the assessment that only a selected subpopulation of the LTR is targeted by Fft2 and the recruitment is regulated by Rrp6 and Mtl1 but not Mmi1 and maintained by the N-terminal extension.

## 5.5 Heterochromatin maintenance and nucleosome exchange are no essential part of Fft2's molecular function.

While recruitment regulation and RNA-binding ability are investigated in this work, the actual molecular functions of Fft2 are still unclear. Described functions for SMARCAD1 family members include maintenance of genome integrity [Lo et al. 2021], nucleosome exchange activity [Markert et al. 2021] nucleosome sliding [Byeon et al. 2013], meiotic recombination [Storey et al. 2018], heterochromatin maintenance [Strålfors et al. 2011; Steglich et al. 2015] and regulation of retrotransposons [Persson et al. 2016].

While recruitment to LTR and ncRNA has already been discussed (chapter 5.4), a clear functionality for Fft2 is missing. ChIP experiments for H3K9me2 (Figure 31) and for the influence of H2A.Z orthologue Pht1 (Figure 32) were performed to investigate the function of Fft2 in heterochromatin maintenance and histone exchange. *Δfft2* did not alter the heterochromatin status of constitutive (*dg*, centromeric repeat) and facultative heterochromatin (*mei4, ssm4*: meiotic genes) (Figure 32). It appears that the deletion of Fft2 has no general effect on heterochromatin status, or that the effect is compensated by the Fft2 paralogue Fft3. Moreover, Fft2 recruitment is very low at *mei4* sites and undetectable at *ssm4*, *dg* and *adh1*. Here, it is questionable whether *Δfft2* can affect heterochromatin for these genes, and it may give further insights to test chromatin status at highly recruited Fft2 chromatin regions known to be regulated by heterochromatin, such as LTRs [Grewal and Moazed 2003; Gao et al. 2008]. Deletion of Clr4, the major histone methyltransferase in *S. pombe*, also has no effect on Fft2 recruitment to the gene *mei4* (Figure 32 B), evaluating that the CLRC complex is not involved in recruiting of Fft2 at chromatin regions, as well that loss of heterochromatin is not affecting Fft2 recruitment in these regions.

So far, in my work I have not determined the influence of *Δfft2* on histone exchange rates. However, I monitored the incorporation of the histone variant Pht1 in ChIP experiments and compared the occurrence of this histone variant in *Δfft2* strain and Fft2-HTP recruitment in a

*Δpht1* background (Figure 32). Here I observed ambivalent effects. While the occurrence of Pht1 in a certain gene region is not influenced by *Δfft2*, the Fft2-HTP signal in a Pht1 deletion background leads to an altered recruitment in different tested gene classes. A slight tendency can be seen that with a higher signal of Pht1 in a certain gene region, there tends to be a reduction of the Fft2 recruitment signal in a *Δpht1* background strain. On the other hand, a low signal of Pht1 in a particular gene region tends to increase the Fft2 recruitment signal in a *Δpht1* background. Whether the results shown are reproducible is not certain due to the small number of replicates, so these small differences in the recruitment of Fft2 from the corresponding regions could be due to a change in chromatin structure. This changes the accessibility of the chromatin non-specifically, which means that the differences do not have to be due to a direct interaction between Pht1 and Fft2.

In conclusion, a clear functional designation of Fft2 is still pending. While the data suggest that Fft2 is not involved in histone exchange and maintenance of heterochromatin, other interesting assays of nucleosome sliding activity could be performed as described for FUN30 [Byeon et al. 2013]. Truncations assayed for RNA binding and chromatin recruitment (Figure 23, Figure 31) could reveal altered function and elucidate functional properties related to protein sequence. Finally, *in vitro* experiments can provide tremendous insight into the functional properties of SMARCAD1 orthologues, as exemplified in [Markert et al. 2021].

# 6 Conclusion

In this study, I investigated the role of the SMARCAD1 orthologue Fft2 in *S. pombe*. Based on the experiments performed, it can be reliably concluded that Fft2 has a novel direct RNA-binding activity and is associated with the nuclear RNA exosome in complex formation and chromatin recruitment. The data also suggest that Fft2 recruitment on chromatin is mediated by its interactions with the nuclear RNA exosome, which is by itself responsible for the degradation of RNA molecules in the cell [Harigaya et al. 2006; Kilchert et al. 2015; Kilchert et al. 2016]. A functional difference between Fft members detected by RIP and growth defect analyses holds potential for further investigations. A schematic representation of the findings of this study is illustrated in Figure 33.

These results provide new insights into the mechanisms of SMARCAD1 like-helicase and have important implications in the field of SNF-ATPase and its multivariate function in a broad range of cellular mechanisms, but other questions are still not answered. Especially the function of Fft2 in meiosis is still unknown, while deletion of Fft2 positively affect the sporulation initiation. Therefore, an obvious recommendation is the analyse of Fft2 characteristics in the process of meiosis for its molecular function and RNA binding abilities. Another open question is, if the interaction of Fft2 with Mtl1 or Rrp6 is of a direct or indirect nature and cannot stated from the obtained data without doubt. Fft2 is involved in Mtl1 dependent complexes (Figure 17) but its interaction with exosome proteins should additionally verified in *in vitro* experiments, especially with generated truncation (Figure 30) and a possible N-terminal truncation. Last but not least, the RNA binding is shown for the C-terminal truncation (Figure 23), but it is not clear if the exosome complex is needed in this RNA binding activity, despite a visible RNA accumulation in exosome deficiency mutants is detected for Fft2 (Figure 8). Because the nature of zero-distance crosslinking in PAR-CLIP, a direct RNA binding is demonstrated, but if this activity is already modified by potential Rrp6 and MTREC interaction is still open and should be analysed to fully reveal the nature of this newly found interaction.

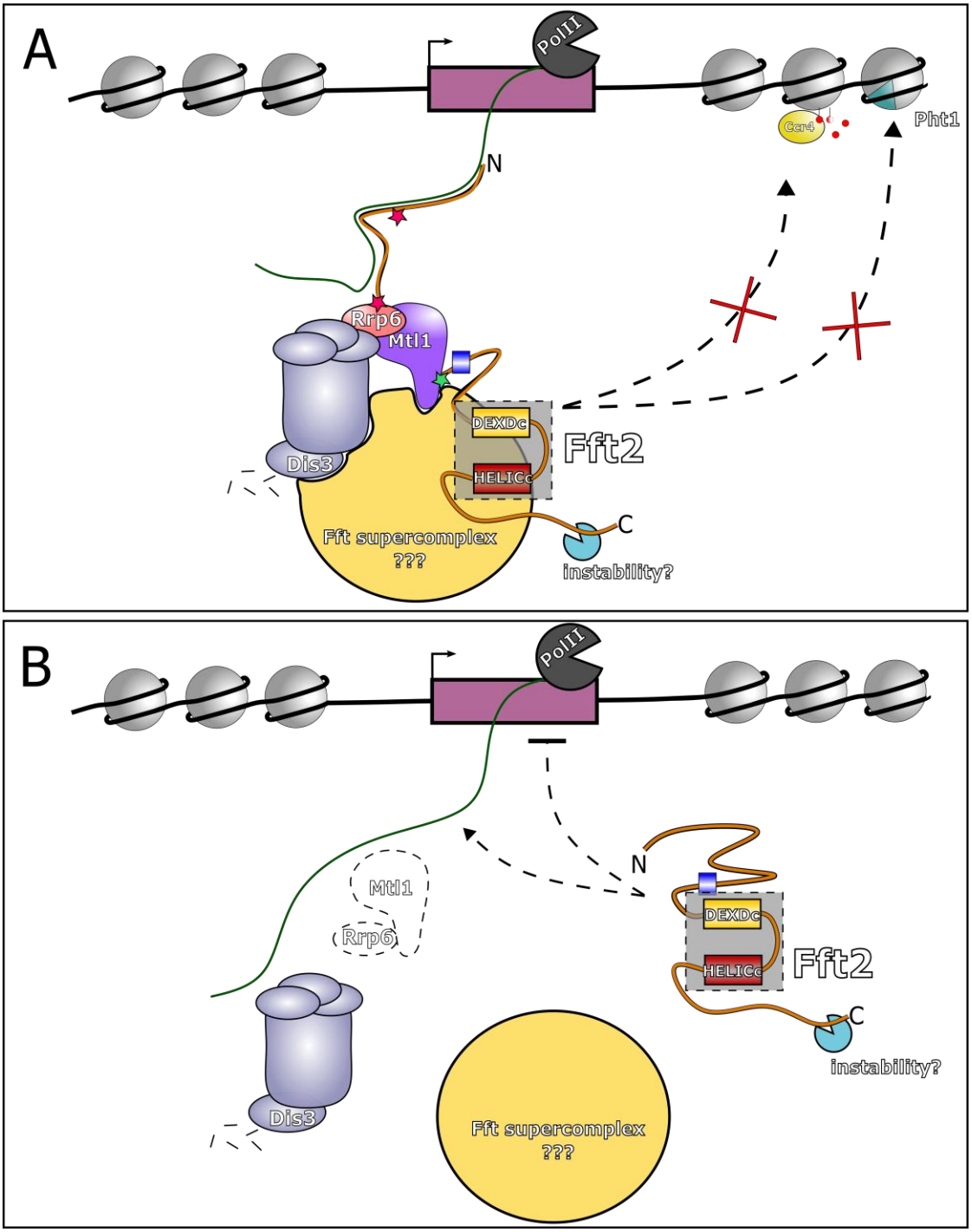


*Figure 33 Fft2 is involved in an exosome dependent manner and recruits to chromatin and RNA*

Schematic overview of the general findings in this work. A) steady state in cell connects Fft2 with the exosome at Mtl1 dependent complex (Figure 17) and its chromatin recruitment depends on Rrp6 (Figure 25) and Mtl1 (Figure 28). Also, Fft2 binds to RNA with its N-terminal extension (Figure 23), which is also sufficient for its chromatin recruitment (Figure 30). A correlation between Fft2 recruitment with the occurrence of Pht1 (Figure 32) or heterochromatin (Figure 31) is not given by my experimental data. B) Exosome deficiency mutants lead to a loss of chromatin recruitment of Fft2, while it is accumulating on RNA is not impaired (Figure 8). Also, it is not finally clear if the stability of Fft2 is enhanced by potential structure change of N-terminal and C-terminal extensions, but stability enhancement of Fft2 truncations suggest a relation between both.

# 7 Appendix

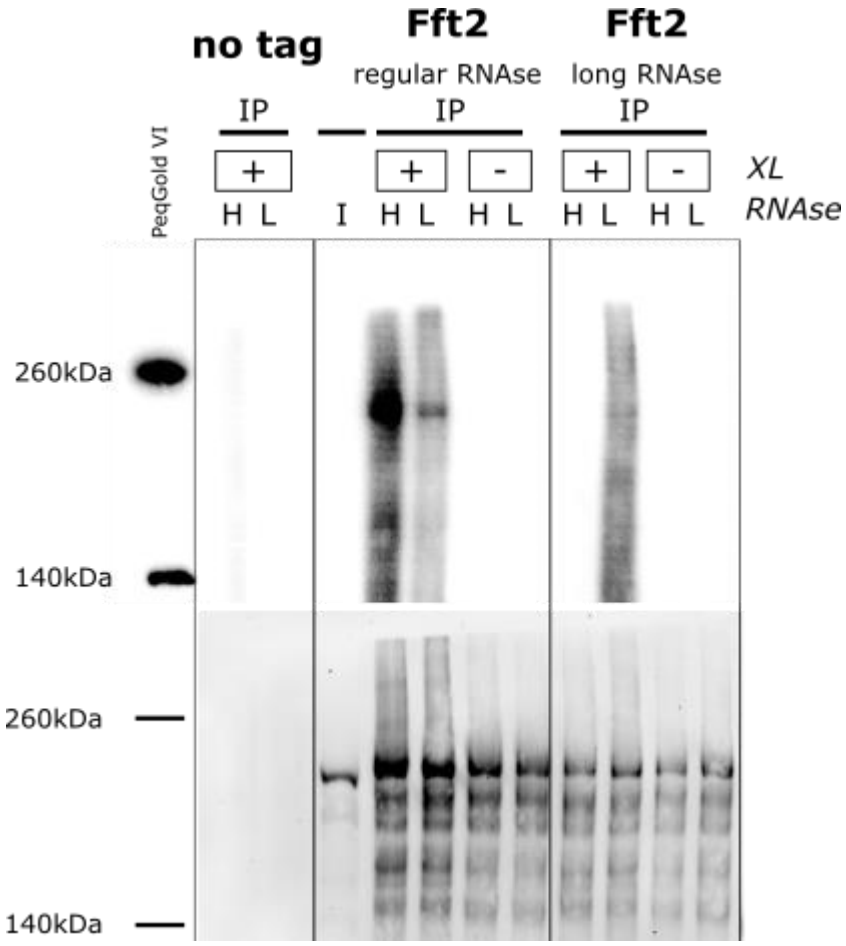


*App. figure 1 time related RNase digest in Fft2-HTP (YPCK9)*

The radionucleotide signal obtained with regular RNase treatment of the lysate (3 minutes) is compared with long RNase treatment (12 minutes). UV crosslinking shows a method background, while a high RNase concentration (H) shows a stronger signal in contrast to a low concentration (L). This pattern reverses after prolonged RNase treatment, mirroring the pattern shown for Mtl1 and Fft3 (Figure 17). It is noteworthy that prolonged RNase treatment has no significant effect on the overall stability of Fft2.

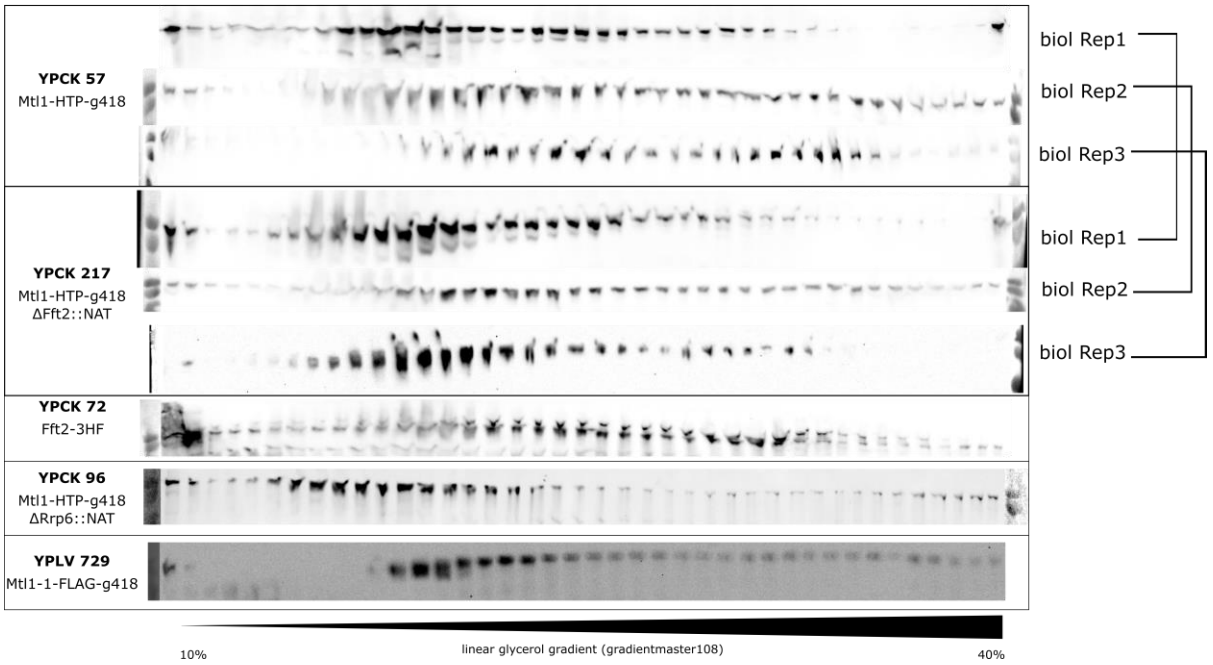


*App. figure 2 single western blot of glycerol gradients*

Western blot of glycerol gradient after fractionation and precipitation of protein. Biological replicates are indicated by parentheses. Signal obtained by α-PAP, Fft2-3xHA 3xFlag (YPCK72) signal with α-HA. While a significant shift is observed for Mtl1-HTP in a *Δfft2* background, a comparable shift is found in the Mtl1-1-HTP strain and Mtl1-HTP in a *Δrrp6* background, suggesting a relationship between complex size and gradient signal shift. The Fft2-3HF signal is detected in fractions with high glycerol content, suggesting a likely interaction with Mtl1 at same high glycerol fractions.

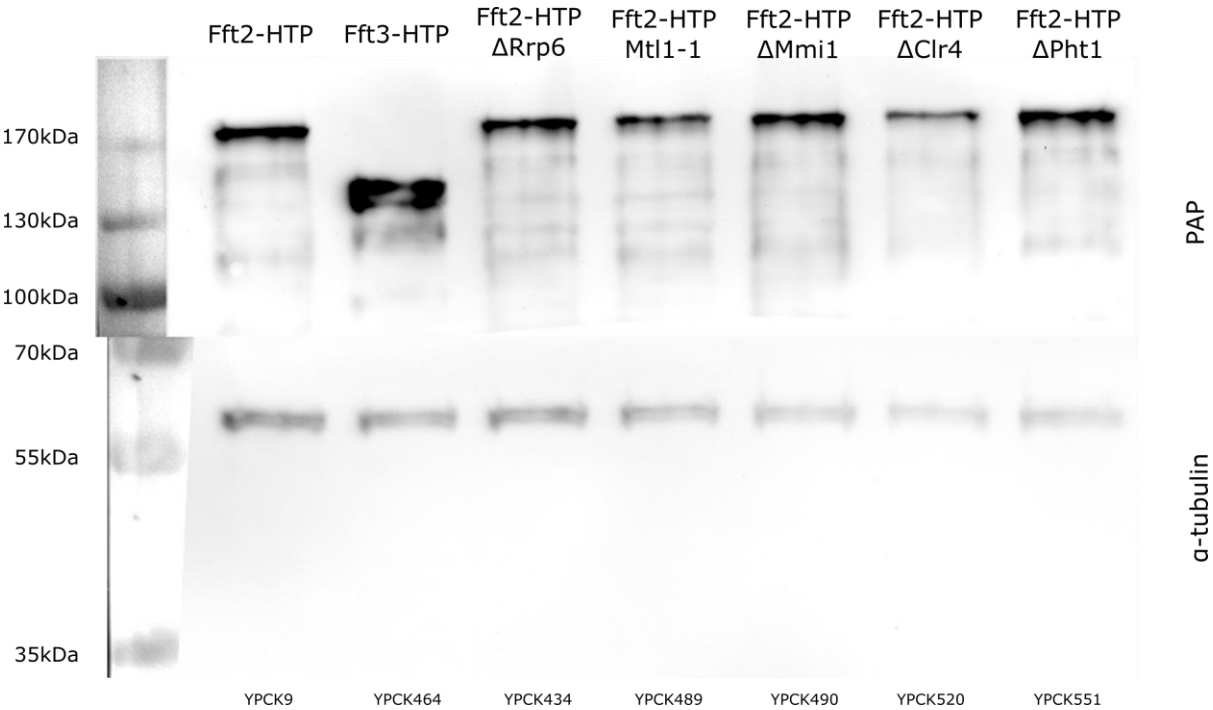


*App. figure 3 control of Fft2 and Fft3 level in respective mutants. A-PAP for detecting of HTP tag, α-tubulin for loading control*

*App. table 1 Differentially expressed genes found in Δfft2 RNAseq with minimum $Log_2$ FC > 1 / < -1*

| ID | name | Log2FC | pvalue | FDR | PANTHER family |
|---|---|---|---|---|---|
| SPNCRNA.1260 | SPNCRNA.1260 | 3,15 | 0 | 0 | |
| SPNCRNA.1259 | SPNCRNA.1259 | 2,89 | 0 | 0 | |
| SPAC186.07c | SPAC186.07c | 2,29 | 0,02 | 0,59 | 2-HYDROXYACID DEHYDROGENASE HOMOLOG 1-RELATED (PTHR43026:SF1) |
| SPBC30B4.09 | SPBC30B4.09 | 2,06 | 0,02 | 0,57 | |
| SPBC23G7.13c | SPBC23G7.13c | 2,01 | 0 | 0 | UREA ACTIVE TRANSPORTER (PTHR46154:SF4) |
| SPBC660.05 | SPBC660.05 | 1,89 | 0 | 0 | |
| SPAC17A2.10c | SPAC17A2.10c | 1,86 | 0,06 | 0,81 | |
| SPAC186.03 | SPAC186.03 | 1,74 | 0,08 | 0,87 | |
| SPNCRNA.1530 | SPNCRNA.1530 | 1,7 | 0,11 | 0,96 | |
| SPNCRNA.917 | SPNCRNA.917 | 1,7 | 0,13 | 0,98 | |
| SPNCRNA.310 | SPNCRNA.310 | 1,6 | 0,21 | 1 | |
| SPNCRNA.201 | SPNCRNA.201 | 1,55 | 0,2 | 1 | |
| SPBC19C7.04c | SPBC19C7.04c | 1,44 | 0 | 0 | MEIOTICALLY UP-REGULATED GENE 9 PROTEIN (PTHR28186:SF1) |
| SPRRNA.31 | SPRRNA.31 | 1,44 | 0,19 | 1 | |
| SPRRNA.49 | SPRRNA.49 | 1,42 | 0,24 | 1 | |
| SPNCRNA.968 | SPNCRNA.968 | 1,39 | 0,01 | 0,33 | |
| SPAC186.02c | SPAC186.02c | 1,36 | 0,17 | 1 | 2-HYDROXYACID DEHYDROGENASE HOMOLOG 1-RELATED (PTHR43026:SF1) |
| SPNCRNA.1039 | SPNCRNA.1039 | 1,29 | 0,04 | 0,73 | |
| SPNCRNA.1084 | SPNCRNA.1084 | 1,29 | 0,12 | 0,97 | |
| SPNCRNA.61 | prl61 | 1,26 | 0,04 | 0,75 | |
| SPCC191.04c | SPCC191.04c | 1,2 | 0,29 | 1 | |
| SPNCRNA.630 | SPNCRNA.630 | 1,18 | 0 | 0,07 | |
| SPAC29A4.12c | mug108 | 1,14 | 0,02 | 0,59 | |
| SPNCRNA.960 | SPAC26H5.04-antisense-1 | 1,09 | 0 | 0,24 | |
| SPAC869.01 | SPAC869.01 | 1,07 | 0,25 | 1 | AMIDASE C869.01-RELATED (PTHR42678:SF25) |
| SPBC119.04 | mei3 | 1,07 | 0,07 | 0,87 | |
| SPAC23H3.15c | SPAC23H3.15c | 1,06 | 0 | 0,14 | |
| SPBC557.05 | SPBC557.05 | 1,06 | 0 | 0,02 | ARRESTIN DOMAIN-CONTAINING PROTEIN C31A2.12 (PTHR11188:SF170) |
| SPNCRNA.1123 | SPNCRNA.1123 | 1,04 | 0,33 | 1 | |

| | | | | | |
|---|---|---|---|---|---|
| SPNCRNA.1653 | cwf28-antisense-1 | 1,02 | 0 | 0,04 | |
| SPNCRNA.457 | ark1-antisense-1 | 1,02 | 0,43 | 1 | |
| SPNCRNA.379 | SPNCRNA.379 | 1 | 0,32 | 1 | |
| SPNCRNA.908 | rpt5-antisense-1 | -1 | 0,01 | 0,46 | |
| SPAC6B12.03c | bit2 | -1,01 | 0,12 | 0,96 | TARGET OF RAPAMYCIN COMPLEX 2 SUBUNIT BIT61-RELATED (PTHR32428:SF2) |
| SPBPB2B2.08 | SPBPB2B2.08 | -1,01 | 0,01 | 0,42 | |
| SPNCRNA.1590 | gar1-antisense-1 | -1,01 | 0,01 | 0,34 | |
| SPNCRNA.240 | SPNCRNA.240 | -1,01 | 0,25 | 1 | |
| SPNCRNA.1245 | rpl2702-antisense-1 | -1,02 | 0,02 | 0,57 | |
| SPNCRNA.1348 | SPNCRNA.1348 | -1,02 | 0,2 | 1 | |
| SPNCRNA.1396 | psy2-antisense-1 | -1,02 | 0,28 | 1 | |
| SPCC1753.03c | rec7 | -1,03 | 0,15 | 1 | |
| SPNCRNA.1611 | hhf3-antisense-1 | -1,03 | 0,06 | 0,84 | |
| SPNCRNA.870 | SPNCRNA.870 | -1,03 | 0,01 | 0,5 | |
| SPNCRNA.1304 | SPNCRNA.1304 | -1,05 | 0,15 | 0,99 | |
| SPNCRNA.1329 | SPNCRNA.1329 | -1,05 | 0,06 | 0,84 | |
| SPNCRNA.1621 | mok13-antisense-1 | -1,05 | 0,02 | 0,57 | |
| SPNCRNA.562 | nop12-antisense-1 | -1,05 | 0,04 | 0,72 | |
| SPNCRNA.602 | SPNCRNA.602 | -1,05 | 0,03 | 0,66 | |
| SPNCRNA.1249 | SPNCRNA.1249 | -1,06 | 0,13 | 0,98 | |
| SPNCRNA.388 | SPNCRNA.388 | -1,06 | 0,02 | 0,52 | |
| SPNCRNA.741 | rpl2001-antisense-1 | -1,07 | 0,01 | 0,42 | |
| SPNCRNA.791 | rad55-antisense-1 | -1,07 | 0,2 | 1 | |
| SPAC1F8.02c | shu1 | -1,08 | 0,22 | 1 | |
| SPNCRNA.1017 | sup45-antisense-1 | -1,08 | 0,01 | 0,49 | |
| SPNCRNA.572 | cmc1-antisense-1 | -1,08 | 0,22 | 1 | |
| SPNCRNA.454 | SPNCRNA.454 | -1,1 | 0,3 | 1 | |
| SPNCRNA.932 | SPAC15E1.10-antisense-1 | -1,1 | 0,23 | 1 | |
| SPBPB2B2.06c | SPBPB2B2.06c | -1,11 | 0,03 | 0,66 | PHOSPHOPROTEIN PHOSPHATASE (PTHR11575:SF49) |
| SPNCRNA.136 | SPNCRNA.136 | -1,11 | 0,34 | 1 | |
| SPNCRNA.1072 | SPAP8A3.07c-antisense-1 | -1,12 | 0,01 | 0,5 | |
| SPNCRNA.1376 | tef103-antisense-1 | -1,12 | 0,04 | 0,74 | |
| SPAC13F5.07c | hpz2 | -1,13 | 0,02 | 0,52 | |
| SPBPB8B6.04c | grt1 | -1,14 | 0 | 0 | ZINC FINGER PROTEIN GRT1 (PTHR47424:SF14) |
| SPNCRNA.850 | SPAC6F6.12-antisense-1 | -1,14 | 0,14 | 0,99 | |
| SPAC6G10.06 | SPAC6G10.06 | -1,15 | 0,22 | 1 | OXIDOREDUCTASE TDA3-RELATED (PTHR13847:SF150) |
| SPCC663.14c | trp663 | -1,15 | 0,1 | 0,92 | TRP-LIKE ION CHANNEL (PTHR31145:SF7) |

| | | | | | |
|---|---|---|---|---|---|
| SPBC1289.17 | Tf2-11 | -1,16 | 0,3 | 1 | TRANSPOSON TF2-1 POLYPROTEIN-RELATED (PTHR47266:SF28) |
| SPAC1F8.04c | SPAC1F8.04c | -1,17 | 0 | 0,01 | |
| SPNCRNA.603 | SPNCRNA.603 | -1,17 | 0,28 | 1 | |
| SPNCRNA.1328 | SPBC660.08-antisense-1 | -1,2 | 0,03 | 0,64 | |
| SPAC977.04 | SPAC977.04 | -1,21 | 0,25 | 1 | |
| SPNCRNA.685 | SPAC16C9.01c-antisense-1 | -1,21 | 0 | 0,08 | |
| SPNCRNA.860 | SPNCRNA.860 | -1,22 | 0,12 | 0,97 | |
| SPNCRNA.923 | SPNCRNA.923 | -1,22 | 0,01 | 0,52 | |
| SPNCRNA.912 | SPNCRNA.912 | -1,23 | 0,24 | 1 | |
| SPNCRNA.1242 | SPNCRNA.1242 | -1,24 | 0,05 | 0,78 | |
| SPNCRNA.1322 | SPBC1198.05-antisense-1 | -1,24 | 0,02 | 0,59 | |
| SPAC27E2.13 | SPAC27E2.13 | -1,26 | 0,11 | 0,95 | |
| SPNCRNA.620 | aps1-antisense-1 | -1,26 | 0,07 | 0,85 | |
| SPNCRNA.1632 | utp4-antisense-1 | -1,27 | 0,04 | 0,72 | |
| SPNCRNA.25 | prl25 | -1,27 | 0,06 | 0,81 | |
| SPNCRNA.1594 | rpl1801-antisense-1 | -1,28 | 0,01 | 0,32 | |
| SPNCRNA.787 | ebp2-antisense-1 | -1,3 | 0,02 | 0,63 | |
| SPAC2F7.06c | pol4 | -1,41 | 0,01 | 0,39 | DNA POLYMERASE TYPE-X FAMILY PROTEIN POL4 (PTHR11276:SF29) |
| SPNCRNA.847 | SPAC6F6.03c-antisense-1 | -1,42 | 0,01 | 0,41 | |
| SPAC20G4.09 | SPAC20G4.09 | -1,45 | 0,12 | 0,97 | |
| SPNCRNA.843 | hcs1-antisense-1 | -1,45 | 0,01 | 0,5 | |
| SPBC21C3.18 | spo4 | -1,46 | 0,16 | 1 | CELL DIVISION CYCLE 7-RELATED PROTEIN KINASE (PTHR11909:SF7) |
| SPNCRNA.715 | mug54-antisense-1 | -1,49 | 0 | 0,25 | |
| SPNCRNA.924 | SPNCRNA.924 | -1,49 | 0,34 | 1 | |
| SPNCRNA.1079 | rad2-antisense-1 | -1,52 | 0 | 0 | |
| SPNCRNA.567 | atp3-antisense-1 | -1,56 | 0,02 | 0,53 | |
| SPNCRNA.130 | omt3 | -1,57 | 0 | 0,04 | |
| SPNCRNA.263 | SPNCRNA.263 | -1,59 | 0,1 | 0,94 | |
| SPNCRNA.826 | cpc2-antisense-1 | -1,6 | 0 | 0,11 | |
| SPNCRNA.568 | ade7-antisense-1 | -1,61 | 0,03 | 0,71 | |
| SPBC23G7.10c | SPBC23G7.10c | -1,63 | 0 | 0 | NADPH DEHYDROGENASE C23G7.10C-RELATED (PTHR43303:SF4) |
| SPNCRNA.1578 | rpl102-antisense-1 | -1,66 | 0 | 0,11 | |
| SPAC186.09 | pdc102 | -1,68 | 0 | 0,18 | PYRUVATE DECARBOXYLASE C186.09-RELATED (PTHR43452:SF6) |
| SPNCRNA.1076 | sum1-antisense-1 | -1,68 | 0,01 | 0,5 | |

| | | | | | |
|---|---|---|---|---|---|
| SPAC750.01 | SPAC750.01 | -2,64 | 0 | 0 | ARYL-ALCOHOL DEHYDROGENASE AAD16-RELATED (PTHR43364:SF15) |
| SPAC750.06c | SPAC750.06c | -3,27 | 0 | 0,07 | |
| SPCC1235.05c | fft2 | -3,82 | 0 | 0 | ATP-DEPENDENT HELICASE FFT2 (PTHR10799:SF1002) |
| SPAC750.05c | SPAC750.05c | -4,6 | 0 | 0 | |

*App. table 2 missregulated meiotic transcripts in EDM compared to a differentially expression in Δfft2 compared to steady state level*

| | ***Δrrp6*** | ***mtl1-1*** | ***Δmmi1*** | ***Δfft2*** |
|---|---|---|---|---|
| *SPBC19C7.04c* | | x | x | x |
| *mug108* | | | x | x |
| *mei3* | x | x | x | |
| *rec7* | | | x | |
| *spo4* | | | | |
| *omt3* | x | | | x |

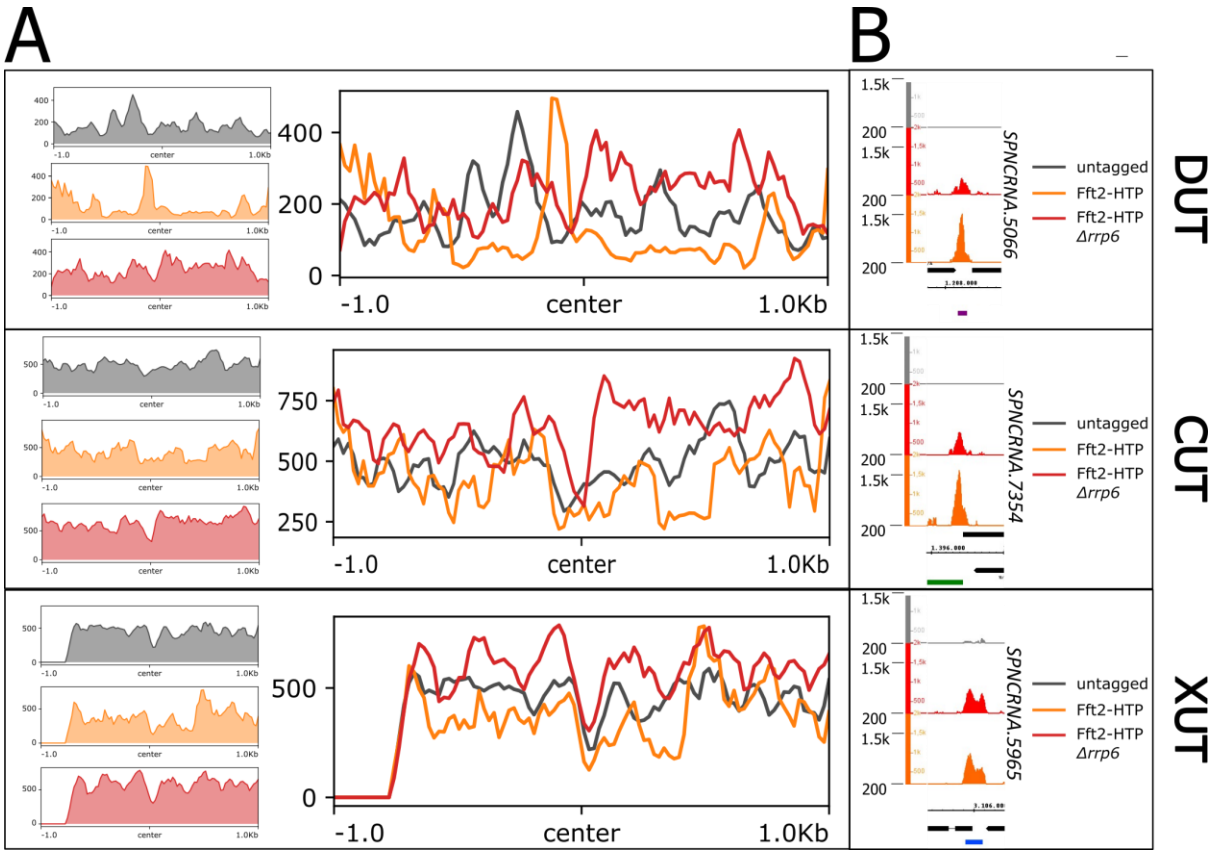


*App. figure 4 Fft2 recruitment at regions of unstable transcripts*

A) Fft2 recruitment to regions of unstable transcripts is presented as a metagene plot processed in galaxy [The galaxy community 2022]. The annotations of DUT, CUT and XUT originate from the paper [Atkinson et al. 2018] and were manually written into a gtf file for analysis. The metagene plot was processed using the "reference point" method, which reflects the +/- 1kB ChIPseq signal around the annotation start point. In contrast to the LTR metagene plot, all plots for cryptic transcripts missing a clear pattern for recruitment of Fft2-HTP. Also, no clear reduction in Fft2 recruitment is observable for the Δrrp6 background. Reasons for this recruitment could be overlapping annotations or very small annotations which provide for an inaccuracy of the analysis, as well as the lack of input normalisation for ChIPseq analysis. B) ChIPseq for selected targets of DUT, CUT and XUT class which represents

# 8 References


AIT-SAADA, A., KHOROSJUTINA, O., CHEN, J., KRAMARZ, K., MAKSIMOV, V., SVENSSON, J.P., LAMBERT, S., AND EKWALL, K. 2019. Chromatin remodeler Fft3 plays a dual role at blocked DNA replication forks. *Life Sci. Alliance 2*, 5, e201900433.

AL KUBAISY, E., ARAFAT, K., WEVER, O. DE, HASSAN, A.H., AND ATTOUB, S. 2016. SMARCAD1 knockdown uncovers its role in breast cancer cell migration, invasion, and metastasis. *Expert opinion on therapeutic targets 20*, 9, 1035–1043.

ALLEN, H.F., WADE, P.A., AND KUTATELADZE, T.G. 2013. The NuRD architecture. *Cellular and molecular life sciences : CMLS 70*, 19, 3513–3524.

ALLIS, C.D., JENUWEIN, T., REINBERG, D., AND CAPARROS, M.-L. 2007. *Epigenetics*. CSH Press/Cold Spring Harbor Laboratory Press, Cold Spring Harbor, N.Y.

ALLMANG, C., PETFALSKI, E., PODTELEJNIKOV, A., MANN, M., TOLLERVEY, D., AND MITCHELL, P. 1999. The yeast exosome and human PM-Scl are related complexes of 3' -- 5' exonucleases. *Genes & Development 13*, 16, 2148–2158.

ALLSHIRE, R.C., AND MADHANI, H.D. 2018. Ten principles of heterochromatin formation and function. *Nature Reviews Molecular Cell Biology 19*, 4, 229–244.

AMBRO, V.H. AND PARKER, R., 1999. The Exosome : A Proteasome for RNA ? Minireview. *Cell 99*, 4, 347–350.

ANDERSEN, P.R., DOMANSKI, M., KRISTIANSEN, M.S., STORVALL, H., NTINI, E., VERHEGGEN, C., SCHEIN, A., BUNKENBORG, J., POSER, I., HALLAIS, M., SANDBERG, R., HYMAN, A., LACAVA, J., ROUT, M.P., ANDERSEN, J.S., BERTRAND, E., AND JENSEN, T.H. 2013. The human cap-binding complex is functionally connected to the nuclear RNA exosome. *Nature structural & molecular biology 20*, 12, 1367–1376.

ANDRIC, V., AND ROUGEMAILLE, M. 2021. Long Non-Coding RNAs in the Control of Gametogenesis: Lessons from Fission Yeast. *Non-coding RNA 7*, 2.

ARAKI, YASUHIRO & TAKAHASHI, SHINYA & KOBAYASHI, TETSUO & KAJIHO, HIROAKI & HOSHINO, SHIN-ICHI & KATADA, TOSHIAKI. 2001. Ski7p G protein interacts with the exosome and the Ski complex for 3'-to-5' mRNA decay in yeast. *The EMBO Journal*. 20. 4684-4693.

ASAKAWA, H., AND HIRAOKA, Y., 2009. Live-cell fluorescence imaging of meiotic chromosome dynamics in Schizosaccharomyces pombe. *Methods in molecular biology (Clifton, N.J.) 558*, 53–64.

ATKINSON, S.R., MARGUERAT, S., BITTON, D.A., RODRÍGUEZ-LÓPEZ, M., RALLIS, C., LEMAY, J.-F., COTOBAL, C., MALECKI, M., SMIALOWSKI, P., MATA, J., KORBER, P., BACHAND, F., AND BÄHLER, J.

2018. Long noncoding RNA repertoire and targeting by nuclear exosome, cytoplasmic exonuclease, and RNAi in fission yeast. *RNA 24*, 9, 1195–1213.

BALASUBRAMANIAN, M.K., BI, E., AND GLOTZER, M. 2004. Comparative Analysis of Cytokinesis in Budding Yeast, Fission Yeast and Animal Cells. *Current biology : CB 14*, 18, R806-R818.

BANTELE, S.C.S., AND PFANDER, B. 2019. Nucleosome Remodeling by Fun30SMARCAD1 in the DNA Damage Response. *Frontiers in molecular biosciences 6*, 78.

BAO, X., GUO, X., YIN, M., TARIQ, M., LAI, Y., KANWAL, S., ZHOU, J., LI, N., LV, Y., PULIDO-QUETGLAS, C., WANG, X., JI, L., KHAN, M.J., ZHU, X., LUO, Z., SHAO, C., LIM, D.-H., LIU, X., LI, N., WANG, W., HE, M., LIU, Y.-L., WARD, C., WANG, T., ZHANG, G., WANG, D., YANG, J., CHEN, Y., ZHANG, C., JAUCH, R., YANG, Y.-G., WANG, Y., QIN, B., ANKO, M.-L., HUTCHINS, A.P., SUN, H., WANG, H., FU, X.-D., ZHANG, B., AND ESTEBAN, M.A. 2018. Capturing the interactome of newly transcribed RNA. *Nature methods 15*, 3, 213–220.

BAYNE, E.H., WHITE, S.A., KAGANSKY, A., BIJOS, D.A., SANCHEZ-PULIDO, L., HOE, K.-L., KIM, D.-U., PARK, H.-O., PONTING, C.P., RAPPSILBER, J., AND ALLSHIRE, R.C. 2010. Stc1: a critical link between RNAi and chromatin modification required for heterochromatin integrity. *Cell 140*, 5, 666–677.

BEACH, D., AND NURSE, P. 1981. High-frequency transformation of the fission yeast Schizosaccharomyces pombe. *Nature 290*, 5802, 140–142.

BECKMANN COULTER. *Intellifuge*. Beckmann Coulter.

BECKMANN, B.M., HOROS, R., FISCHER, B., CASTELLO, A., EICHELBAUM, K., ALLEAUME, A.M., SCHWARZL, T., CURK, T., FOEHR, S., HUBER, W., KRIJGSVELD, J., AND HENTZE, M.W., 2015. The RNA-binding proteomes from yeast to man harbour conserved enigmRBPs. *Nature Communications 6*.

BENNETT, R.J., AND TURGEON, B.G. 2016. Fungal Sex: The Ascomycota. *Microbiology spectrum 4*, 5.

BERNARD, P., MAURE, J.F., PARTRIDGE, J.F., GENIER, S., JAVERZAT, J.P., AND ALLSHIRE, R.C. 2001. Requirement of heterochromatin for cohesion at centromeres. *Science (New York, N.Y.) 294*, 5551, 2539–2542.

BERNSTEIN, J., AND TOTH, E.A., 2012. Yeast nuclear RNA processing *3*, 1.

BEVILACQUA, A., CERIANI, M.C., CAPACCIOLI, S., AND NICOLIN, A. 2003. Post-transcriptional regulation of gene expression by degradation of messenger RNAs. *Journal of cellular physiology 195*, 3, 356–372.

BIROT, A., KUS, K., PRIEST, E., AL ALWASH, A., CASTELLO, A., MOHAMMED, S., VASILJEVA, L., AND KILCHERT, C. 2022. RNA-binding protein Mub1 and the nuclear RNA exosome act to fine-tune environmental stress response. *Life science alliance 5*, 2.

BONNEAU, F., BASQUIN, J., EBERT, J., LORENTZEN, E., AND CONTI, E., 2009. The Yeast Exosome Functions as a Macromolecular Cage to Channel RNA Substrates for Degradation. *Cell 139*, 3, 547–559.

BRIGGS, M.W., BURKARD, K.T.D., AND BUTLER, J.S., 1998. Rrp6p, the yeast homologue of the human PM-Scl 100-kDa autoantigen, is essential for efficient 5.8 S rRNA 3' end formation. *Journal of Biological Chemistry 273*, 21, 13255–13263.

BROWN, J.T., BAI, X., AND JOHNSON, A.W., 2000. The yeast antiviral proteins Ski2p, Ski3p, and Ski8p exist as a complex in vivo. *RNA 6*, 3, 449-457

BÜHLER, M., HAAS, W., GYGI, S.P., AND MOAZED, D., 2007. RNAi-dependent and -independent RNA turnover mechanisms contribute to heterochromatic gene silencing. *Cell 129*, 4, 707–721.

BURNETTE, W.N., 1981. "Western blotting": electrophoretic transfer of proteins from sodium dodecyl sulfate--polyacrylamide gels to unmodified nitrocellulose and radiographic detection with antibody and radioiodinated protein A. *Analytical biochemistry 112*, 2, 195–203.

BURTON, R.F., 1859. *The Lake Regions of Central Equatorial Africa. with Notices of the Lunar Mountains and the Sources of the White Nile; being the Results of an Expedition Undertaken Under the Patronage of Her Majesty's Government and the Royal Geographical Society of London, in the Years 1857-1859*. The First "Lake Regions". Journal of the Royal Geographical Society.

BYEON, B., WANG, W., BARSKI, A., RANALLO, R.T., BAO, K., SCHONES, D.E., ZHAO, K., WU, C., AND WU, W.-H. 2013. The ATP-dependent chromatin remodeling enzyme Fun30 represses transcription by sliding promoter-proximal nucleosomes. *The Journal of biological chemistry 288*, 32, 23182–23193.

CALLAHAN, K.P., AND BUTLER, J.S., 2008. Evidence for core exosome independent function of the nuclear exoribonuclease Rrp6p. *Nucleic Acids Research 36*, 21, 6645–6655.

CANADELL, D., GARCÍA-MARTÍNEZ, J., ALEPUZ, P., PÉREZ-ORTÍN, J.E., AND ARIÑO, J., 2015. Impact of high pH stress on yeast gene expression: A comprehensive analysis of mRNA turnover during stress responses. *Biochimica et biophysica acta 1849*, 6, 653–664.

CAPUT, D., BEUTLER, B., HARTOG, K., THAYER, R., BROWN-SHIMER, S., AND CERAMI, A., 1986. Identification of a common nucleotide sequence in the 3'-untranslated region of mRNA molecules specifying inflammatory mediators. *Proceedings of the National Academy of Sciences of the United States of America 83*, 6, 1670–1674.

CARNEIRO, T., CARVALHO, C., BRAGA, J., RINO, J., MILLIGAN, L., TOLLERVEY, D., AND CARMO-FONSECA, M., 2007. Depletion of the yeast nuclear exosome subunit Rrp6 results in

accumulation of polyadenylated RNAs in a discrete domain within the nucleolus. *Molecular and Cellular Biology 27*, 11, 4157–4165.

CARR, A.M., DORRINGTON, S.M., HINDLEY, J., PHEAR, G.A., AVES, S.J., AND NURSE, P., 1994. Analysis of a histone H2A variant from fission yeast: evidence for a role in chromosome stability. *Molecular & general genetics : MGG 245*, 5, 628–635.

CASTELLO, A., FISCHER, B., EICHELBAUM, K., HOROS, R., BECKMANN, B.M., STREIN, C., DAVEY, N.E., HUMPHREYS, D.T., PREISS, T., STEINMETZ, L.M., KRIJGSVELD, J., AND HENTZE, M.W., 2012. Insights into RNA biology from an atlas of mammalian mRNA-binding proteins. *Cell 149*, 6, 1393–1406.

CASTELLO, A., HOROS, R., STREIN, C., FISCHER, B., EICHELBAUM, K., STEINMETZ, L.M., KRIJGSVELD, J., AND HENTZE, M.W., 2013. System-wide identification of RNA-binding proteins by interactome capture. *Nature protocols 8*, 3, 491–500.

CAUDRON-HERGER, M., RUSIN, S.F., ADAMO, M.E., SEILER, J., SCHMID, V.K., BARREAU, E., KETTENBACH, A.N., AND DIEDERICHS, S., 2019. R-DeeP: Proteome-wide and Quantitative Identification of RNA-Dependent Proteins by Density Gradient Ultracentrifugation. *Molecular Cell 75*, 1, 184-199.e10.

CHAKRABORTY, S., PANDITA, R.K., HAMBARDE, S., MATTOO, A.R., CHARAKA, V., AHMED, K.M., IYER, S.P., HUNT, C.R., AND PANDITA, T.K., 2018. SMARCAD1 Phosphorylation and Ubiquitination Are Required for Resection during DNA Double-Strand Break Repair. *iScience 2*, 123–135.

CHANG, H.M., TRIBOULET, R., THORNTON, J.E., AND GREGORY, R.I., 2013. A role for the Perlman syndrome exonuclease Dis3l2 in the Lin28-let-7 pathway. *Nature 497*, 7448, 244–248.

CHEN, D., TOONE, W.M., MATA, J., LYNE, R., BURNS, G., KIVINEN, K., BRAZMA, A., JONES, N., AND BÄHLER, J., 2003. Global transcriptional responses of fission yeast to environmental stress. *Molecular biology of the cell 14*, 1, 214–229.

CHEN, J.W., ROMERO, P., UVERSKY, V.N., AND DUNKER, A.K., 2006. Conservation of intrinsic disorder in protein domains and families: II. functions of conserved disorder. *Journal of proteome research 5*, 4, 888–898.

CLAPIER, C.R., IWASA, J., CAIRNS, B.R., AND PETERSON, C.L., 2017. Mechanisms of action and regulation of ATP-dependent chromatin-remodelling complexes. *Nature Reviews Molecular Cell Biology 18*, 7, 407–422.

DANAN, C., MANICKAVEL, S., AND HAFNER, M., 2016. PAR-CLIP: A Method for Transcriptome-Wide Identification of RNA Binding Protein Interaction Sites. *Methods in molecular biology (Clifton, N.J.) 1358*, 153–173.

DAVIS, C.A., AND ARES, M., 2006. Accumulation of unstable promoter-associated transcripts upon loss of the nuclear exosome subunit Rrp6p in Saccharomyces cerevisiae.

*Proceedings of the National Academy of Sciences of the United States of America 103*, 9, 3262–3267.

DAVIS, M.W., AND JORGENSEN, E.M., 2022. ApE, A Plasmid Editor: A Freely Available DNA Manipulation and Visualization Program. *Frontiers in bioinformatics 2*, 818619.

DELAN-FORINO, C., SCHNEIDER, C., AND TOLLERVEY, D., 2017. Transcriptome-wide analysis of alternative routes for RNA substrates into the exosome complex. *PLoS genetics 13*, 3, e1006699.

DEUTSCHER, M.P., 2006. Degradation of RNA in bacteria: comparison of mRNA and stable RNA. *Nucleic Acids Research 34*, 2, 659–666.

DIEDERICHS, S., AND HABER, D.A., 2007. Dual role for argonautes in microRNA processing and posttranscriptional regulation of microRNA expression. *Cell 131*, 6, 1097–1108.

DIEDERICHS LAB/PROJECTS. 2018. *r-deep.dkfz.de. a table of all listed RNA-dependent proteins in humans*. https://r-deep.dkfz.de/session/8e4b670029eedefbfe58212204519061/download/down.RBPtable?w=. Accessed 17 January 2023.

DING, D.Q., HARAGUCHI, T., AND HIRAOKA, Y., 2013. The role of chromosomal retention of noncoding RNA in meiosis. *Chromosome research : an international journal on the molecular, supramolecular and evolutionary aspects of chromosome biology 21*, 6-7, 665–672.

DING, D.-Q., OKAMASA, K., KATOU, Y., OYA, E., NAKAYAMA, J., CHIKASHIGE, Y., SHIRAHIGE, K., HARAGUCHI, T., AND HIRAOKA, Y., 2019. Chromosome-associated RNA-protein complexes promote pairing of homologous chromosomes during meiosis in Schizosaccharomyces pombe. *Nature Communications 10*, 1, 5598.

DING, R., WEST, R.R., MORPHEW, D.M., OAKLEY, B.R., AND MCINTOSH, J.R., 1997. The spindle pole body of Schizosaccharomyces pombe enters and leaves the nuclear envelope as the cell cycle proceeds. *Molecular biology of the cell 8*, 8, 1461–1479.

DOMA, M.K., AND PARKER, R., 2007. *RNA Quality Control in Eukaryotes*. *Cell 131*.

DU, J., JOHNSON, L.M., JACOBSEN, S.E., AND PATEL, D.J., 2015. DNA methylation pathways and their crosstalk with histone methylation. *Nature Reviews Molecular Cell Biology 16*, 9, 519–532.

DZIEMBOWSKI, A., LORENTZEN, E., CONTI, E., AND SERAPHIN, B., 2007. A single subunit, Dis3, is essentially responsible for yeast exosome core activity. *Nat. Struct. Mol. Biol. 14*, 15–22.

EGAN, E.D., BRAUN, C.R., GYGI, S.P., AND MOAZED, D., 2014. Post-transcriptional regulation of meiotic genes by a nuclear RNA silencing complex. *RNA 20*, 6, 867–881.

EGEL, R., 1971. Physiological aspects of conjugation in fission yeast. *Planta 98*, 1, 89–96. https://pubmed.ncbi.nlm.nih.gov/24493310/.

EGEL, R., 1977. Selective spore survival during replica-plating of fission yeast. *Archives of microbiology 112*, 1, 109–110.

EISSENBERG, J.C., 2012. Structural biology of the chromodomain: form and function. *Gene 496*, 2, 69–78.

FANTES, P.A., AND HOFFMAN, C.S., 2016. A Brief History of Schizosaccharomyces pombe Research: A Perspective Over the Past 70 Years. *Genetics 203*, 2, 621–629.

FRANKE, V., GANESH, S., KARLIC, R., MALIK, R., PASULKA, J., HORVAT, F., KUZMAN, M., FULKA, H., CERNOHORSKA, M., URBANOVA, J., SVOBODOVA, E., MA, J., SUZUKI, Y., AOKI, F., SCHULTZ, R.M., VLAHOVICEK, K., AND SVOBODA, P., 2017. Long terminal repeats power evolution of genes and gene expression programs in mammalian oocytes and zygotes. *Genome research 27*, 8, 1384–1394.

FREESE, N.H., NORRIS, D.C., AND LORAINE, A.E., 2016. Integrated genome browser: visual analytics platform for genomics. *Bioinformatics (Oxford, England) 32*, 14, 2089–2095.

GAO, X., HOU, Y., EBINA, H., LEVIN, H.L., AND VOYTAS, D.F., 2008. Chromodomains direct integration of retrotransposons to heterochromatin. *Genome research 18*, 3, 359–369.

GHEDIRA, K., Ed. 2018. *Transcriptional and Post-transcriptional Regulation*. InTech.

GLATZ, A., PILBAT, A.-M., NÉMETH, G.L., VINCE-KONTÁR, K., JÓSVAY, K., HUNYA, Á., UDVARDY, A., GOMBOS, I., PÉTER, M., BALOGH, G., HORVÁTH, I., VÍGH, L., AND TÖRÖK, Z., 2016. Involvement of small heat shock proteins, trehalose, and lipids in the thermal stress management in Schizosaccharomyces pombe. *Cell stress & chaperones 21*, 2, 327–338.

GÖKE, J., AND NG, H.H., 2016. CTRL+INSERT: retrotransposons and their contribution to regulation and innovation of the transcriptome. *EMBO Reports 17*, 8, 1131–1144.

GÓRNA, M.W., CARPOUSIS, A.J., AND LUISI, B.F., 2012. From conformational chaos to robust regulation: the structure and function of the multi-enzyme RNA degradosome. *Quarterly reviews of biophysics 45*, 2, 105–145.

GREWAL, S.I.S., AND MOAZED, D., 2003. Heterochromatin and epigenetic control of gene expression. *Science 301*, 5634, 798–802.

HARIGAYA, Y., TANAKA, H., YAMANAKA, S., TANAKA, K., WATANABE, Y., TSUTSUMI, C., CHIKASHIGE, Y., HIRAOKA, Y., YAMASHITA, A., AND YAMAMOTO, M., 2006. Selective elimination of messenger RNA prevents an incidence of untimely meiosis. *Nature 442*, 7098, 45–50.

HARRIS, M.A., RUTHERFORD, K.M., HAYLES, J., LOCK, A., BÄHLER, J., OLIVER, S.G., MATA, J., AND WOOD, V., 2022. Fission stories: using PomBase to understand Schizosaccharomyces pombe biology. *Genetics 220*, 4.

HIGUCHI, Y., MORI, H., KUBOTA, T., AND TAKEGAWA, K., 2018. Analysis of ambient pH stress response mediated by iron and copper intake in Schizosaccharomyces pombe. *Journal of bioscience and bioengineering 125*, 1, 92–96.

HO, L., AND CRABTREE, G.R., 2010. Chromatin remodelling during development. *Nature 463*, 7280, 474–484.

HOFFMAN, C.S., WOOD, V., AND FANTES, P.A., 2015. An ancient yeast for young geneticists: A primer on the Schizosaccharomyces pombe model system. *Genetics 201*, 2, 403–423.

HORN, P.J., BASTIE, J.N., AND PETERSON, C.L., 2005. A Rik1-associated, cullin-dependent E3 ubiquitin ligase is essential for heterochromatin formation. *Genes & Development 19*, 14, 1705–1714.

IMADA, K., AND NAKAMURA, T., 2016. The exocytic Rabs Ypt3 and Ypt2 regulate the early step of biogenesis of the spore plasma membrane in fission yeast. *Molecular biology of the cell 27*, 21, 3317–3328.

IMAI, Y., AND YAMAMOTO, M., 1994. The fission yeast mating pheromone P-factor: its molecular structure, gene structure, and ability to induce gene expression and G1 arrest in the mating partner. *Genes & Development 8*, 3, 328–338.

INKSCAPE-DEVELOPMENT TEAM, 2022. *Inkscape*. Inkscape-development team.

IVANOVA, A.V., BONADUCE, M.J., IVANOV, S.V., AND KLAR, A.J., 1998. The chromo and SET domains of the Clr4 protein are essential for silencing in fission yeast. *Nature genetics 19*, 2, 192–195.

HAN, J., AND AMBRO, V.H., 2016. The RNA Exosome Channeling and Direct Access Conformations Have Distinct In Vivo Functions. *Cell Reports 16*, 12, 3348–3358.

HOUSELEY, J., AND TOLLERVEY, D., 2009. The Many Pathways of RNA Degradation. *Cell 136*, 4, 763–776.

JANUSZYK, K., AND LIMA, C.D., 2010. Structural components and architectures of RNA exosomes. *Advances in experimental medicine and biology 702*, 9–28.

JANUSZYK, K., LIU, Q., AND LIMA, C.D., 2011. Activities of human RRP6 and structure of the human RRP6 catalytic domain. *RNA 17*, 8, 1566–1577.

JANUSZYK, K., AND LIMA, C.D., 2014. The eukaryotic RNA exosome. *Current Opinion in Structural Biology 24*.

JIA, S., KOBAYASHI, R., AND GREWAL, S.I.S., 2005. Ubiquitin ligase component Cul4 associates with Clr4 histone methyltransferase to assemble heterochromatin. *Nature cell biology 7*, 10, 1007–1013.

KAGALWALA, M.N., GLAUS, B.J., DANG, W., ZOFALL, M., AND BARTHOLOMEW, B., 2004. Topography of the ISW2-nucleosome complex: insights into nucleosome spacing and chromatin remodeling. *The EMBO journal 23*, 10, 2092–2104.

KILCHERT, C., AND VASILJEVA, L., 2013. mRNA quality control goes transcriptional. *Biochemical Society Transactions 41*, 6, 1666–1672.

KILCHERT, C., WITTMANN, S., PASSONI, M., SHAH, S., GRANNEMAN, S., AND VASILJEVA, L., 2015. Regulation of mRNA Levels by Decay-Promoting Introns that Recruit the Exosome Specificity Factor Mmi1. *Cell Reports 13*, 11, 2504–2515.

KILCHERT, C., WITTMANN, S., AND VASILJEVA, L., 2016. The regulation and functions of the nuclear RNA exosome complex. *Nature Reviews Molecular Cell Biology 17*, 4, 435–439.

KILCHERT, C., KECMAN, T., PRIEST, E., HESTER, S., AYDIN, E., KUS, K., ROSSBACH, O., CASTELLO, A., MOHAMMED, S., AND VASILJEVA, L., 2020. System-wide analyses of the fission yeast poly(A)+ RNA interactome reveal insights into organization and function of RNA-protein complexes. *Genome research 30*, 7, 1012–1026.

KIM, H.S., *S.pombe – Transformation (LiAOc)*. https://www.researchgate.net/profile/Aashiq_Kachroo/post/Why_did_my_transformation_in_S_pombe_with_the_lithium_acetate_method_fails/attachment/59d61de379197b807797bdda/AS%3A273821184004120%401442295465860/download/PombeTransformation+1.pdf. Accessed 12 January 2023.

KIM, D.U., HAYLES, J., KIM, D., WOOD, V., PARK, H.-O., WON, M., YOO, H.S., DUHIG, T., NAM, M., PALMER, G., HAN, S., JEFFERY, L., BAEK, S.T., LEE, H., SHIM, Y.S., LEE, M., KIM, L., HEO, K.S., NOH, E.J., LEE, A.R., JANG, Y.J., CHUNG, K.S., CHOI, S.J., PARK, J.Y., PARK, Y., KIM, H.M., PARK, S.K., PARK, H.J., KANG, E.-J., KIM, H.B., KANG, H.S., PARK, H.M., KIM, K., SONG, K., SONG, K.B., NURSE, P., AND HOE, K.L., 2010. Analysis of a genome-wide set of gene deletions in the fission yeast Schizosaccharomyces pombe. *Nature biotechnology 28*, 6, 617–623.

KIM, H.S., VANOOSTHUYSE, V., FILLINGHAM, J., ROGUEV, A., WATT, S., KISLINGER, T., TREYER, A., CARPENTER, L.R., BENNETT, C.S., EMILI, A., GREENBLATT, J.F., HARDWICK, K.G., KROGAN, N.J., BÄHLER, J., AND KEOGH, M.C., 2009. An acetylated form of histone H2A.Z regulates chromosome architecture in Schizosaccharomyces pombe. *Nature structural & molecular biology 16*, 12, 1286–1293.

KINOSHITA, N., GOEBL, M., AND YANAGIDA, M., 1991. The fission yeast dis3+ gene encodes a 110-kDa essential protein implicated in mitotic control. *Molecular and Cellular Biology 11*, 12, 5839–5847.

KITAMURA, K., AND SHIMODA, C., 1991. The Schizosaccharomyces pombe mam2 gene encodes a putative pheromone receptor which has a significant homology with the Saccharomyces cerevisiae Ste2 protein. *The EMBO journal 10*, 12, 3743–3751.

KJAERULFF, S., DAVEY, J., AND NIELSEN, O., 1994. Analysis of the structural genes encoding M-factor in the fission yeast Schizosaccharomyces pombe: identification of a third gene, mfm3. *Molecular and Cellular Biology 14*, 6, 3895–3905.

KJAERULFF, S., LAUTRUP-LARSEN, I., TRUELSEN, S., PEDERSEN, M., AND NIELSEN, O., 2005. Constitutive activation of the fission yeast pheromone-responsive pathway induces ectopic meiosis and reveals ste11 as a mitogen-activated protein kinase target. *Molecular and Cellular Biology 25*, 5, 2045–2059.

KORESSAAR, T., AND REMM, M., 2007. Enhancements and modifications of primer design program Primer3. *Bioinformatics (Oxford, England) 23*, 10, 1289–1291.

KRUEGER, F., 2021. *Trim Galore*. GitHub.

KUSCU, C., ZARATIEGUI, M., KIM, H.S., WAH, D.A., MARTIENSSEN, R.A., SCHALCH, T., AND JOSHUA-TOR, L., 2014. CRL4-like Clr4 complex in Schizosaccharomyces pombe depends on an exposed surface of Dos1 for heterochromatin silencing. *Proceedings of the National Academy of Sciences of the United States of America 111*, 5, 1795–1800.

LACAVA, J., HOUSELEY, J., SAVEANU, C., PETFALSKI, E., THOMPSON, E., JACQUIER, A., AND TOLLERVEY, D., 2005. RNA degradation by the exosome is promoted by a nuclear polyadenylation complex. *Cell 121*, 5, 713–724.

LAI, A.Y., AND WADE, P.A., 2011. Cancer biology and NuRD: a multifaceted chromatin remodelling complex. *Nature reviews. Cancer 11*, 8, 588–596.

LANGMEAD, B., AND SALZBERG, S.L., 2012. Fast gapped-read alignment with Bowtie 2. *Nature methods 9*, 4, 357–359.

LAUREAU, R., DYATEL, A., DURSUK, G., BROWN, S., ADEOYE, H., YUE, J.-X., CHIARA, M. DE, HARRIS, A., ÜNAL, E., LITI, G., ADAMS, I.R., AND BERCHOWITZ, L.E., 2021. Meiotic Cells Counteract Programmed Retrotransposon Activation via RNA-Binding Translational Repressor Assemblies. *Developmental cell 56*, 1, 22-35.e7.

LEE, J., CHOI, E.S., SEO, H.D., KANG, K., GILMORE, J.M., FLORENS, L., WASHBURN, M.P., CHOE, J., WORKMAN, J.L., AND LEE, D., 2017. Chromatin remodeller Fun30Fft3 induces nucleosome disassembly to facilitate RNA polymerase II elongation. *Nature Communications 8*, 14527.

LEE, N.N., CHALAMCHARLA, V.R., REYES-TURCU, F., MEHTA, S., ZOFALL, M., BALACHANDRAN, V., DHAKSHNAMOORTHY, J., TANEJA, N., YAMANAKA, S., ZHOU, M., AND GREWAL, S.I.S., 2013. Mtr4-like protein coordinates nuclear RNA processing for heterochromatin assembly and for telomere maintenance. *Cell 155*, 5, 1061–1074.

LEHRBACH, N.J., ARMISEN, J., LIGHTFOOT, H.L., MURFITT, K.J., BUGAUT, A., BALASUBRAMANIAN, S., AND MISKA, E.A., 2009. LIN-28 and the poly(U) polymerase PUP-2 regulate let-7 microRNA processing in Caenorhabditis elegans. *Nature structural & molecular biology 16*, 10, 1016–1020.

LEJEUNE, F., LI, X., AND MAQUAT, L.E., 2003. Nonsense-Mediated mRNA Decay in Mammalian Cells Involves Decapping, Deadenylating, and Exonucleolytic Activities. *Molecular Cell 12*.

LEMIEUX, C., MARGUERAT, S., LAFONTAINE, J., BARBEZIER, N., BÄHLER, J., AND BACHAND, F., 2011. A Pre-mRNA degradation pathway that selectively targets intron-containing genes requires the nuclear poly(A)-binding protein. *Molecular Cell 44*, 1, 108–119.

LEUPOLD, U., 1949. *Die Vererbung von Homothallie und Heterothallie bei Schizosaccharomyces pombe*. Dissertation.

LIAO, Y., SMYTH, G.K., AND SHI, W., 2014. featureCounts: an efficient general purpose program for assigning sequence reads to genomic features. *Bioinformatics (Oxford, England) 30*, 7, 923–930.

LINDNER, P., 1893. Schizosaccharomyces pombe n. sp. neuer Gärungserreger. *Wochenschrift für Brauerei*, 10, 1298–1300.

LIPARDI, C., WEI, Q., AND PATERSON, B.M., 2001. RNAi as random degradative PCR: siRNA primers convert mRNA into dsRNAs that are degraded to generate new siRNAs. *Cell 107*, 3, 297–307.

LIU, J.J., NIU, C.Y., WU, Y., TAN, D., WANG, Y., DA YE, M., LIU, Y., ZHAO, W., ZHOU, K., LIU, Q.S., DAI, J., YANG, X., QIU DONG, M., HUANG, N., AND WANG, H.W., 2016. CryoEM structure of yeast cytoplasmic exosome complex. *Cell Research 26*, 7, 822–837.

LIU, Q., GREIMANN, J.C., AND LIMA, C.D., 2006. Reconstitution, Activities, and Structure of the Eukaryotic RNA Exosome. *Cell 127*, 6, 1223–1237.

LIU, W., XIE, Y., MA, J., LUO, X., NIE, P., ZUO, Z., LAHRMANN, U., ZHAO, Q., ZHENG, Y., ZHAO, Y., XUE, Y., AND REN, J., 2015. IBS: an illustrator for the presentation and visualization of biological sequences. *Bioinformatics (Oxford, England) 31*, 20, 3359–3361.

LIVAK, K.J., AND SCHMITTGEN, T.D., 2001. Analysis of relative gene expression data using real-time quantitative PCR and the 2(-Delta Delta C(T)) Method. *Methods (San Diego, Calif.) 25*, 4, 402–408. https://pubmed.ncbi.nlm.nih.gov/11846609/.

LO, C.S.Y., VAN TOORN, M., GAGGIOLI, V., PAES DIAS, M., ZHU, Y., MANOLIKA, E.M., ZHAO, W., VAN DER DOES, M., MUKHERJEE, C., G S C SOUTO GONÇALVES, J., VAN ROYEN, M.E., FRENCH, P.J., DEMMERS, J., SMAL, I., LANS, H., WHEELER, D., JONKERS, J., CHAUDHURI, A.R., MARTEIJN, J.A., AND TANEJA, N., 2021. SMARCAD1-mediated active replication fork stability maintains genome integrity. *Science Advances 7*, 19.

LORENTZEN, E., AND CONTI, E., 2005. Structural basis of 3′ end RNA recognition and exoribonucleolytic cleavage by an exosome RNase PH core. *Molecular Cell 20*, 3, 473–481.

LORENTZEN, E., WALTER, P., FRIBOURG, S., EVGUENIEVA-HACKENBERG, E., KLUG, G., AND CONTI, E., 2005. The archaeal exosome core is a hexameric ring structure with three catalytic subunits. *Nature structural & molecular biology 12*, 7, 575–581.

LUBAS, M., CHRISTENSEN, M.S., KRISTIANSEN, M.S., DOMANSKI, M., FALKENBY, L.G., LYKKE-ANDERSEN, S., ANDERSEN, J.S., DZIEMBOWSKI, A., AND JENSEN, T.H., 2011. Interaction profiling identifies the human nuclear exosome targeting complex. *Molecular Cell 43*, 4, 624–637.

MALECKI, M., VIEGAS, S.C., CARNEIRO, T., GOLIK, P., DRESSAIRE, C., FERREIRA, M.G., AND ARRAIANO, C.M., 2013. The exoribonuclease Dis3L2 defines a novel eukaryotic RNA degradation pathway. *The EMBO journal 32*, 13, 1842–1854.

MALET, H., TOPF, M., CLARE, D.K., EBERT, J., BONNEAU, F., BASQUIN, J., DRAZKOWSKA, K., TOMECKI, R., DZIEMBOWSKI, A., CONTI, E., SAIBIL, H.R., AND LORENTZEN, E., 2010. RNA channelling by the eukaryotic exosome. *EMBO Reports 11*, 12, 936–942.

MARAYATI, B.F., HOSKINS, V., BOGER, R.W., TUCKER, J.F., FISHMAN, E.S., BRAY, A.S., AND ZHANG, K., 2016. The fission yeast MTREC and EJC orthologs ensure the maturation of meiotic transcripts during meiosis. *RNA 22*, 9, 1349–1359.

MARGUERAT, S., SCHMIDT, A., CODLIN, S., CHEN, W., AEBERSOLD, R., AND BÄHLER, J., 2012. Quantitative Analysis of Fission Yeast Transcriptomes and Proteomes in Proliferating and Quiescent Cells. *Cell 151*, 3, 671–683.

MARKERT, J., ZHOU, K., AND LUGER, K., 2021. SMARCAD1 is an ATP-dependent histone octamer exchange factor with de novo nucleosome assembly activity. *Science Advances 7*, 42, eabk2380.

MARTIENSSEN, R., AND MOAZED, D., 2015. RNAi and heterochromatin assembly. *Cold Spring Harbor perspectives in biology 7*, 8, a019323.

MARTÍN CABALLERO, L., CAPELLA, M., BARRALES, R.R., DOBREV, N., VAN EMDEN, T., HIRANO, Y., SUMA SREECHAKRAM, V.N., FISCHER-BURKART, S., KINUGASA, Y., NEVERS, A., ROUGEMAILLE, M., SINNING, I., FISCHER, T., HIRAOKA, Y., AND BRAUN, S., 2022. The inner nuclear membrane protein Lem2 coordinates RNA degradation at the nuclear periphery. *Nature structural & molecular biology 29*, 9, 910–921.

MAURYA, P.K., GARAI, P., GOEL, K., BHATT, H., DUTTA, A., GOYAL, A., DEWASTHALE, S., GUPTA, M., HAOKIP, D.T., BARIK, S., AND MUTHUSWAMI, R., 2022. Fun30 and Rtt109 Mediate Epigenetic Regulation of the DNA Damage Response Pathway in C. albicans. *Journal of fungi (Basel, Switzerland) 8*, 6.

MEOLA, N., DOMANSKI, M., KARADOULAMA, E., CHEN, Y., GENTIL, C., PULTZ, D., VITTING-SEERUP, K., LYKKE-ANDERSEN, S., ANDERSEN, J.S., SANDELIN, A., AND JENSEN, T.H., 2016. Identification of a Nuclear Exosome Decay Pathway for Processed Transcripts. *Molecular Cell 64*, 3, 520–533. https://www.cell.com/molecular-cell/pdf/S1097-2765(16)30574-3.pdf.

MIGNONE, F., GISSI, C., LIUNI, S., AND PESOLE, G., 2002. Untranslated regions of mRNAs. *Genome biology 3*, 3, REVIEWS0004.

MIKOLASKOVA, B., JURCIK, M., CIPAKOVA, I., SELICKY, T., JURCIK, J., POLAKOVA, S.B., STUPENOVA, E., DUDAS, A., SIVAKOVA, B., BELLOVA, J., BARATH, P., ARONICA, L., GREGAN, J., AND CIPAK, L., 2021. Identification of Nrl1 Domains Responsible for Interactions with RNA-Processing Factors and Regulation of Nrl1 Function by Phosphorylation. *International journal of molecular sciences 22*, 13.

MITA, P., AND BOEKE, J.D., 2016. How retrotransposons shape genome regulation. *Current opinion in genetics & development 37*, 90–100.

MITCHELL, P., PETFALSKI, E., SHEVCHENKO, A., MANN, M., AND TOLLERVEY, D., 1997. The exosome: A conserved eukaryotic RNA processing complex containing multiple 3’→5’ exoribonucleases. *Cell 91*, 4, 457–466.

MITCHISON, J.M., 1990. The fission yeast, Schizosaccharomyces pombe. *BioEssays : news and reviews in molecular, cellular and developmental biology 12*, 4, 189–191.

MOCHIZUKI, N., AND YAMAMOTO, M., 1992. Reduction in the intracellular cAMP level triggers initiation of sexual development in fission yeast. *Molecular & general genetics : MGG 233*, 1-2, 17–24.

MOLNAR, M., PARISI, S., KAKIHARA, Y., NOJIMA, H., YAMAMOTO, A., HIRAOKA, Y., BOZSIK, A., SIPICZKI, M., AND KOHLI, J., 2001. Characterization of rec7, an early meiotic recombination gene in Schizosaccharomyces pombe. *Genetics 157*, 2, 519–532.

MONTAVON, T., SHUKEIR, N., ERIKSON, G., ENGIST, B., ONISHI-SEEBACHER, M., RYAN, D., MUSA, Y., MITTLER, G., MEYER, A.G., GENOUD, C., AND JENUWEIN, T., 2021. Complete loss of H3K9 methylation dissolves mouse heterochromatin organization. *Nature Communications 12*, 1, 4359.

MOURIER, T., AND WILLERSLEV, E., 2010. Large-scale transcriptome data reveals transcriptional activity of fission yeast LTR retrotransposons. *BMC genomics 11*, 167.

MUKHERJEE, K., GARDIN, J., FUTCHER, B., AND LEATHERWOOD, J., 2016. Relative contributions of the structural and catalytic roles of Rrp6 in exosomal degradation of individual mRNAs. *RNA 22*, 9, 1311–1319.

MURCHISON, E.P., AND HANNON, G.J., 2004. miRNAs on the move: miRNA biogenesis and the RNAi machinery. *Current Opinion in Cell Biology 16*, 3, 223–229. https://www.sciencedirect.com/science/article/pii/S0955067404000547.

NAKAYAMA, J., RICE, J.C., STRAHL, B.D., ALLIS, C.D., AND GREWAL, S.I.S., 2001. Role of histone H3 lysine 9 methylation in epigenetic control of heterochromatin assembly. *Science (New York, N.Y.) 292*, 5514, 110–113.

NEVES-COSTA, A., WILL, W.R., VETTER, A.T., MILLER, J.R., AND VARGA-WEISZ, P., 2009. The SNF2-family member Fun30 promotes gene silencing in heterochromatic loci. *PLoS ONE 4*, 12, e8111.

NIELSEN, O., AND DAVEY, J., 1995. Pheromone communication in the fission yeast Schizosaccharomyces pombe. *Seminars in cell biology 6*, 2, 95–104.

NIMMO, E.R., CRANSTON, G., AND ALLSHIRE, R.C., 1994. Telomere-associated chromosome breakage in fission yeast results in variegated expression of adjacent genes. *The EMBO journal 13*, 16, 3801–3811.

NISHI, H., HASHIMOTO, K., AND PANCHENKO, A.R., 2011. Phosphorylation in protein-protein binding: effect on stability and function. *Structure 19*, 12, 1807–1815.

OGAMI, K., 2018. RNA Surveillance by the Nuclear RNA Exosome: Mechanisms and Significance.

OHTSUKA, H., IMADA, K., SHIMASAKI, T., AND AIBA, H., 2022. Sporulation: A response to starvation in the fission yeast Schizosaccharomyces pombe. *MicrobiologyOpen 11*, 3, e1303.

ONO, Y., KATAYAMA, K., ONUMA, T., KUBO, K., TSUYUZAKI, H., HAMADA, M., AND SATO, M., 2022. Structure-based screening for functional non-coding RNAs in fission yeast identifies a factor repressing untimely initiation of sexual differentiation. *Nucleic Acids Research 50*, 19, 11229–11242.

ORIGINLAB CORPORATION., 2022. *OriginPro*. OriginLab Corporation, Northampton, MA, USA.

OYA, E., NAKAGAWA, R., YOSHIMURA, Y., TANAKA, M., NISHIBUCHI, G., MACHIDA, S., SHIRAI, A., EKWALL, K., KURUMIZAKA, H., TAGAMI, H., AND NAKAYAMA, J., 2019. H3K14 ubiquitylation promotes H3K9 methylation for heterochromatin assembly. *EMBO Reports 20*, 10, e48111.

PADEKEN, J., METHOT, S.P., AND GASSER, S.M., 2022. Establishment of H3K9-methylated heterochromatin and its functions in tissue differentiation and maintenance. *Nature Reviews Molecular Cell Biology 23*, 9, 623–640.

PAPAMICHOS-CHRONAKIS, M., WATANABE, S., RANDO, O.J., AND PETERSON, C.L., 2011. Global regulation of H2A.Z localization by the INO80 chromatin-remodeling enzyme is essential for genome integrity. *Cell 144*, 2, 200–213.

PERSSON, J., STEGLICH, B., SMIALOWSKA, A., BOYD, M., BORNHOLDT, J., ANDERSSON, R., SCHURRA, C., ARCANGIOLI, B., SANDELIN, A., NIELSEN, O., AND EKWALL, K., 2016. Regulating retrotransposon activity through the use of alternative transcription start sites. *EMBO Reports 17*, 5, 753–768.

PETERSEN, J., AND RUSSELL, P., 2016. Growth and the Environment of Schizosaccharomyces pombe. *Cold Spring Harbor protocols 2016*, 3, pdb.top079764.

PORRUA, O., AND LIBRI, D., 2015. Transcription termination and the control of the transcriptome: why, where and how to stop. *Nature Reviews Molecular Cell Biology 16*, 3, 190–202.

PRATT, A.J., AND MACRAE, I.J., 2009. The RNA-induced Silencing Complex: A Versatile Gene-silencing Machine*. *The Journal of biological chemistry 284*, 27, 17897–17901.

RAMÍREZ, F., RYAN, D.P., GRÜNING, B., BHARDWAJ, V., KILPERT, F., RICHTER, A.S., HEYNE, S., DÜNDAR, F., AND MANKE, T., 2016. deepTools2: a next generation web server for deep-sequencing data analysis. *Nucleic Acids Research 44*, W1, W160-5.

REA, S., EISENHABER, F., O'CARROLL, D., STRAHL, B.D., SUN, Z.W., SCHMID, M., OPRAVIL, S., MECHTLER, K., PONTING, C.P., ALLIS, C.D., AND JENUWEIN, T., 2000. Regulation of chromatin structure by site-specific histone H3 methyltransferases. *Nature 406*, 6796, 593–599.

REYES-TURCU, F.E., ZHANG, K., ZOFALL, M., CHEN, E., AND GREWAL, S.I.S., 2011. Defects in RNA quality control factors reveal RNAi-independent nucleation of heterochromatin. *Nature structural & molecular biology 18*, 10, 1132–1138.

RHIND, N., CHEN, Z., YASSOUR, M., THOMPSON, D.A., HAAS, B.J., HABIB, N., WAPINSKI, I., ROY, S., LIN, M.F., HEIMAN, D.I., YOUNG, S.K., FURUYA, K., GUO, Y., PIDOUX, A., CHEN, H.M., ROBBERTSE, B., GOLDBERG, J.M., AOKI, K., BAYNE, E.H., BERLIN, A.M., DESJARDINS, C.A., DOBBS, E., DUKAJ, L., FAN, L., FITZ GERALD, M.G., FRENCH, C., GUJJA, S., HANSEN, K., KEIFENHEIM, D., LEVIN, J.Z., MOSHER, R.A., MÜLLER, C.A., PFIFFNER, J., PRIEST, M., RUSS, C., SMIALOWSKA, A., SWOBODA, P., SYKES, S.M., VAUGHN, M., VENGROVA, S., YODER, R., ZENG, Q., ALLSHIRE, R., BAULCOMBE, D., BIRREN, B.W., BROWN, W., EKWALL, K., KELLIS, M., LEATHERWOOD, J., LEVIN, H., MARGALIT, H., MARTIENSSEN, R., NIEDUSZYNSKI, C.A., SPATAFORA, J.W., FRIEDMAN, N., DALGAARD, J.Z., BAUMANN, P., NIKI, H., REGEV, A., NUSBAUM, C., 2011. Comparative functional genomics of the fission yeasts. *Science 20,* 332, 930-936

RIO, D.C., 2014. 5'-end labeling of RNA with γ-32PATP and T4 polynucleotide kinase. *Cold Spring Harbor protocols 2014*, 4, 441–443.

ROWBOTHAM, S.P., BARKI, L., NEVES-COSTA, A., SANTOS, F., DEAN, W., HAWKES, N., CHOUDHARY, P., WILL, W.R., WEBSTER, J., OXLEY, D., GREEN, C.M., VARGA-WEISZ, P., AND MERMOUD, J.E., 2011. Maintenance of silent chromatin through replication requires SWI/SNF-like chromatin remodeler SMARCAD1. *Molecular Cell 42*, 3, 285–296.

SCHINDELIN, J., ARGANDA-CARRERAS, I., FRISE, E., KAYNIG, V., LONGAIR, M., PIETZSCH, T., PREIBISCH, S., RUEDEN, C., SAALFELD, S., SCHMID, B., TINEVEZ, J.-Y., WHITE, D.J., HARTENSTEIN, V., ELICEIRI, K., TOMANCAK, P., AND CARDONA, A., 2012. Fiji: an open-source platform for biological-image analysis. *Nature methods 9*, 7, 676–682.

SEIKE, T., AND NIKI, H., 2022. Pheromone Response and Mating Behavior in Fission Yeast. *Microbiology and molecular biology reviews : MMBR 86*, 4, e0013022.

SHAN, C.-M., KIM, J.-K., WANG, J., BAO, K., SUN, Y., CHEN, H., YUE, J.-X., STIRPE, A., ZHANG, Z., LU, C., SCHALCH, T., LITI, G., NAGY, P.L., TONG, L., QIAO, F., AND JIA, S., 2021. The histone H3K9M mutation synergizes with H3K14 ubiquitylation to selectively sequester histone H3K9 methyltransferase Clr4 at heterochromatin. *Cell Reports 35*, 7, 109137.

SHICHINO, Y., OTSUBO, Y., KIMORI, Y., YAMAMOTO, M., AND YAMASHITA, A., 2018. YTH-RNA-binding protein prevents deleterious expression of meiotic proteins by tethering their mRNAs to nuclear foci. *eLife 7*.

SHICHINO, Y., YAMASHITA, A., AND YAMAMOTO, M., 2014. Meiotic long non-coding meiRNA accumulates as a dot at its genetic locus facilitated by Mmi1 and plays as a decoy to lure Mmi1. *Open Biology 4*, 6, 140022.

SIEVERS, F., WILM, A., DINEEN, D., GIBSON, T.J., KARPLUS, K., LI, W., LOPEZ, R., MCWILLIAM, H., REMMERT, M., SÖDING, J., THOMPSON, J.D., AND HIGGINS, D.G., 2011. Fast, scalable generation of high-quality protein multiple sequence alignments using Clustal Omega. *Molecular systems biology 7*, 539.

SIGOVA, A., RHIND, N., AND ZAMORE, P.D., 2004. A single Argonaute protein mediates both transcriptional and posttranscriptional silencing in Schizosaccharomyces pombe. *Genes & Development 18*, 19, 2359–2367.

SIPICZKI, M., 2000. Where does fission yeast sit on the tree of life? *Genome biology 1*, 2,

SMITH, C.L., MATSUMOTO, T., NIWA, O., KLCO, S., FAN, J.B., YANAGIDA, M., AND CANTOR, C.R., 1987. An electrophoretic karyotype for Schizosaccharomyces pombe by pulsed field gel electrophoresis. *Nucleic Acids Research 15*, 11, 4481–4489.

SPENCER KIMBALL, P.M., 2022. *GIMP 2*. GIMP-development team.

STAALS, R.H.J., BRONKHORST, A.W., SCHILDERS, G., SLOMOVIC, S., SCHUSTER, G., HECK, A.J.R., RAIJMAKERS, R., AND PRUIJN, G.J.M., 2010. Dis3-like 1: a novel exoribonuclease associated with the human exosome. *The EMBO journal 29*, 14, 2358–2367.

STEBEL, S., BREUER, J., AND ROSSBACH, O., 2022. Studying miRNA-mRNA Interactions: An Optimized CLIP-Protocol for Endogenous Ago2-Protein. *Methods and protocols 5*, 6.

STEGLICH, B., STRÅLFORS, A., KHOROSJUTINA, O., PERSSON, J., SMIALOWSKA, A., JAVERZAT, J.-P., AND EKWALL, K., 2015. The Fun30 chromatin remodeler Fft3 controls nuclear organization and chromatin structure of insulators and subtelomeres in fission yeast. *PLoS genetics 11*, 3, e1005101.

STELZER, G., ROSEN, N., PLASCHKES, I., ZIMMERMAN, S., TWIK, M., FISHILEVICH, S., STEIN, T.I., NUDEL, R., LIEDER, I., MAZOR, Y., KAPLAN, S., DAHARY, D., WARSHAWSKY, D., GUAN-GOLAN, Y., KOHN, A., RAPPAPORT, N., SAFRAN, M., AND LANCET, D., 2016. The GeneCards Suite: From Gene Data Mining to Disease Genome Sequence Analyses. *Current protocols in bioinformatics 54*, 1.30.1-1.30.33.

STEVENSON, A.L., AND NORBURY, C.J., 2006. The Cid1 family of non-canonical poly(A) polymerases. *Yeast 23*, 13, 991–1000.

STOREY, A.J., WANG, H.-P., PROTACIO, R.U., DAVIDSON, M.K., TACKETT, A.J., AND WAHLS, W.P., 2018. Chromatin-mediated regulators of meiotic recombination revealed by proteomics of a recombination hotspot. *Epigenetics & chromatin 11*, 1, 64.

STRÅLFORS, A., WALFRIDSSON, J., BHUIYAN, H., AND EKWALL, K., 2011. The FUN30 chromatin remodeler, Fft3, protects centromeric and subtelomeric domains from euchromatin formation. *PLoS genetics 7*, 3, e1001334.

SUGIYAMA, T., AND SUGIOKA-SUGIYAMA, R., 2011. Red1 promotes the elimination of meiosis-specific mRNAs in vegetatively growing fission yeast. *The EMBO journal 30*, 6, 1027–1039.

SUGIYAMA, T., WANATABE, N., KITAHATA, E., TANI, T., AND SUGIOKA-SUGIYAMA, R., 2013. Red5 and three nuclear pore components are essential for efficient suppression of specific mRNAs during vegetative growth of fission yeast. *Nucleic Acids Research 41*, 13, 6674–6686.

TAHARA, Y.O., MIYATA, M., AND NAKAMURA, T., 2020. Quick-Freeze, Deep-Etch Electron Microscopy Reveals the Characteristic Architecture of the Fission Yeast Spore. *Journal of fungi (Basel, Switzerland) 7*, 1.

TANAKA, K., DAVEY, J., IMAI, Y., AND YAMAMOTO, M., 1993. Schizosaccharomyces pombe map3+ encodes the putative M-factor receptor. *Molecular and Cellular Biology 13*, 1, 80–88.

TANAKA, K., AND HIRATA, A., 1982. Ascospore development in the fission yeasts Schizosaccharomyces pombe and S. japonicus. *Journal of cell science 56*, 263–279.

TANEJA, N., ZOFALL, M., BALACHANDRAN, V., THILLAINADESAN, G., SUGIYAMA, T., WHEELER, D., ZHOU, M., AND GREWAL, S.I.S., 2017. SNF2 Family Protein Fft3 Suppresses Nucleosome

Turnover to Promote Epigenetic Inheritance and Proper Replication. *Molecular Cell 66*, 1, 50-62.e6.

TASHIRO, S., ASANO, T., KANOH, J., AND ISHIKAWA, F., 2013. Transcription-induced chromatin association of RNA surveillance factors mediates facultative heterochromatin formation in fission yeast. *Genes to cells : devoted to molecular & cellular mechanisms 18*, 4, 327–339.

TEJADA-ARRANZ, A., CRÉCY-LAGARD, V., AND REUSE, H., 2020. Bacterial RNA Degradosomes: Molecular Machines under Tight Control. *Trends in biochemical sciences 45*, 1, 42–57.

THE GALAXY COMMUNITY, 2022. The Galaxy platform for accessible, reproducible and collaborative biomedical analyses: 2022 update. *Nucleic Acids Research 50*, W1, W345-51.

THOMAS, P.D., EBERT, D., MURUGANUJAN, A., MUSHAYAHAMA, T., ALBOU, L.-P., AND MI, H., 2022. PANTHER: Making genome-scale phylogenetics accessible to all. *Protein science : a publication of the Protein Society 31*, 1, 8–22.

THOMS, M., THOMSON, E., BAßLER, J., GNÄDIG, M., GRIESEL, S., AND HURT, E., 2015. The Exosome Is Recruited to RNA Substrates through Specific Adaptor Proteins. *Cell 162*, 5, 1029–1038.

TOMECKI, R., KRISTIANSEN, M.S., LYKKE-ANDERSEN, S., CHLEBOWSKI, A., LARSEN, K.M., SZCZESNY, R.J., DRAZKOWSKA, K., PASTULA, A., ANDERSEN, J.S., STEPIEN, P.P., DZIEMBOWSKI, A., AND JENSEN, T.H., 2010. The human core exosome interacts with differentially localized processive RNases: hDIS3 and hDIS3L. *The EMBO journal 29*, 14, 2342–2357.

TONG, Z.-B., AI, H.-S., AND LI, J.-B., 2020. The Mechanism of Chromatin Remodeler SMARCAD1/Fun30 in Response to DNA Damage. *Frontiers in cell and developmental biology 8*, 560098.

TRAN, H.G., STEGER, D.J., IYER, V.R., AND JOHNSON, A.D., 2000. The chromo domain protein chd1p from budding yeast is an ATP-dependent chromatin-modifying factor. *The EMBO journal 19*, 10, 2323–2331.

TROJER, P., AND REINBERG, D., 2007. Facultative heterochromatin: is there a distinctive molecular signature? *Molecular Cell 28*, 1, 1–13.

TUDEK, A., LLORET-LLINARES, M., AND JENSEN, T.H., 2018. The multitasking polyA tail: nuclear RNA maturation, degradation and export. *Philosophical transactions of the Royal Society of London. Series B, Biological sciences 373*, 1762.

VALENTIN, M.N., SOLOMON, B.D., RICHARD, G., FERREIRA, C.R., AND KIRKORIAN, A.Y., 2018. Basan gets a new fingerprint: Mutations in the skin-specific isoform of SMARCAD1 cause ectodermal dysplasia syndromes with adermatoglyphia. *American journal of medical genetics. Part A 176*, 11, 2451–2455.

VAN ATTIKUM, H., FRITSCH, O., AND GASSER, S.M., 2007. Distinct roles for SWR1 and INO80 chromatin remodeling complexes at chromosomal double-strand breaks. *The EMBO journal 26*, 18, 4113–4125.

VAN DER LEE, R., BULJAN, M., LANG, B., WEATHERITT, R.J., DAUGHDRILL, G.W., DUNKER, A.K., FUXREITER, M., GOUGH, J., GSPONER, J., JONES, D.T., KIM, P.M., KRIWACKI, R.W., OLDFIELD, C.J., PAPPU, R.V., TOMPA, P., UVERSKY, V.N., WRIGHT, P.E., AND BABU, M.M., 2014. Classification of intrinsically disordered regions and proteins. *Chemical reviews 114*, 13, 6589–6631.

VAN DIJK, E.L., SCHILDERS, G., AND PRUIJN, G.J.M., 2007. Human cell growth requires a functional cytoplasmic exosome, which is involved in various mRNA decay pathways. *RNA (New York, N.Y.) 13*, 7, 1027–1035.

VARADI, M., ANYANGO, S., DESHPANDE, M., NAIR, S., NATASSIA, C., YORDANOVA, G., YUAN, D., STROE, O., WOOD, G., LAYDON, A., ŽÍDEK, A., GREEN, T., TUNYASUVUNAKOOL, K., PETERSEN, S., JUMPER, J., CLANCY, E., GREEN, R., VORA, A., LUTFI, M., FIGURNOV, M., COWIE, A., HOBBS, N., KOHLI, P., KLEYWEGT, G., BIRNEY, E., HASSABIS, D., AND VELANKAR, S., 2022. AlphaFold Protein Structure Database: massively expanding the structural coverage of protein-sequence space with high-accuracy models. *Nucleic Acids Research 50*, D1, D439-D444.

VERDEL, A., JIA, S., GERBER, S., SUGIYAMA, T., GYGI, S., GREWAL, S.I.S., AND MOAZED, D., 2004. RNAi-mediated targeting of heterochromatin by the RITS complex. *Science 303*, 5658, 672–676.

VO, T.V., DAS, J., MEYER, M.J., CORDERO, N.A., AKTURK, N., WEI, X., FAIR, B.J., DEGATANO, A.G., FRAGOZA, R., LIU, L.G., MATSUYAMA, A., TRICKEY, M., HORIBATA, S., GRIMSON, A., YAMANO, H., YOSHIDA, M., ROTH, F.P., PLEISS, J.A., XIA, Y., AND YU, H., 2016. A Proteome-wide Fission Yeast Interactome Reveals Network Evolution Principles from Yeasts to Human. *Cell 164*, 1-2, 310–323.

VOLPE, T.A., KIDNER, C., HALL, I.M., TENG, G., GREWAL, S.I.S., AND MARTIENSSEN, R.A., 2002. Regulation of heterochromatic silencing and histone H3 lysine-9 methylation by RNAi. *Science 297*, 5588, 1833–1837.

WAN, J., YOURSHAW, M., MAMSA, H., RUDNIK-SCHÖNEBORN, S., MENEZES, M.P., HONG, J.E., LEONG, D.W., SENDEREK, J., SALMAN, M.S., CHITAYAT, D., SEEMAN, P., MOERS, A. VON, GRAUL-NEUMANN, L., KORNBERG, A.J., CASTRO-GAGO, M., SOBRIDO, M.-J., SANEFUJI, M., SHIEH, P.B., SALAMON, N., KIM, R.C., VINTERS, H.V., CHEN, Z., ZERRES, K., RYAN, M.M., NELSON, S.F., AND JEN, J.C., 2012. Mutations in the RNA exosome component gene EXOSC3 cause pontocerebellar hypoplasia and spinal motor neuron degeneration. *Nature genetics 44*, 6, 704–708.

WANG, H.W., WANG, J., DING, F., CALLAHAN, K., BRATKOWSKI, M.A., BUTLER, J.S., NOGALES, E., AND KE, A., 2007. Architecture of the yeast Rrp44-exosome complex suggests routes of RNA recruitment for 3′ end processing. *Proceedings of the National Academy of Sciences of the United States of America 104*, 43, 16844–16849.

WANG, X., JIA, H., JANKOWSKY, E., AND ANDERSON, J.T., 2008. Degradation of hypomodified tRNAiMet in vivo involves RNA-dependent ATPase activity of the DExH helicase Mtr4p. *RNA (New York, N.Y.) 14*, 1, 107–116.

WASMUTH, E.V., JANUSZYK, K., AND LIMA, C.D., 2014. Structure of an Rrp6-RNA exosome complex bound to polyA RNA. *Nature 176*, 5, 139–148.

WATANABE, Y., LINO, Y., FURUHATA, K., SHIMODA, C., AND YAMAMOTO, M., 1988. The S.pombe mei2 gene encoding a crucial molecule for commitment to meiosis is under the regulation of cAMP. *The EMBO journal 7*, 3, 761–767.

WATANABE, Y., SHINOZAKI-YABANA, S., CHIKASHIGE, Y., HIRAOKA, Y., AND YAMAMOTO, M., 1997. Phosphorylation of RNA-binding protein controls cell cycle switch from mitotic to meiotic in fission yeast. *Nature 386*, 6621, 187–190.

WATERHOUSE, A.M., PROCTER, J.B., MARTIN, D.M.A., CLAMP, M., AND BARTON, G.J., 2009. Jalview Version 2--a multiple sequence alignment editor and analysis workbench. *Bioinformatics (Oxford, England) 25*, 9, 1189–1191.

WEICK, E.M., PUNO, M.R., JANUSZYK, K., ZINDER, J.C., DIMATTIA, M.A., AND LIMA, C.D., 2018. Helicase-Dependent RNA Decay Illuminated by a Cryo-EM Structure of a Human Nuclear RNA Exosome-MTR4 Complex. *Cell 173*, 7, 1663-1677.e21.

WILSON, B.G., AND ROBERTS, C.W.M., 2011. SWI/SNF nucleosome remodellers and cancer. *Nature reviews. Cancer 11*, 7, 481–492.

WILSON, G.M., SUTPHEN, K., MOUTAFIS, M., SINHA, S., AND BREWER, G., 2001. Structural remodeling of an A + U-rich RNA element by cation or AUF1 binding. *Journal of Biological Chemistry 276*, 42, 38400–38409.

WOOD, V., GWILLIAM, R., RAJANDREAM, M.-A., LYNE, M., LYNE, R., STEWART, A., SGOUROS, J., PEAT, N., HAYLES, J., BAKER, S., BASHAM, D., BOWMAN, S., BROOKS, K., BROWN, D., BROWN, S., CHILLINGWORTH, T., CHURCHER, C., COLLINS, M., CONNOR, R., CRONIN, A., DAVIS, P., FELTWELL, T., FRASER, A., GENTLES, S., GOBLE, A., HAMLIN, N., HARRIS, D., HIDALGO, J., HODGSON, G., HOLROYD, S., HORNSBY, T., HOWARTH, S., HUCKLE, E.J., HUNT, S., JAGELS, K., JAMES, K., JONES, L., JONES, M., LEATHER, S., MCDONALD, S., MCLEAN, J., MOONEY, P., MOULE, S., MUNGALL, K., MURPHY, L., NIBLETT, D., ODELL, C., OLIVER, K., O'NEIL, S., PEARSON, D., QUAIL, M.A., RABBINOWITSCH, E., RUTHERFORD, K., RUTTER, S., SAUNDERS, D., SEEGER, K., SHARP, S., SKELTON, J., SIMMONDS, M., SQUARES, R., SQUARES, S., STEVENS, K., TAYLOR, K., TAYLOR, R.G.,

TIVEY, A., WALSH, S., WARREN, T., WHITEHEAD, S., WOODWARD, J., VOLCKAERT, G., AERT, R., ROBBEN, J., GRYMONPREZ, B., WELTJENS, I., VANSTREELS, E., RIEGER, M., SCHÄFER, M., MÜLLER-AUER, S., GABEL, C., FUCHS, M., DÜSTERHÖFT, A., FRITZC, C., HOLZER, E., MOESTL, D., HILBERT, H., BORZYM, K., LANGER, I., BECK, A., LEHRACH, H., REINHARDT, R., POHL, T.M., EGER, P., ZIMMERMANN, W., WEDLER, H., WAMBUTT, R., PURNELLE, B., GOFFEAU, A., CADIEU, E., DRÉANO, S., GLOUX, S., LELAURE, V., MOTTIER, S., GALIBERT, F., AVES, S.J., XIANG, Z., HUNT, C., MOORE, K., HURST, S.M., LUCAS, M., ROCHET, M., GAILLARDIN, C., TALLADA, V.A., GARZON, A., THODE, G., DAGA, R.R., CRUZADO, L., JIMENEZ, J., SÁNCHEZ, M., DEL REY, F., BENITO, J., DOMÍNGUEZ, A., REVUELTA, J.L., MORENO, S., ARMSTRONG, J., FORSBURG, S.L., CERUTTI, L., LOWE, T., MCCOMBIE, W.R., PAULSEN, I., POTASHKIN, J., SHPAKOVSKI, G.V., USSERY, D., BARRELL, B.G., AND NURSE, P., 2002. The genome sequence of Schizosaccharomyces pombe. *Nature 415*, 6874, 871–880.

Wu G., Schmid M., Rib L., Polak P., Meola N., Sandelin A., Jensen T.H., 2020. A Two-Layered Targeting Mechanism Underlies Nuclear RNA Sorting by the Human Exosome, Cell Reports, 30, 7, 2387-2401

WU Y., WU X. AND LI S., 2021. Retrotransposons: Jump to Cancer? *Trends in cancer 7*, 7, 577–579.

XIONG, Y., CHEN, T., YU, J., ZHOU, H., LU, B., CHEN, L., SUN, L., WANG, C., LI, S., AND WU, B., 2022. Association between Mutation in SMARCAD1 and Basan Syndrome with Cutaneous Squamous Cell Carcinoma. *Disease Markers 2022*, 7840710.

YAMAMOTO, A., WEST, R.R., MCINTOSH, J.R., AND HIRAOKA, Y., 1999. A cytoplasmic dynein heavy chain is required for oscillatory nuclear movement of meiotic prophase and efficient meiotic recombination in fission yeast. *The Journal of cell biology 145*, 6, 1233–1249.

YAMASHITA, A., SAKUNO, T., WATANABE, Y., AND YAMAMOTO, M., 2017. Analysis of Schizosaccharomyces pombe Meiosis. *Cold Spring Harbor protocols 2017*, 9, pdb.top079855.

YAMASHITA, A., SHICHINO, Y., TANAKA, H., HIRIART, E., TOUAT-TODESCHINI, L., VAVASSEUR, A., DING, D.-Q., HIRAOKA, Y., VERDEL, A., AND YAMAMOTO, M., 2012. Hexanucleotide motifs mediate recruitment of the RNA elimination machinery to silent meiotic genes. *Open Biology 2*, 3, 120014.

YAMASHITA, A., TAKAYAMA, T., IWATA, R., AND YAMAMOTO, M., 2013. A novel factor Iss10 regulates Mmi1-mediated selective elimination of meiotic transcripts. *Nucleic Acids Research 41*, 21, 9680–9687.

YAP, K.L., AND ZHOU, M.M., 2011. Structure and mechanisms of lysine methylation recognition by the chromodomain in gene transcription. *Biochemistry 50*, 12, 1966–1980.

SHICHINO, Y., OTSUBO, Y., YAMAMOTO, M., AND YAMASHITA, A., 2020. Meiotic gene silencing complex MTREC/NURS recruits the nuclear exosome to YTH-RNA-binding protein Mmi1. *PLoS genetics 16*, 2, e1008598.

ZHANG, K., MOSCH, K., FISCHLE, W., AND GREWAL, S.I.S., 2008. Roles of the Clr4 methyltransferase complex in nucleation, spreading and maintenance of heterochromatin. *Nature structural & molecular biology 15*, 4, 381–388.

ZHONGHAO SHI, WEI ZEN YANG, SUE LIN-CHAO, KIN FU CHAK, AND HANNA S. YUAN., 2008. Crystal structure of Escherichia coli PNPase: Central channel residues are involved in processive RNA degradation. *RNA (New York, N.Y.) 14*, 11, 2361–2371.

ZHOU, Y., ZHU, J., SCHERMANN, G., OHLE, C., BENDRIN, K., SUGIOKA-SUGIYAMA, R., SUGIYAMA, T., AND FISCHER, T., 2015. The fission yeast MTREC complex targets CUTs and unspliced pre-mRNAs to the nuclear exosome. *Nature Communications 6*, May, 1–11.

ZOFALL, M., FISCHER, T., ZHANG, K., ZHOU, M., CUI, B., VEENSTRA, T.D., GREWAL, S.I.S., 2009. Histone H2A.Z cooperates with RNAi and heterochromatin factors to suppress antisense RNAs. *Nature 461*, 7262, 419-422

ZOFALL, M., YAMANAKA, S., REYES-TURCU, F.E., ZHANG, K., RUBIN, C., AND GREWAL, S.I.S., 2012. RNA elimination machinery targeting meiotic mRNAs promotes facultative heterochromatin formation. *Science 335*, 6064, 96–100.